

# For Reference

---

NOT TO BE TAKEN FROM THIS ROOM

For Reference

---

NOT TO BE TAKEN FROM THIS ROOM

Ex LIBRIS  
UNIVERSITATIS  
ALBERTAE NSIS













THE UNIVERSITY OF ALBERTA

LAMINAR FORCED CONVECTION HEAT TRANSFER  
IN CURVED RECTANGULAR CHANNELS

by



MITSUBU AKIYAMA

A THESIS  
SUBMITTED TO THE FACULTY OF GRADUATE STUDIES  
IN PARTIAL FULFILMENT OF THE REQUIREMENTS FOR THE DEGREE  
OF MASTER OF SCIENCE

DEPARTMENT OF MECHANICAL ENGINEERING

EDMONTON, ALBERTA

Spring, 1969



UNIVERSITY OF ALBERTA  
FACULTY OF GRADUATE STUDIES

The undersigned certify that they have read, and recommend to the Faculty of Graduate Studies for acceptance, a thesis entitled "LAMINAR FORCED CONVECTION HEAT TRANSFER IN CURVED RECTANGULAR CHANNELS" submitted by MITSUNOBU AKIYAMA in partial fulfilment of the requirements for the degree of Master of Science.



## ABSTRACT

Numerical results for flow and heat transfer are obtained by finite difference method for steady fully developed laminar flow in curved rectangular channels under the thermal boundary conditions of axially uniform wall heat flux and peripherally uniform wall temperature at any axial position.

It is found that the parameter  $K$  (Dean number) is important for the governing equations under consideration. The numerical method yields solutions for a reasonably wide range of Dean number for the curved rectangular channels with aspect ratios  $\gamma = 0.2, 0.5, 1, 2$ , and  $5$  considered in this study. The method used complements the boundary layer approximation which is available in the literature and is applicable for high Dean number region only.

Graphical results for  $Pr = 0.73$  are presented for the ratios of Nusselt numbers, and products of friction factor and Reynolds number between the curved and straight channels,  $Nu/(Nu)_0$  and  $(fRe)/(fRe)_0$ , respectively, with Dean Number as a parameter. Typical examples for axial velocity distributions, temperature profiles, isotherms, and streamlines and velocity profiles for secondary flow are also shown. For square channel, the effect of Prandtl number on the heat transfer results is also investigated.

Comparison of the present result with the results for the curved square channel available in the literature shows clearly that reasonable estimate can be made for the flow and heat transfer results for the Dean number ranging from 150 to 1000 where currently accurate solutions are not available.





## ACKNOWLEDGEMENTS

- The author wishes to extend his appreciation to
- Dr. K.C. Cheng for his supervision of this thesis,
  - Drs. M. Nakayama and Y. Uchida, and Mr. G.J. Hwang for their valuable suggestions and discussions,
  - Drs. N. Nishiwaki and M. Hirata of Tokyo University and Dr. A. Tsuchida of Seikei University for their inspiring guidance during his earlier professional development,
  - Miss H. Mozniuk for her patience in typing this thesis,
  - The National Research Council of Canada for research assistantship through Grant NRC A-1655,
  - His parents and wife for their constant encouragement.



## TABLE OF CONTENTS

	Page
CHAPTER I      INTRODUCTION	1
1.1    Review of the Literature on Flow and Heat Transfer in Curved Pipes	2
1.2    Review of the Literature on Flow and Heat Transfer in Curved Rectangular or Other Noncircular Channels	6
1.3    Purpose of Present Investigation	8
CHAPTER II     THEORETICAL ANALYSIS	10
2.1    General Analysis of Fundamental Equations for the Curved Channel Flow	10
2.2    Basic Equations for Fully Developed Flows in Curved Rectangular Channels and Boundary Conditions	20
CHAPTER III    NUMERICAL SOLUTION	26
3.1    Finite-Difference Approximation	26
3.2    Iterative Method	36
3.3    Point Successive-Overrelaxation Method	41
CHAPTER IV    FLOW AND HEAT TRANSFER RESULTS	43
4.1    Flow and Heat Transfer Characteristics	43
4.2    The Effect of Dean Number on Velocity and Temperature Fields	46
4.3    The Effect of Aspect Ratio on Velocity and Temperature Fields	50
4.4    The Effect of Prandtl Number on Temperature Field	53



	Page
4.5 Flow Resistance	54
4.6 Heat Transfer	56
CHAPTER V CONCLUDING REMARKS	60
REFERENCES	65
APPENDIX FORTRAN PROGRAM	73





## LIST OF FIGURES

Figure		Page
1	Coordinate system and numerical grid for a curved rectangular channel	84
2	Effect of grid size on flow and heat transfer results for a curved square channel ( $\gamma = 1$ ) with $Pr = 0.73$	85
3	Effect of grid size on computing time for a curved square channel ( $\gamma = 1$ ) with $Pr = 0.73$	86
4	A relation between error $\varepsilon_1$ and computing time for a curved square channel $\gamma = 1$ with $Pr = 10^2$	87
5	Numerical experiment on the behavior of the equations at high parameter regime	88
6	Dimensionless axial velocity distribution in a curved square channel $\gamma = 1$ with $K$ as a parameter	89
7	Dimensionless temperature distribution in a curved square channel $\gamma = 1$ and $Pr = 0.73$ with $K$ as a parameter	90
8	Secondary flow streamlines and dimensionless isothermals for a curved square channel $\gamma = 1$ with $K = 51.9$ and $Pr = 0.73$	91
9	Distribution of dimensionless secondary velocity components ( $u, v$ ) in two directions ( $X$ and $Y$ ) passing through the center of circulation for a curved square channel ( $\gamma = 1$ ) with $K$ as a parameter	92





Figure		Page
10	Dimensionless axial velocity distribution in a curved rectangular channel $\gamma = 2$ with $K$ as a parameter	93
11	Dimensionless temperature distribution in a curved rectangular channel $\gamma = 2$ and $Pr = 0.73$ with $K$ as a parameter	94
12	Secondary flow streamlines and dimensionless isothermals for a curved rectangular channel $\gamma = 2$ with $K = 58.8$ and $Pr = 0.73$	95
13	Distribution of dimensionless secondary velocity components $(u,v)$ in two directions $(X$ and $Y)$ passing through the center of circulation for a curved rectangular channel $(\gamma = 2)$ with $K$ as a parameter	96
14	Dimensionless axial velocity distribution in a curved rectangular channel $\gamma = 5$ with $K$ as a parameter	97
15	Dimensionless temperature distribution in a curved rectangular channel $\gamma = 5$ and $Pr = 0.73$ with $K$ as a parameter	98
16	Secondary flow streamlines and dimensionless isothermals for a curved rectangular channel $\gamma = 5$ with $K = 88.1$ and $Pr = 0.73$	99
17	Dimensionless axial velocity distribution in a curved rectangular channel $\gamma = 0.5$ with $K$ as a parameter	100



Figure		Page
18	Dimensionless temperature distribution in a curved rectangular channel $\gamma = 0.5$ and $Pr = 0.73$ with $K$ as a parameter	101
19	Secondary flow streamlines and dimensionless isothermals for a curved rectangular channel $\gamma = 0.5$ with $K = 103.4$ and $Pr = 0.73$	102
20	Distribution of dimensionless secondary velocity components $(u,v)$ in two directions $(X$ and $Y)$ passing through the center of circulation for a curved rectangular channel ( $\gamma = 0.5$ ) with $K$ as a parameter	103
21	Dimensionless axial velocity distribution in a curved rectangular channel $\gamma = 0.2$ with $K$ as a parameter	104
22	Dimensionless temperature distribution in a curved rectangular channel $\gamma = 0.2$ and $Pr = 0.73$ with $K$ as a parameter	105
23	Secondary flow streamlines and dimensionless isothermals for a curved rectangular channel $\gamma = 0.2$ with $K = 79.3$ and $Pr = 0.73$	106
24	Dimensionless temperature distribution in a curved square channel $\gamma = 1$ with $K$ as a parameter and $Pr = 0.1$	107
25	Dimensionless temperature distribution in a curved square channel $\gamma = 1$ with $K$ as a parameter and $Pr = 10^2$	108



Figure		Page
26	Dimensionless temperature distribution in a curved square channel $\gamma = 1$ with $K$ as a parameter and $Pr = 10^3$	109
27	$\bar{w}/(\bar{w})_0$ versus $K$ with aspect ratio $\gamma$ as a parameter	110
28	$(fRe)/(fRe)_0$ versus $K$ with aspect ratio $\gamma$ as a parameter	111
29	Comparison of the results for friction factor from this work with the theoretical and experimental results available in literature	112
30	$\bar{\theta}/(\bar{\theta})_0$ versus $K$ with aspect ratio as a parameter and $Pr = 0.73$	113
31	$\bar{\theta}/(\bar{\theta})_0$ versus $K$ with Prandtl number $Pr$ as a parameter in a curved square channel $\gamma = 1$	114
32	$Nu/(Nu)_0$ versus $K$ with aspect ratio $\gamma$ as a parameter and $Pr = 0.73$	115
33	$Nu/(Nu)_0$ versus $K$ with Prandtl number $Pr$ as a parameter in a curved square channel $\gamma = 1$	116
34	Comparison of heat transfer results from this work with theoretical results available in literature	117





# LIST OF TABLES

Table		Page
1	Numerical results for a curved square channel $\gamma = 1$ with $Pr = 0.73$ (1)	118
2	Numerical results for a curved square channel $\gamma = 1$ with $Pr = 0.73$ (2)	119
3	Numerical results for aspect ratio $\gamma = 0.2$ with $Pr = 0.73$	120
4	Numerical results for aspect ratio $\gamma = 0.5$ with $Pr = 0.73$	121
5	Numerical results for aspect ratio $\gamma = 2$ with $Pr = 0.73$	122
6	Numerical results for aspect ratio $\gamma = 5$ with $Pr = 0.73$	123
7	Numerical results for a curved square channel $\gamma = 1$ with $Pr = 0.1$	124
8	Numerical results for a curved square channel $\gamma = 1$ with $Pr = 0.71$	125
9	Numerical results for a curved square channel $\gamma = 1$ with $Pr = 1$	126
10	Numerical results for a curved square channel $\gamma = 1$ with $Pr = 10$	127
11	Numerical results for a curved square channel $\gamma = 1$ with $Pr = 10^2$	128





Table		Page
12	Numerical results for a curved square channel $\gamma = 1$ with $Pr = 10^3$	129
13	Numerical results for a curved square channel $\gamma = 1$ with $Pr = 10^4$	130
14	Comparison of numerical results with exact values for $K = 0$ (straight channel)	131
15	Numerical results of $(\frac{\partial \bar{w}}{\partial n})_w$ , $\bar{w}$ , and $4X \frac{\partial \bar{\theta}}{\partial n} _w$ for $Pr = 0.73$	132



## NOMENCLATURE

$A$	= cross-section area
$a$	= width of a curved rectangular channel
$b$	= height of a curved rectangular channel
$C_0, C_1, C_1'$	= constants defined in equation (3-2)
$c$	= $-c_1 D_e^3 / 4\nu\mu$
$c_p$	= specific heat at constant pressure
$c_0$	= constant defined in equation (2-12)
$c_1$	= axial pressure gradient, $-\partial P_0 / \partial Z$
$c_2$	= temperature gradient, $\partial T / \partial Z$ or $\partial T / R \partial \Phi$
$D_e$	= equivalent hydraulic diameter, $4A/S = 2ab/(a+b)$
$Ec$	= Eckert number, $W_c^2 / c_p (T - T_W)$
$F_1$	= function defined in equation (3-1)
$F_2$	= function defined in equation (3-8)
$f$	= friction factor, $2 \bar{\tau}_W / (\rho \bar{W}^2)$
$G$	= heat generation
$Gr$	= Grashof number, $D_e^4 g \beta c_2 / \nu^2$
$g$	= gravitational acceleration
$h$	= dimensionless grid spacing, $a / M D_e = b / 2 N D_e$
$\bar{h}$	= average heat transfer coefficient
$K$	= Dean number, $Re(D_e / R_c)^{1/2}$ , see equation (2-19) or (4-11)
$k$	= thermal conductivity
$M$	= number of divisions in the X-direction



$N$	= number of divisions in the Y-direction
$Nu$	= Nusselt number, $\bar{h} D_e/k$
$n$	= dimensionless inward-drawn normal or nth iteration for superscript
$n'$	= dimensional inward-drawn normal
$P$	= pressure
$P'$	= pressure deviation which is a function of X and Y only
$P_0$	= axial pressure distribution measured along the centerline of the main stream and a function of Z only
$Pr$	= Prandtl number, $\nu/\alpha$
$R, \phi, Y$	= cylindrical coordinates
$R_c$	= radius of curvature of a curved rectangular channel
$Re$	= Reynolds number, $D_e W_c/\nu$ or $D_e \bar{W}/\nu$
$Re_a$	= Reynolds number, $a W_c/\nu$
$r_c$	= dimensionless radius of curvature of a curved rectangular channel
$S$	= circumference of cross-section
$T$	= local temperature
$T_M$	= mixed mean temperature difference
$T_W$	= wall temperature
$U, V, W$	= velocity components in X, Y and Z directions in Cartesian coordinates or in R, Y and $\phi$ directions in cylindrical coordinates





$u, v, w$  = dimensionless velocity components in  $x, y$ , and  $z$ -  
directions in Cartesian coordinates or in  $x, y$  and  
 $\phi$ -directions in cylindrical coordinates  
 $X, Y, Z$  = Cartesian coordinates  
 $x, y, z$  = dimensionless Cartesian coordinates  
 $x, y, \phi$  = dimensionless cylindrical coordinates

#### GREEK LETTERS

$\alpha$  = thermal diffusivity  
 $\beta$  = coefficient of thermal expansion  
 $\Gamma$  =  $(\rho W_c^2 / R_c) / (\mu W_c^2 / D_e^2)$   
 $\gamma$  = aspect ratio of rectangular channel,  $a/b$   
 $\epsilon$  = a prescribed error  
 $\zeta$  = dimensionless vorticity,  $\partial v / \partial x - \partial u / \partial y$   
 $\theta_c$  = characteristic temperature difference  
 $\theta$  = dimensionless temperature difference  
 $\lambda$  =  $D_e / R_c$   
 $\lambda_a$  =  $a / R_c$   
 $\mu$  = viscosity  
 $\nu$  = kinematic viscosity  
 $\xi$  = vorticity,  $\partial V / \partial X - \partial U / \partial Y$   
 $\rho$  = density  
 $\sigma$  =  $D_e / R_c \Omega$





$\sigma_a$	= $a/R_c \Omega$
$\overline{\tau}_W$	= mean shearing stress at wall
$\Phi$	= angular coordinate
$\phi$	= dimensionless angular coordinate
$\psi$	= dimensionless stream function
$\Omega$	= characteristic angle in the $\Phi$ -direction
$\omega$	= relaxation factor
$\nabla_\gamma^2$	= dimensionless Laplacian operator, $\partial^2/\partial x^2 + \gamma^2 \partial^2/\partial y^2$
$\nabla^2$	= dimensional or dimensionless Laplacian operator

#### SUBSCRIPTS

a	= value with respect to a
c	= characteristic quantity
i,j	= space subscripts of grid point in X and Y directions
0	= value for straight channel or axial direction
W	= value at wall
x,y	= derivative with respect to x and y, respectively

#### SUPERSCRIPTS

( )	= number inside parentheses indicates an order of the derivative, or number of iteration
-	= average value



## CHAPTER I

### INTRODUCTION

The influence of the dominating body force on the flow and heat transfer characteristics in pipes or channels of various cross sectional shapes has been the subject of many investigations in recent years. The forced convection problems with body force effect are frequently encountered in various heat exchangers, cooling or heating systems, reactors and heat engines. The familiar sources of body force acting on fluid element are gravitational, centrifugal, Coriolis, magnetic and any artificial acceleration forces. It is noted that body force also results due to thermal radiation but this effect is negligibly small in most problems of interest. In general a body force can act at any angle with the main flow in the channel. However in this study consideration will be given only to the case where the body force is acting normal to the main flow. Due to the body forces acting in the cross section perpendicular to the main flow, the flow is now three-dimensional and helical even for the fully developed situation. This means that the additional two velocity components arise in the plane of the cross section and these velocity components together are usually called the secondary flow.

Under certain conditions, a secondary flow due to body force will not be established until a critical value of the characteristic parameter based on body force and the flow field is reached. The stability





problem relating to the onset of the secondary flow due to centrifugal or Coriolis forces and the thermal-convective instability problem (due to buoyant force) have also attracted much attention in the past [1,2,3].

A number of combinations concerning the kinds of body forces and the geometrical shapes of the flow passages are possible in forced convective heat transfer problems [4,5]. However, in this study consideration will be given only to a particular combination dealing with centrifugal force and rectangular channel, namely, curved rectangular channel. For a flow in the curved channel, the critical value of the characteristic parameter (Dean number) is zero. As the Dean number increases, the intensity of the secondary flow increases; consequently, the flow and temperature fields are affected by the secondary flow. Since forced convective heat transfer in curved pipes is closely related to the present problem, a review of the pertinent works on flow and heat transfer in curved pipes is in order.

### 1.1 Review of the Literature on Flow and Heat Transfer in Curved Pipes

The literature on flow in curved pipes is very extensive because of its technical importance. The effect of centrifugal force on flow in pipe bends was first mentioned by Thomson [6] in 1876. Experimental investigations of the secondary flow in curved pipes were made by Eustice [7,8], White [9], Taylor [10] and Yarnell and Nagler [11]. The theoretical analysis was first given by Dean [12,13] for fully developed laminar flow of incompressible fluid in a curved pipe of circular cross-section. Dean employed a perturbation method and his analysis is



applicable only in a low Dean number region ( $0 \leq K < \sim 25$ ). However, Dean's work appears to have sparked a series of works on curved pipes thereafter. Adler [14] introduced the important concept of boundary layer for secondary flow along the wall in his analysis for laminar flow with large Reynolds number. His experimental work covers a wide range encompassing both laminar and turbulent flows and involves the measurements of velocity distributions. Barua's [15] analysis on secondary flow in stationary curved pipes employed boundary layer approximation along the wall for the laminar flow when the Dean number is large and complements Dean's work. Ito [16] proposed accurate empirical formulas on friction factors for fully developed turbulent flow in curved pipes and the empirical equation for transition from laminar to turbulent flow. He also presented asymptotic expressions for friction factors deduced from the 1/7 th-power and the logarithmic velocity distribution laws based on boundary layer approximation. Ito [17] also reported theoretical and experimental investigation on laminar flow in curved pipes. Weske [18] found that the turbulent flow in curved ducts may be analyzed by methods adopted from the theory of boundary layers. Cuming [19] gave solutions for flow in curved pipes of circular, elliptic and rectangular sections in power series of the curvature of the pipe. Topakoglu [20] employed similar method for steady laminar flow of an incompressible viscous fluid in curved pipes of circular and concentric annular sections. By assuming that the actual secondary motion is approximately a uniform stream for the most part of the section, Dean and Hurst [21] obtained





solution for the motion of fluid in curved pipes of circular and square sections. Hawthorne [22] and Detra [23] analyzed the secondary flow problems in curved pipes based on inviscid-fluid theory. It is seen that the published works on flow in curved pipes are numerous; the above review deals only with the literature which is readily available.

Jeschke's experimental work on heat transfer for turbulent flow of air in helically coiled tubes was quoted by McAdams [24]. Hawes' [23] experimental investigation concerned with the measurements of the velocity and temperature distributions of the water in a coiled pipe, but his temperature profiles showed somewhat unusual character. Pratt's [26] work is directed toward developing empirical equations of turbulent flow for both the internal and external film coefficients of heat transfer in a cooling coil immersed in a stirred liquid contained in a tank. Ede [27] pointed out the lack of heat transfer data on various pipe bends and reported the results on local heat transfer coefficient for water in a right-angled pipe bend covering a range of Reynolds number from 500 to 50,000. He noted that with laminar flow the effect of the ratio of bend radius to pipe radius is large. Recently, Seban and McLaughlin [28] presented friction and heat transfer results for the laminar flow of oil and the turbulent flow of water in tube coils with uniform heating having the ratios of coil to tube diameter of 17 and 104, for Reynolds numbers from 12 to 65,000. They too noted the need for additional experimental data to properly define the heat transfer in curved tubes. Rogers and Mayhew [29] provided additional experimental results



for forced convection heat transfer and friction factors using water in steam heated helically coiled tubes with turbulent flow.

At this point it is quite clear that additional experimental investigations and theoretical analysis for heat transfer and pressure loss in curved pipes are still badly needed. Mori and Nakayama [30, 31, 32] presented a series of comprehensive studies on forced convective heat transfer in curved pipes for both laminar and turbulent regions. The results of theoretical analysis based on boundary layer approximation along the pipe wall for fully developed laminar flow in a curved pipe under the condition of uniform heat flux at large Dean numbers were shown to be in good agreement with experimental study using air. For fully developed turbulent flow under the condition of uniform heat flux, the results of theoretical analysis assuming a boundary layer along the pipe wall and experimental results using air were again shown to be in good agreement. The theoretical analysis under the condition of uniform wall temperature and the presentation of practical formulae for both laminar and turbulent flows rounded out this series of investigations. Kubair and Kuloor [33] presented empirical correlations on pressure drop and heat transfer for laminar flow in coiled pipes under constant tube wall temperature conditions. Very recently, Özisik and Topakoglu [34] presented heat transfer results for hydrodynamically and thermally fully developed laminar flow in a curved pipe under the conditions of axially uniform heat flux and uniform peripheral wall temperature at any cross





section for small Dean number region using a method of series expansion; the results are applicable for small curvatures. It is noted that solution for laminar forced convection in a curved pipe for the intermediate Dean number region is still unavailable and some work can be expected in the near future for this region. Finally, it may be of some interest to note that analytical solutions [35,36] for flow of some non-Newtonian fluids in curved pipes are also available.

## 1.2 Review of the Literature on Flow and Heat Transfer in Curved Rectangular or Other Noncircular Channels

In contrast to the number of published papers dealing with flow and heat transfer characteristics in curved pipes, the published works relating to flow and heat transfer in rectangular or other non-circular channels are rather limited in spite of its significance in practical applications.

Ito [37] first reported theory on laminar flows through curved pipes of elliptic and rectangular cross sections using series expansion in Dean number. As noted earlier Cuming [19] also presented theoretical analysis for flow in curved pipes of elliptic and rectangular sections using perturbation method. Dean and Hurst [21] as mentioned before obtained some analytical results for laminar flow in curved square channel by assuming uniform stream for secondary flow. Using boundary layer approximation along the wall, Ludwig [38] presented analytical results for friction factors for fully developed laminar flow in helically coiled square channels rotating around its axis. Extensive experimental results





covering both laminar and turbulent flows are compared against the theoretical results for laminar flow only with good agreement. Experimental results for friction factors are also presented for the case of stationary curved square channel with laminar and turbulent flows. Kapur, Tyagi and Srivastava [39] solved the fully developed laminar flow problem in a curved annulus of concentric circular cross sections for the case when the radius of curvature of the annulus is large compared with the radius of the outer curved pipe. Topakoglu's [20] solution for secondary flow between two concentric torus shaped pipes shows the existence of four vortices as compared to a pair of vortices found by Kapur et al. based on simplified analysis. Eichenberger [40] analysed entrance region problem in a curved rectangular channel with secondary flow by assuming an inviscid flow. Experimental investigations on fully developed turbulent flows in a plane curved channel between concentric circular walls were reported by Wattendorf [41] and Eskinazi and Yeh [42].

Using boundary layer approximation, Mori and Uchida [43] presented analytical results for fully developed laminar flow in a curved square channel under the thermal condition of axially uniform wall temperature gradient. Their results for flow and heat transfer are applicable only for the regime where Dean number is large. Velocity and temperature fields were obtained by dividing the cross section into core and boundary regions and considering the balances of kinetic energy and entropy production for the boundary layers.

Neglecting secondary flow effect, Kreith [44] calculated the



Nusselt numbers for turbulent flow in a curved channel formed by the annulus between two concentric cylinders with the fluid flowing in a direction perpendicular to their common axis showing good agreement with the results from heat-transfer experiments. Mori and Uchida [45] also carried out theoretical investigation on forced convective heat transfer for fully developed laminar and turbulent flows in a curved channel under the condition of constant wall heat flux and compared the theoretical results with experimental measurements. Ustimenko, Zhurgembaev and Nusupbekova [46] presented flow and heat transfer results for fully developed laminar flow in curved flat channels with different ratios of heat fluxes at the inner and outer walls with no secondary flow effect.

It is quite clear from the above brief review that more theoretical and experimental work is certainly required to bring our knowledge of flow and heat transfer in curved channels comparable to the level provided by the rather extensive data relating to flow and heat transfer in straight channels.

### 1.3 Purpose of Present Investigation

The purpose of this work is to present an accurate numerical solution on forced convective heat transfer for steady fully developed laminar flow in curved rectangular channels with various aspect ratios under the thermal boundary conditions of axially uniform wall heat flux and peripherally uniform wall temperature at any axial position. It is noted that Mori and Uchida's [43] analytical solution using boundary layer approximation is valid only for the flow regime when the Dean number is





large. The numerical method complements the boundary layer technique for high Dean number regime and yields accurate solutions up to a reasonably high Dean number region for the aspect ratios  $\gamma = 0.2, 0.5, 1, 2$  and 5 considered in this study. This work is confined to a study of the effect of centrifugal force field on fully developed laminar flow and heat transfer characteristics in curved rectangular channels assuming constant physical properties; it deals only with one type of body force and one kind of geometrical shape. Moreover this study concerns only with one aspect of a broad class of forced convection heat transfer problems in rotating, bent and heated horizontal tubes involving secondary flow caused by body forces. In order to understand the physical meaning of the various dimensionless parameters pertaining to the problem under consideration and the relative importance of each term in the differential equations expressing the conservation of momentum and energy for an incompressible fluid in a curved channel, a general analysis for the continuity, Navier-Stokes and energy equations will be made next.



## CHAPTER II

### THEORETICAL ANALYSIS

#### 2.1 General Analysis of Fundamental Equations for the Curved Channel Flow

Consider a laminar flow with constant viscosity and thermal conductivity coefficients in a channel of rectangular cross-section whose horizontal axis is bent into a circle of radius  $R_c$  with buoyancy force effect. Taking the origin of cylindrical coordinates  $(R, \Phi, Y)$  at the center of curvature with  $(R, \Phi)$  in the horizontal plane, the differential equations expressing the conservation of mass, momentum and energy for a viscous heat generating fluid are

Continuity Equation:

$$\frac{\partial U}{\partial R} + \frac{U}{R} + \frac{1}{R} \frac{\partial W}{\partial \Phi} + \frac{\partial V}{\partial Y} = 0 \quad (2-1)$$

R-Momentum Equation:

$$\begin{aligned} & U \frac{\partial U}{\partial R} + \frac{W}{R} \frac{\partial U}{\partial \Phi} - \frac{W^2}{R} + V \frac{\partial U}{\partial Y} \\ &= - \frac{1}{\rho} \frac{\partial P'}{\partial R} + \nu \left( \frac{\partial^2 U}{\partial R^2} + \frac{1}{R} \frac{\partial U}{\partial R} - \frac{U}{R^2} + \frac{1}{R^2} \frac{\partial^2 U}{\partial \Phi^2} - \frac{2}{R^2} \frac{\partial W}{\partial \Phi} + \frac{\partial^2 U}{\partial Y^2} \right) \end{aligned} \quad (2-2)$$





$\Phi$ -Momentum Equation:

$$\begin{aligned}
 & U \frac{\partial W}{\partial R} + \frac{W}{R} \frac{\partial W}{\partial \Phi} + \frac{UW}{R} + V \frac{\partial W}{\partial Y} \\
 & = - \frac{1}{\rho} \frac{1}{R} \frac{\partial P_0}{\partial \Phi} + \nu \left( \frac{\partial^2 W}{\partial R^2} + \frac{1}{R} \frac{\partial W}{\partial R} - \frac{W}{R^2} + \frac{1}{R^2} \frac{\partial^2 W}{\partial \Phi^2} + \frac{2}{R^2} \frac{\partial U}{\partial \Phi} + \frac{\partial^2 W}{\partial Y^2} \right) \quad (2-3)
 \end{aligned}$$

$Y$ -Momentum Equation:

$$\begin{aligned}
 & U \frac{\partial V}{\partial R} + \frac{W}{R} \frac{\partial V}{\partial \Phi} + V \frac{\partial V}{\partial Y} \\
 & = \beta g(T - T_w) - \frac{1}{\rho} \frac{\partial P'}{\partial Y} + \nu \left( \frac{\partial^2 V}{\partial R^2} + \frac{1}{R} \frac{\partial V}{\partial R} + \frac{1}{R^2} \frac{\partial^2 V}{\partial \Phi^2} + \frac{\partial^2 V}{\partial Y^2} \right) \quad (2-4)
 \end{aligned}$$

where  $P = P'(R, Y) + P_0(\Phi) - \beta gY$

Energy Equation:

$$\begin{aligned}
 & U \frac{\partial T}{\partial R} + \frac{W}{R} \frac{\partial T}{\partial \Phi} + V \frac{\partial T}{\partial Y} \\
 & = \alpha \left[ \frac{\partial^2 T}{\partial R^2} + \frac{1}{R} \frac{\partial T}{\partial R} + \frac{1}{R^2} \frac{\partial^2 T}{\partial \Phi^2} + \frac{\partial^2 T}{\partial Y^2} \right] \\
 & + \frac{\mu}{\rho c_p} \left\{ 2 \left[ \left( \frac{\partial U}{\partial R} \right)^2 + \frac{1}{R^2} \left( \frac{\partial W}{\partial \Phi} + U \right)^2 + \left( \frac{\partial V}{\partial Y} \right)^2 \right] \right. \\
 & + \left. \left( \frac{\partial W}{\partial Y} + \frac{1}{R} \frac{\partial V}{\partial \Phi} \right)^2 + \left( \frac{\partial V}{\partial R} + \frac{\partial U}{\partial Y} \right)^2 + \left[ \frac{1}{R} \frac{\partial U}{\partial \Phi} + R \frac{\partial}{\partial R} \left( \frac{W}{R} \right) \right]^2 \right\} + \frac{G}{\rho c_p} \quad (2-5)
 \end{aligned}$$

Introducing representative lengths,  $a$  and  $b$ , of the rectangular cross-section of the channel, representative radius of curvature,  $R_c$ , of



the channel, representative angle  $\Omega$  for  $\Phi$ , and the reference velocity components  $U_c$ ,  $V_c$  and  $W_c$  in the  $R$ ,  $Y$  and  $\Phi$ -directions, respectively, the following non-dimensional quantities may be defined:

$$R = R_c + ax = R_c(1 + \lambda_a x) \quad , \quad X = ax \quad ,$$

$$Y = by, \quad \Phi = \Omega\phi, \quad U = U_c u, \quad V = V_c v, \quad \text{and} \quad W = W_c w \quad .$$

Using the above relations, the continuity equation (2-1) is reduced to the following non-dimensional form.

$$\begin{aligned} & \left(\frac{U_c}{V_c}\right) \left(\frac{b}{a}\right) \left\{ \frac{\partial u}{\partial x} + \lambda_a \frac{u}{(1 + \lambda_a x)} \right. \\ & \left. + \Omega^{-1} \lambda_a \left(\frac{W_c}{U_c}\right) \frac{1}{(1 + \lambda_a x)} \frac{\partial w}{\partial \phi} \right\} + \frac{\partial v}{\partial y} = 0 \end{aligned} \quad (2-6)$$

since  $\partial u / \partial x$  and  $\partial v / \partial y$  may be expected to be of the same order of magnitude, one may set

$$\left(\frac{U_c}{V_c}\right) \left(\frac{b}{a}\right) = O[1] \quad . \quad (2-7)$$

The continuity equation now becomes

$$\frac{\partial u}{\partial x} + \frac{\partial v}{\partial y} + \lambda_a \frac{u}{(1 + \lambda_a x)} + \Omega^{-1} \lambda_a \left(\frac{W_c}{U_c}\right) \frac{1}{(1 + \lambda_a x)} \frac{\partial w}{\partial \phi} = 0 \quad . \quad (2-8)$$



Eliminating pressure  $P'$  from equations (2-2) and (2-4) and introducing the vorticity function  $\zeta = \partial v / \partial x - \partial u / \partial y$ , the following relation can be obtained by considering that the centrifugal force term and the inertia terms are equally significant

$$U_c = \lambda_a^{\frac{1}{2}} W_c \quad (2-9)$$

This signifies the importance of the secondary motion. The resulting momentum equation in non-dimensional form for the secondary flow is

$$\begin{aligned} & \gamma^{-1} \frac{\partial}{\partial x} (u\zeta) + \frac{\partial}{\partial y} (v\zeta) + \Omega^{-1} \gamma^{-\frac{1}{2}} \lambda_a^{\frac{1}{2}} \frac{1}{(1 + \lambda_a x)} \\ & (\gamma^{-1} \frac{\partial w}{\partial x} \frac{\partial v}{\partial \phi} - \gamma \frac{\partial w}{\partial y} \frac{\partial u}{\partial \phi}) + \Omega^{-1} \lambda_a^{\frac{1}{2}} \gamma^{-\frac{3}{2}} \frac{w}{(1 + \lambda_a x)} \frac{\partial \zeta}{\partial \phi} \\ & = \text{Re}_a^{-1} \gamma^{\frac{1}{2}} \lambda_a^{-\frac{1}{2}} [\nabla_\gamma^2 \zeta + \sigma_a^2 \frac{1}{(1 + \lambda_a x)} \frac{\partial^2 \zeta}{\partial \phi^2} \\ & + 2\gamma^{\frac{1}{2}} \sigma_a \lambda_a^{\frac{1}{2}} \frac{1}{(1 + \lambda_a x)} \frac{\partial^2 w}{\partial \phi \partial y} + \lambda_a \frac{1}{(1 + \lambda_a x)} \frac{\partial \zeta}{\partial x} \\ & + \lambda_a^2 \frac{1}{(1 + \lambda_a x)^2} \frac{\partial u}{\partial y}] + \text{GrRe}_a^{-2} \lambda_a^{-1} \gamma^{-1} \frac{\partial \theta}{\partial x} - \gamma \frac{1}{(1 + \lambda_a x)} \frac{\partial (w)^2}{\partial y} \quad (2-10) \end{aligned}$$

where  $\nabla_\gamma^2 = \frac{\partial^2}{\partial x^2} + \gamma^2 \frac{\partial^2}{\partial y^2}$

$$\gamma = \frac{a}{b}$$





$$\sigma_a = \frac{a}{\Omega R_c}$$

Similarly, the axial momentum equation in non-dimensional form becomes

$$\begin{aligned} & \gamma u \frac{\partial w}{\partial x} + v \frac{\partial w}{\partial y} + \Omega^{-\frac{1}{2}} \sigma_a^{-\frac{1}{2}} \gamma^{-\frac{1}{2}} \left[ \frac{w}{(1 + \lambda_a x)} \frac{\partial w}{\partial \phi} \right] \\ & = \text{Re}_a^{-1} \lambda_a^{-\frac{1}{2}} \gamma^{-\frac{1}{2}} \left[ - \frac{a}{\mu W_c \Omega} \frac{1}{(1 + \lambda_a x)} \frac{\partial P}{\partial \phi} + \nabla_\gamma^2 w \right. \\ & \quad + \sigma_a^2 \frac{1}{(1 + \lambda_a x)^2} \frac{\partial^2 w}{\partial \phi^2} + 2 \sigma_a^2 \lambda_a^{-\frac{1}{2}} \gamma^{-\frac{1}{2}} \frac{1}{(1 + \lambda_a x)} \frac{\partial u}{\partial \phi} \\ & \quad \left. + \lambda_a \frac{1}{(1 + \lambda_a x)} \frac{\partial w}{\partial x} - \lambda_a^2 \frac{w}{(1 + \lambda_a x)^2} \right] - \lambda_a \frac{uw}{(1 + \lambda_a x)} \end{aligned} \quad (2-11)$$

The reference velocity  $W_c$  may be regarded as the average velocity in a straight channel given as

$$W_c = - \frac{a}{\mu \Omega} \frac{\partial P}{\partial \phi} \frac{1}{c_0} \quad (2-12)$$

where  $c_0$  is a constant depending on the geometrical shape of the cross-section.

For the forced convection problem, the axial temperature gradient is usually known or given. Consequently, the reference temperature difference may be defined as

$$T - T_W = \theta_c \theta$$



It is clear that the convective term involving the axial temperature gradient and one lateral conduction terms in the energy equation must be equally significant. From this one may define a characteristic temperature difference as follows:

$$\theta_c = \frac{W_c c_a^2}{\alpha} \quad (2-13)$$

Then, the non-dimensionalized energy equation neglecting heat generation is given as

$$\begin{aligned} & u \frac{\partial \theta}{\partial x} + \frac{w}{(1 + \lambda_a x)} \frac{\partial \theta}{\partial \phi} + v \frac{\partial \theta}{\partial y} \\ &= Re_a^{-1} Pr^{-1} \left[ \lambda_a^{-\frac{1}{2}} \lambda^{-\frac{1}{2}} \nabla_\gamma^2 \theta + \lambda_a^{\frac{1}{2}} \lambda^{-\frac{1}{2}} \frac{1}{(1 + \lambda_a x)} \frac{\partial \theta}{\partial x} \right. \\ &+ \left. \sigma_a \frac{1}{(1 + \lambda_a x)} \frac{\partial^2 \theta}{\partial \phi^2} \right] + Ec Re_a^{-1} \{ 2\gamma \left[ \left( \frac{\partial u}{\partial x} \right)^2 + \left( \frac{\partial v}{\partial y} \right)^2 \right] \right. \\ &+ 2\lambda_a \frac{1}{(1 + \lambda_a x)^2} \left( \Omega^{-1} \frac{\partial w}{\partial \phi} + \lambda_a^{\frac{1}{2}} \lambda^{\frac{1}{2}} u \right)^2 \\ &+ \left. \lambda_a \left[ \lambda_a^{-1} \lambda \frac{\partial w}{\partial y} + \lambda_a^{-\frac{1}{2}} \gamma^{-\frac{1}{2}} \frac{1}{(1 + \lambda_a x)} \frac{\partial w}{\partial \phi} \right]^2 \right\} \end{aligned}$$



$$\begin{aligned}
& + \lambda_a \left[ \lambda_a^{-\frac{1}{2}} \gamma^{-\frac{1}{2}} \frac{\partial w}{\partial x} + \lambda_a^{-\frac{1}{2}} \gamma^{\frac{3}{2}} \frac{\partial u}{\partial y} \right]^2 \\
& + \lambda_a \left[ \lambda_a^{-\frac{1}{2}} \gamma^{\frac{1}{2}} \Omega^{-1} \frac{1}{(1 + \lambda_a x)} \frac{\partial u}{\partial \phi} + \lambda_a^{-1} \frac{\partial w}{\partial x} - \frac{w}{(1 + \lambda_a x)} \right]^2 \}. \quad (2-14)
\end{aligned}$$

For a fully developed flow and neglecting viscous dissipation, one may write

$$Ec \lll 0 \quad [1]$$

$$\Omega \ggg 0 \quad [1] \quad .$$

The last condition implies

$$\sigma_a \equiv \lambda_a / \Omega \lll 0 \quad [1]$$

since geometrically  $\lambda_a$  is restricted as

$$\lambda_a \ll 2 \quad .$$

Define the following quantities

$$\lambda = D_e / R_c \quad , \quad \sigma = D_e / R_c \Omega \lll 0 \quad [1]$$

and  $\gamma = a/b = 0 \quad [1]$  where  $D_e = 2ab/(a + b)$





and replacing  $\lambda_a$  and  $\sigma_a$  in equations (2-8), (2-10), (2-11) and (2-14), by  $\lambda$  and  $\sigma$ , respectively, the following simplified equations result.

The Continuity Equation:

$$\frac{\partial u}{\partial x} + \frac{\partial v}{\partial y} = 0 \quad (2-15)$$

The Momentum Equation for Secondary Flow:

$$\begin{aligned} & u \frac{\partial \zeta}{\partial x} + v \frac{\partial \zeta}{\partial y} \\ &= \text{Re}^{-1} \left[ \lambda^{-\frac{1}{2}} \nabla^2 \zeta + \lambda^{\frac{1}{2}} \frac{1}{(1 + \lambda x)} \frac{\partial \zeta}{\partial x} + \lambda^{\frac{3}{2}} \frac{1}{(1 + \lambda x)^2} \frac{\partial u}{\partial y} \right] \\ &+ \text{Gr} \text{Re}^{-2} \lambda^{-1} \frac{\partial \theta}{\partial x} - \frac{1}{(1 + \lambda x)} \frac{\partial (w)^2}{\partial y} \end{aligned} \quad (2-16)$$

The Axial Momentum Equation:

$$\begin{aligned} & u \frac{\partial w}{\partial x} + v \frac{\partial w}{\partial y} = \text{Re}^{-1} \left[ \lambda^{-\frac{1}{2}} \frac{c_0}{(1 + \lambda x)} \right. \\ &+ \lambda^{-\frac{1}{2}} \nabla^2 w + \lambda^{\frac{1}{2}} \frac{1}{(1 + \lambda x)} \frac{\partial w}{\partial x} - \lambda^{\frac{3}{2}} \frac{w}{(1 + \lambda x)^2} \left. \right] - \lambda \frac{uw}{(1 + \lambda x)} \end{aligned} \quad (2-17)$$

The Energy Equation:

$$\begin{aligned} & u \frac{\partial \theta}{\partial x} + v \frac{\partial \theta}{\partial y} + \frac{w}{(1 + \lambda x)} \frac{\partial \theta}{\partial \phi} \\ &= \text{Re}^{-1} \text{Pr}^{-1} \left[ \lambda^{-\frac{1}{2}} \nabla^2 \theta + \lambda^{\frac{1}{2}} \frac{1}{(1 + \lambda x)} \frac{\partial \theta}{\partial x} \right] \end{aligned} \quad (2-18)$$



where  $\nabla^2 = \frac{\partial}{\partial x^2} + \frac{\partial}{\partial y^2}$

It may be of interest to note that the last term on the right-hand side of equation (2-16) represents a centrifugal force effect due to curvature and the term next to the last represents buoyancy force effect. It is also seen that the last term on the right-hand side of equation (2-17) represents Coriolis force effect.

As stated earlier, for a fully developed flow condition  $\Omega \gg 0[1]$ , and this also implies that  $\lambda \ll 0[1]$ . Thus all the terms involving  $\lambda^{1/2}$ ,  $\lambda^1$  and  $\lambda^{3/2}$  may be neglected as compared with the term of order one. Similarly, the term involving  $\lambda^{-1/2}$  must be retained by considering the contribution due to other non-dimensional characteristic parameters. It is noted that Topakoglu [20] and Özisik and Topakoglu [34] considered the cases of small curvatures for laminar flow and heat transfer in a curved pipe; however, the results of analysis show that the terms involving  $\lambda^{1/2}$ ,  $\lambda$  and  $\lambda^{3/2}$  seem to have negligible effect on the flow and heat transfer results at least for the very low Dean number region.

The following general conclusions may be drawn from the order of magnitude analysis:

(1)  $Re = O[10^{-2}]$  and  $\lambda = O[10^{-2}]$

Observations of the equations of motion show that inertia terms, centrifugal force term and Coriolis force term can be neglected for this case. In addition, the buoyancy force term can be neglected only if  $Gr < O[10^{-6}]$  and must be considered if  $Gr > O[10^{-4}]$ . Observation of the energy equation shows that convective terms may be neglected if  $Pr < O[10]$ .



On the other hand, convective terms cannot be neglected when  $Pr > 0[10^3]$ .

(2)  $Re > 0[10]$

In contrast to the above case, the inertia terms and the convective terms must be considered for this case. The buoyancy force term now depends on the order of magnitude for  $Re \lambda^{1/2}$ . The following case may be of interest:

$$Re \lambda^{\frac{1}{2}} > 0[10^2] .$$

It is noted that the buoyancy force term must be considered if  $Gr > 0[10^3]$ .

It is very likely that this case may occur in practice. On the other hand, if  $Gr < 0[10^2]$ , the buoyancy force term can be neglected. This condition corresponds to the problem under study. It is also noted that the Coriolis force effect is important if  $\lambda = 0[1]$ . However, this condition hardly ever occurs for the fully developed flow situation.

The foregoing general analysis shows clearly that the following dimensionless parameters are of importance for flow and heat transfer characteristics in a curved channel:

Dimensionless parameter representing  
curvature effect

$$\lambda = \frac{D_e}{R_c}$$

Reynolds number

$$Re = D_e \frac{W_c}{\nu}$$

Prandtl number

$$Pr = \frac{\nu}{\alpha}$$

Grashof number

$$Gr = D_e^4 g \beta \frac{c_2}{\nu^2}$$







Observation of the momentum and energy equations shows that the Reynolds number,  $Re$ , and the curvature effect parameter,  $\lambda$ , appear together as  $Re \lambda^{1/2} \equiv K$ . This last characteristic parameter for flow in a curved channel is usually referred to as Dean number in the literature.

In order to gain physical insight into the meaning of this important characteristic parameter, the Dean number, may be rewritten as [2]

$$K = \left[ \frac{\frac{W_c^2}{\rho D_e}}{\frac{W_c^2}{\mu D_e^2}} \cdot \frac{\frac{W_c^2}{\rho R_c}}{\frac{W_c^2}{\mu D_e^2}} \right]^{1/2} = (Re \cdot \Gamma)^{1/2} \quad (2-19)$$

One sees that the Dean number consists of the product of two non-dimensional characteristic parameters  $Re$  and  $\Gamma$ . The meaning of Reynolds number is well understood. The parameter  $\Gamma$  represents the ratio of the centrifugal force effect to the viscous force effect and might be called as the centrifugal Reynolds number. Finally, one notes that the heat generating term in the energy equation (2-5) was included to show that the analysis can be carried out for heat generating fluid. However, for simplicity, the heat generation will be omitted in the remaining analysis.

## 2.2 Basic Equations for Fully Developed Flows in Curved Rectangular Channels and Boundary Conditions

Consider a steady fully developed laminar flow of viscous fluid in a curved rectangular channel under the thermal boundary conditions of



axially uniform wall heat flux and peripherally uniform wall temperature at any axial position. Because of the non-linearity of the basic equations governing the problem, the following simplifying assumptions are made to facilitate the analysis:

1. Velocity and temperature fields are fully developed.
2. The only body force is a centrifugal force caused by the curvature of the channel.
3. The radius of curvature of the rectangular channel is large compared with the hydraulic diameter of the cross-section of the channel.
4. No internal heat generation.
5. Physical properties are constant.
6. Viscous dissipation is negligible.

Taking the origin of the rectangular coordinates (X,Y,Z) at the center of the rectangular cross-section as shown in Figure 1 and applying the assumptions stated above, the governing equations for the present problem are

Continuity Equation:

$$\frac{\partial U}{\partial X} + \frac{\partial V}{\partial Y} = 0 \quad (2-20)$$

Momentum Equation for Secondary Flow:

$$U \frac{\partial \xi}{\partial X} + V \frac{\partial \xi}{\partial Y} = \nu \nabla^2 \xi - \frac{\partial}{\partial Y} \left( \frac{W^2}{R_c} \right) \quad (2-21)$$



Axial Momentum Equation:

$$U \frac{\partial W}{\partial X} + V \frac{\partial W}{\partial Y} = - \frac{1}{\rho} \frac{\partial P_0}{\partial Z} + \nu \nabla^2 W \quad (2-22)$$

Energy Equation:

$$U \frac{\partial T}{\partial X} + V \frac{\partial T}{\partial Y} + W \frac{\partial T}{\partial Z} = \alpha \nabla^2 T \quad (2-23)$$

where

$$\xi = \frac{\partial V}{\partial X} - \frac{\partial U}{\partial Y} \quad (2-24)$$

and the pressure at any point consists of two parts,

$$P = P_0(Z) + P'(X,Y) \quad (2-25)$$

Boundary Conditions:

$$U = V = W = T - T_W = 0$$

along upper and lower walls,

$$Y = \frac{b}{2} \text{ or } Y = -\frac{b}{2} \text{ and } -\frac{a}{2} \leq X \leq \frac{a}{2}$$

$$V = \frac{\partial U}{\partial Y} = \frac{\partial T}{\partial Y} = 0$$

along center line,  $Y = 0$  (2-26)

$$\text{and } -\frac{a}{2} \leq X \leq \frac{a}{2}$$

$$U = V = W = T - T_W = 0$$

along inner and outer walls,

$$X = -\frac{a}{2} \text{ or } X = \frac{a}{2} \text{ and } -\frac{b}{2} \leq Y \leq \frac{b}{2}$$





Introducing the following transformations,

$$X = D_e x, \quad R_c = D_e r_c, \quad Y = D_e y, \quad U = (\nu/D_e) u,$$

$$V = (\nu/D_e) v, \quad W = (\nu c/D_e) w, \quad c = -c_1 D_e^{3/4} \nu \mu,$$

$$T - T_w = (c_2 D_e \text{Pr} c) \theta$$

where  $D_e = \frac{2ab}{(a+b)}$

$$c_1 = -\frac{\partial P_0}{\partial Z}, \quad c_2 = \frac{\partial T}{\partial Z},$$

and a dimensionless stream function  $\psi$

$$u = \frac{\partial \psi}{\partial y}$$

(2-27)

$$v = -\frac{\partial \psi}{\partial x}$$

the above equations may be restated in the following dimensionless forms.

Momentum Equation for Secondary Flow:

$$\frac{\partial \psi}{\partial y} \frac{\partial}{\partial x} \nabla^2 \psi - \frac{\partial \psi}{\partial x} \frac{\partial}{\partial y} \nabla^2 \psi = \nabla^2 \nabla^2 \psi + 2\left(\frac{c^2}{r_c}\right) w \frac{\partial w}{\partial y} \quad (2-28)$$



Axial Momentum Equation:

$$\frac{\partial \psi}{\partial y} \frac{\partial w}{\partial x} - \frac{\partial \psi}{\partial x} \frac{\partial w}{\partial y} = \nabla^2 w + 4 \quad (2-29)$$

Energy Equation:

$$\text{Pr} \left( \frac{\partial \psi}{\partial y} \frac{\partial \theta}{\partial x} - \frac{\partial \psi}{\partial x} \frac{\partial \theta}{\partial y} \right) = \nabla^2 \theta - w \quad (2-30)$$

Because of symmetry with respect to the X-axis, it is only required to consider the lower half of the rectangular cross-section (see Figure 1). Consequently, the boundary conditions are:

$$\begin{aligned} \frac{\partial \psi}{\partial x} = \frac{\partial \psi}{\partial y} = w = \theta = 0 & \quad \text{along lower wall, } y = -\frac{b}{2D_e} \\ & \quad \text{and } -\frac{a}{2D_e} \leq x \leq \frac{a}{2D_e} \\ \\ \frac{\partial \psi}{\partial x} = \frac{\partial^2 \psi}{\partial y^2} = \frac{\partial \theta}{\partial y} = 0 & \quad \text{along center line, } y = 0 \\ & \quad \text{and } -\frac{a}{2D_e} \leq x \leq \frac{a}{2D_e} \\ \\ \frac{\partial \psi}{\partial x} = \frac{\partial \psi}{\partial y} = w = \theta = 0 & \quad \text{along inner and outer walls,} \\ & \quad x = -\frac{a}{2D_e} \text{ or } x = \frac{a}{2D_e} \text{ and} \\ & \quad -\frac{b}{2D_e} \leq y \leq 0 \end{aligned} \quad (2-31)$$

The above set of equations constitutes a formal mathematical statement of the problem under consideration. In contrast to the forced



convection problem with buoyancy effect, one notes that for the problem at hand, the momentum equations and the energy equation are uncoupled; namely, velocity field can be found independently. It is possible to solve the above set of equations analytically by a method of successive approximation in principle as demonstrated in the literature for similar problems [19,20,37], but the process is very tedious and the solution quickly diverges with the increase of the Dean number. In view of the considerable difficulties with the analytical method, the numerical solutions of the exact equations using converging iterative procedures will be presented in this study. The numerical solutions for a similar set of differential equations having non-linear terms are available in the literature [47 to 53].





## CHAPTER III

### NUMERICAL SOLUTION

#### 3.1 Finite-Difference Approximation

In recent years, finite-difference methods have been shown to be a powerful tool for the solution of natural convection problems. The prediction of natural convection by numerical method was recently reviewed by Churchill [47]. Wilkes and Churchill [48] made a study of natural convection in a rectangular enclosure with one vertical wall heated and the other cooled by an implicit alternating direction finite-difference method. Finite-difference methods were also used by Samuels and Churchill [49] to compute hydrodynamic instability due to natural convection in an enclosed horizontal rectangular region heated from below. Barakat and Clark [50] made a study of the two-dimensional transient laminar natural convection in a partially filled liquid container using an explicit finite-difference technique. Recently, Hwang [51,52] presented numerical solution for fully developed combined free and forced laminar convection in horizontal rectangular channels using point successive-overrelaxation method. DeVahl Davis [53] also reported numerical solution for laminar natural convection in an enclosed rectangular cavity by similar successive-overrelaxation method. In this study, the point successive-overrelaxation method was employed to solve a set of elliptic partial differential equations and the associated boundary conditions.



Consider equation (2-29) which may be regarded as

$$\nabla^2 w = F_1(u, v, \frac{\partial w}{\partial x}, \frac{\partial w}{\partial y}) \quad (3-1)$$

The Laplacian function  $\nabla^2 w$  at a mesh point (i,j) may be expressed by

$$\nabla^2 w_{i,j} = C_0 w_{i,j} + C_1(w_{i+1,j} + w_{i-1,j}) + C_1(w_{i,j+1} + w_{i,j-1}) + \dots \quad (3-2)$$

Using Taylor series expansion, the following equations can be written at the four neighboring points of the mesh point (i,j).

$$\begin{aligned} w_{i+1,j} &= w_{i,j} + h w_{i,jx}^{(1)} + \frac{h^2}{2!} w_{i,jx}^{(2)} + \frac{h^3}{3!} w_{i,jx}^{(3)} \\ &\quad + \frac{h^4}{4!} w_{i,jx}^{(4)} + \frac{h^5}{5!} w_{i,jx}^{(5)} + \frac{h^6}{6!} w_{i,jx}^{(6)} + \dots \\ w_{i-1,j} &= w_{i,j} - h w_{i,jx}^{(1)} + \frac{h^2}{2!} w_{i,jx}^{(2)} - \frac{h^3}{3!} w_{i,jx}^{(3)} \\ &\quad + \frac{h^4}{4!} w_{i,jx}^{(4)} - \frac{h^5}{5!} w_{i,jx}^{(5)} + \frac{h^6}{6!} w_{i,jx}^{(6)} - \dots \\ w_{i,j+1} &= w_{i,j} + h w_{i,jy}^{(1)} + \frac{h^2}{2!} w_{i,jy}^{(2)} + \frac{h^3}{3!} w_{i,jy}^{(3)} \\ &\quad + \frac{h^4}{4!} w_{i,jy}^{(4)} + \frac{h^5}{5!} w_{i,jy}^{(5)} + \frac{h^6}{6!} w_{i,jy}^{(6)} + \dots \\ w_{i,j-1} &= w_{i,j} - h w_{i,jy}^{(1)} + \frac{h^2}{2!} w_{i,jy}^{(2)} - \frac{h^3}{3!} w_{i,jy}^{(3)} \\ &\quad + \frac{h^4}{4!} w_{i,jy}^{(4)} - \frac{h^5}{5!} w_{i,jy}^{(5)} + \frac{h^6}{6!} w_{i,jy}^{(6)} - \dots \end{aligned} \quad (3-3)$$



It is noted that identical dimensionless mesh size ( $h$ ) is used in X and Y-directions. Substituting equation (3-3) into equation (3-2) and evaluating the coefficients  $C_0, C_1, C_1'$ , the Laplacian function at the mesh point  $(i,j)$  becomes

$$\begin{aligned} \nabla^2 w_{i,j} = & -\frac{4}{h^2} w_{i,j} + \frac{1}{h^2} (w_{i+1,j} + w_{i-1,j} + w_{i,j+1} + w_{i,j-1}) \\ & + \frac{h^2}{12} (w_{i,jx}^{(4)} + w_{i,jy}^{(4)}) + \dots \end{aligned} \quad (3-4)$$

Comparing equations (2-29) and (3-1), the function  $F$  at the mesh point  $(i,j)$  may be expressed as

$$\begin{aligned} F_{i,j} = & \frac{1}{2h} (w_{i+1,j} - w_{i-1,j}) u_{i,j} + \frac{1}{2h} (w_{i,j+1} - w_{i,j-1}) v_{i,j} \\ & - 4 - \frac{h^2}{6} (w_{i,jx}^{(3)} u_{i,j} + w_{i,jy}^{(3)} v_{i,j}) + \dots \end{aligned} \quad (3-5)$$

Equating equations (3-4) and (3-5) and neglecting higher order terms, the finite-difference equation for the axial momentum equation (2-29) may be expressed as

$$\begin{aligned} w_{i,j} = & \frac{1}{4} (w_{i+1,j} + w_{i-1,j} + w_{i,j+1} + w_{i,j-1}) \\ & - \frac{h^2}{4} \left\{ u_{i,j} \frac{w_{i+1,j} - w_{i-1,j}}{2h} + v_{i,j} \frac{w_{i,j+1} - w_{i,j-1}}{2h} - 4 \right\} \end{aligned} \quad (3-6)$$







Applying similar method, the finite-difference equation for the energy equation (2-30) becomes

$$\begin{aligned} \theta_{i,j} = & \frac{1}{4}(\theta_{i+1,j} + \theta_{i-1,j} + \theta_{i,j+1} + \theta_{i,j-1}) \\ & - \frac{h^2}{4} \left\{ \text{Pr}[u_{i,j} \frac{\theta_{i+1,j} - \theta_{i-1,j}}{2h} + v_{i,j} \frac{\theta_{i,j+1} - \theta_{i,j-1}}{2h}] + w_{i,j} \right\} \end{aligned} \quad (3-7)$$

To obtain the finite-difference equation for equation (2-28), one notes that equation (2-28) may be regarded as the inhomogeneous biharmonic equation in the following form.

$$\nabla^2 \nabla^2 \psi = F_2 \left[ \left( \frac{\partial}{\partial x}, \frac{\partial}{\partial y} \right) \psi, \left( \frac{\partial}{\partial x}, \frac{\partial}{\partial y} \right) \nabla^2 \psi, w, \frac{\partial w}{\partial y} \right] \quad (3-8)$$

Omitting details, the finite-difference equation for the secondary flow stream function  $\psi$  at the mesh point  $(i,j)$  may be obtained by double application of the procedure transforming equation (3-1) into its finite-difference form. The result is

$$\begin{aligned} \psi_{i,j} = & \left( \frac{4}{10} - \frac{h}{10} u_{i,j} \right) \psi_{i+1,j} + \left( \frac{4}{10} + \frac{h}{10} u_{i,j} \right) \psi_{i-1,j} \\ & + \left( \frac{4}{10} - \frac{h}{10} v_{i,j} \right) \psi_{i,j+1} + \left( \frac{4}{10} + \frac{h}{10} v_{i,j} \right) \psi_{i,j-1} \\ & + \left( -\frac{1}{20} + \frac{h}{40} u_{i,j} \right) \psi_{i+2,j} + \left( -\frac{1}{20} - \frac{h}{40} u_{i,j} \right) \psi_{i-2,j} \end{aligned}$$



$$\begin{aligned}
& + \left(-\frac{1}{20} + \frac{h}{40} v_{i,j}\right) \psi_{i,j+2} + \left(-\frac{1}{20} - \frac{h}{40} v_{i,j}\right) \psi_{i,j-2} \\
& + \left(-\frac{1}{10} + \frac{h}{40} u_{i,j} + \frac{h}{40} v_{i,j}\right) \psi_{i+1,j+1} \quad (3-9) \\
& + \left(-\frac{1}{10} + \frac{h}{40} u_{i,j} - \frac{h}{40} v_{i,j}\right) \psi_{i+1,j-1} \\
& + \left(-\frac{1}{10} - \frac{h}{40} u_{i,j} + \frac{h}{40} v_{i,j}\right) \psi_{i-1,j+1} \\
& + \left(-\frac{1}{10} - \frac{h}{40} u_{i,j} - \frac{h}{40} v_{i,j}\right) \psi_{i-1,j-1} \\
& - \frac{h^3}{120} \left(\frac{c}{r_c}\right)^2 w_{i,j} (-w_{i,j+2} + 8w_{i,j+1} - 8w_{i,j-1} + w_{i,j-2})
\end{aligned}$$

It is noted that for the derivative  $\partial w / \partial y$  in equation (2-28), five-point formula is used.

It is well to note that the finite-difference expression for the stream function at the mesh point next to the boundary takes the following forms after satisfying the boundary condition for  $\psi$ :

At the points  $i = 2, j = 3, 4 \dots N + 1$ ,  $\psi_{2,j}$  is

$$\begin{aligned}
\psi_{2,j} = & [\psi_{3,j} \left(\frac{4}{10} - u_{2,j} \frac{h}{10}\right) + \psi_{2,j+1} \left(\frac{4}{10} - v_{2,j} \frac{h}{10}\right) \\
& + \psi_{2,j-1} \left(\frac{4}{10} + v_{2,j} \frac{h}{10}\right) \\
& + \psi_{3,j+1} \left(-\frac{1}{10} + u_{2,j} \frac{h}{40} + v_{2,j} \frac{h}{40}\right)
\end{aligned}$$



$$\begin{aligned}
& + \psi_{3,j-1} \left( -\frac{1}{10} + u_{2,j} \frac{h}{40} - v_{2,j} \frac{h}{40} \right) \\
& + \psi_{2,j-2} \left( -\frac{1}{20} - v_{2,j} \frac{h}{40} \right) \\
& + \psi_{4,j} \left( -\frac{1}{20} + u_{2,j} \frac{h}{40} \right) \\
& + \psi_{2,j+2} \left( -\frac{1}{20} + v_{2,j} \frac{h}{40} \right) \\
& - \frac{h^3}{120} \left( \frac{c^2}{r_c} \right) w_{2,j} \left( -w_{2,j+2} + 8w_{2,j+1} - 8w_{2,j-1} + w_{2,j-2} \right) / \\
& \left[ 1 - \frac{1}{20} - u_{2,j} \frac{h}{40} \right] \tag{3-10}
\end{aligned}$$

At the points  $i = M, j = 3, 4 \dots N + 1$ ,  $\psi_{M,j}$  is

$$\begin{aligned}
\psi_{M,j} = & [\psi_{M-1,j} \left( \frac{4}{10} + u_{M,j} \frac{h}{10} \right) + \psi_{M,j+1} \left( \frac{4}{10} - v_{M,j} \frac{h}{10} \right) \\
& + \psi_{M,j-1} \left( \frac{4}{10} + v_{M,j} \frac{h}{10} \right) \\
& + \psi_{M-1,j+1} \left( -\frac{1}{10} - u_{M,j} \frac{h}{40} + v_{M,j} \frac{h}{40} \right) \\
& + \psi_{M-1,j-1} \left( -\frac{1}{10} - u_{M,j} \frac{h}{40} - v_{M,j} \frac{h}{40} \right) \\
& + \psi_{M-2,j} \left( -\frac{1}{20} - u_{M,j} \frac{h}{40} \right)
\end{aligned}$$





$$\begin{aligned}
& + \psi_{M,j+2} \left( -\frac{1}{20} + v_{M,j} \frac{h}{40} \right) \\
& + \psi_{M,j-2} \left( -\frac{1}{20} - v_{M,j} \frac{h}{40} \right) \\
& - \frac{h^3}{120} \left( \frac{c^2}{r_c} \right) w_{M,j} \left( -w_{M,j+2} + 8w_{M,j+1} - 8w_{M,j-1} + w_{M,j-2} \right) ] / \\
& \left[ 1 - \frac{1}{20} + u_{M,j} \frac{h}{40} \right] \tag{3-11}
\end{aligned}$$

At the point  $i = 2, j = 2$ ,  $\psi_{2,2}$  is

$$\begin{aligned}
\psi_{2,2} = & [\psi_{3,2} \left( \frac{4}{10} - u_{2,2} \frac{h}{10} \right) + \psi_{2,3} \left( \frac{4}{10} - v_{2,2} \frac{h}{10} \right) \\
& + \psi_{3,3} \left( -\frac{1}{10} + u_{2,2} \frac{h}{40} + v_{2,2} \frac{h}{40} \right) \\
& + \psi_{4,2} \left( -\frac{1}{20} + u_{2,2} \frac{h}{40} \right) \\
& + \psi_{2,4} \left( -\frac{1}{20} + v_{2,2} \frac{h}{40} \right) \\
& - \left( \frac{h^3}{120} \right) \left( \frac{c^2}{r_c} \right) w_{2,2} (w_{2,5} - 6w_{2,4} + 18w_{2,3} - 10w_{2,2}) ] / \\
& \left[ 1 - \frac{1}{10} - u_{2,2} \frac{h}{40} - v_{2,2} \frac{h}{40} \right] \tag{3-12}
\end{aligned}$$

At the point  $i = M, j = 2$ ,  $\psi_{M,2}$  is



$$\begin{aligned}
\psi_{M,2} = & [\psi_{M-1,2} (\frac{4}{10} + u_{M,2} \frac{h}{10}) + \psi_{M,3} (\frac{4}{10} - v_{M,2} \frac{h}{10}) \\
& + \psi_{M-1,3} (-\frac{1}{10} - u_{i,j} \frac{h}{40} + v_{i,j} \frac{h}{40}) \\
& + \psi_{M-2,2} (-\frac{1}{20} - u_{i,j} \frac{h}{40}) \\
& + \psi_{M,4} (-\frac{1}{20} + v_{i,j} \frac{h}{40}) \\
& - (\frac{h^3}{120}) (\frac{c^2}{r_c}) w_{M,2} (w_{M,5} - 6w_{M,4} + 18w_{M,3} - 10w_{M,2}) / \\
& [1 - \frac{1}{10} + u_{M,2} \frac{h}{40} - v_{M,2} \frac{h}{40}]
\end{aligned} \tag{3-13}$$

At the points  $i = 3, 4 \dots M - 1$ ,  $j = 2$ ,  $\psi_{i,2}$  becomes

$$\begin{aligned}
\psi_{i,2} = & [\psi_{i+1,2} (\frac{4}{10} - u_{i,2} \frac{h}{10}) + \psi_{i,3} (\frac{4}{10} - v_{i,2} \frac{h}{10}) \\
& + \psi_{i-1,2} (\frac{4}{10} + u_{i,2} \frac{h}{10}) \\
& + \psi_{i+1,3} (-\frac{1}{10} + u_{i,2} \frac{h}{40} + v_{i,2} \frac{h}{40}) \\
& + \psi_{i-1,3} (-\frac{1}{10} - u_{i,2} \frac{h}{40} + v_{i,2} \frac{h}{40}) \\
& + \psi_{i-2,2} (-\frac{1}{20} - u_{i,2} \frac{h}{40}) \\
& + \psi_{i+2,2} (-\frac{1}{20} + u_{i,2} \frac{h}{40})
\end{aligned}$$



$$\begin{aligned}
& + \psi_{i,4} \left( -\frac{1}{20} + v_{i,2} \frac{h}{40} \right) \\
& - \left( \frac{h^3}{120} \right) \left( \frac{c^2}{r_c} \right) w_{i,2} (w_{i,5} - 6w_{i,4} + 18w_{i,3} - 10w_{i,2}) / \\
& \left[ 1 - \frac{1}{20} - v_{i,2} \frac{h}{40} \right]
\end{aligned} \tag{3-14}$$

It is noted that in the derivation of equations (3-10), (3-11), (3-12), (3-13) and (3-14) for equation (2-28) higher-order approximation is used for  $\partial w / \partial y$  as compared with the inertia terms.

The finite-difference approximations for the secondary flow velocity components  $u, v$  are:

At the points  $i = 2, 3 \dots M, j = 3, 4 \dots N + 1$

$$u_{i,j} = \frac{(\psi_{i,j-2} - 8\psi_{i,j-1} + 8\psi_{i,j+1} - \psi_{i,j+2})}{12h} \tag{3-15}$$

At the points  $i = 2, 3 \dots M, j = 2$

$$u_{i,2} = \frac{(\psi_{i,5} - 6\psi_{i,4} + 18\psi_{i,3} - 10\psi_{i,2})}{12h}$$

At the points  $i = 3, 4 \dots M - 1, j = 2, 3 \dots N + 1$

$$v_{i,j} = \frac{(\psi_{i+2,j} - 8\psi_{i+1,j} + 8\psi_{i-1,j} - \psi_{i-2,j})}{12h}$$

At the points  $i = 2, j = 2, 3 \dots N + 1$





$$v_{2,j} = \frac{(\psi_{5,j} - 6\psi_{4,j} + 18\psi_{3,j} - 10\psi_{2,j})}{-12h} \quad (3-16)$$

At the points  $i = M, j = 2, 3 \dots N + 1$

$$v_{M,j} = \frac{(\psi_{M-3,j} - 6\psi_{M-2,j} + 18\psi_{M-1,j} - 10\psi_{M,j})}{12h}$$

The finite-difference expressions for the boundary conditions (equation (2-31)) are:

(1) Along the lower horizontal surface,

$$i = 1, 2 \dots M + 1, j = 1$$

$$w_{i,1} = \theta_{i,1} = \psi_{i,j} = u_{i,1} = v_{i,1} = 0$$

(2) Along the horizontal center line,

$$i = 1, 2 \dots M + 1, j = N$$

$$w_{i,N} = w_{i,N+2}, \theta_{i,N} = \theta_{i,N+2},$$

$$\psi_{i,N} = -\psi_{i,N+2}, \psi_{i,N-1} = -\psi_{i,N+3}$$

(3-17)

$$\psi_{i,N+1} = v_{i,N+1} = 0$$

(3) Along the inner wall,

$$i = 1, j = 1, 2 \dots N + 1$$



$$w_{1,j} = \theta_{1,j} = \psi_{1,j} = u_{1,j} = v_{1,j} = 0$$

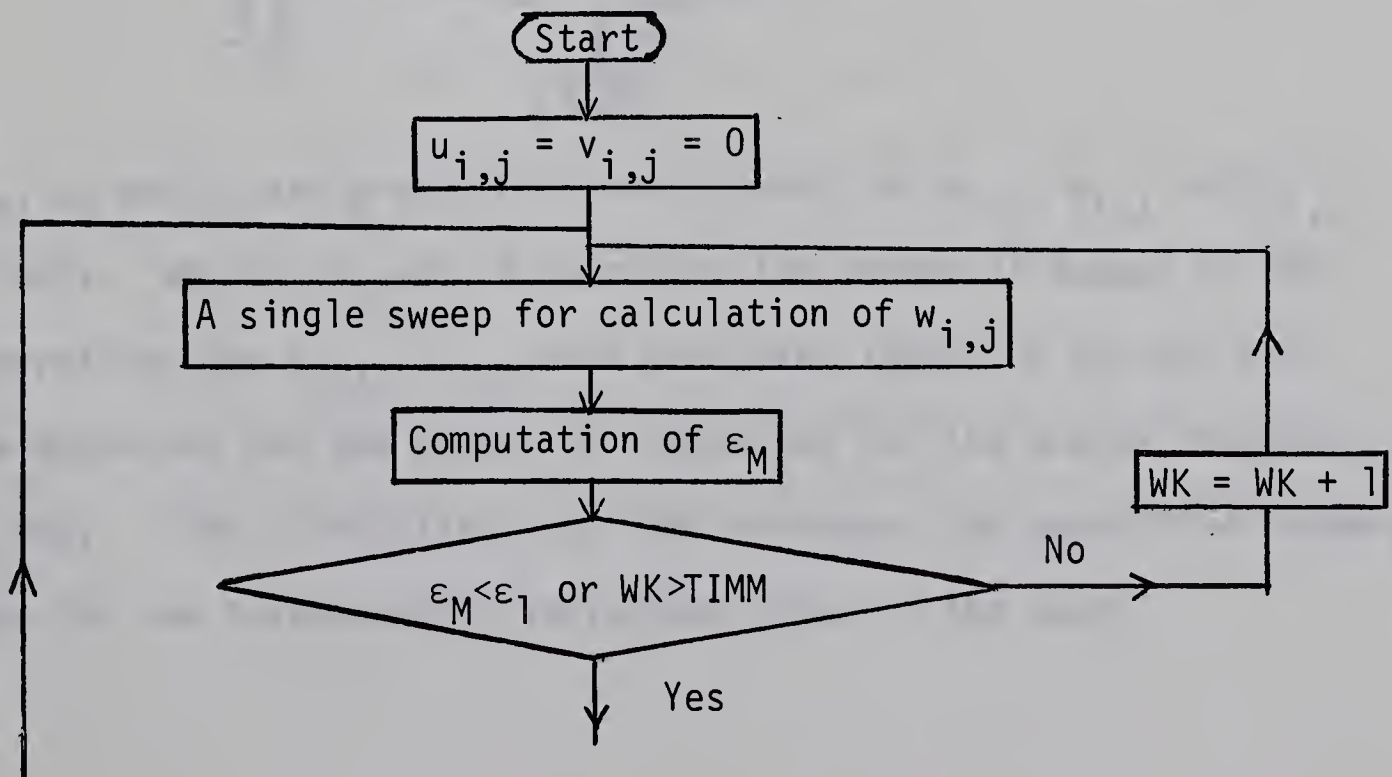
(4) Along the outer wall,

$$i = M + 1, j = 1, 2 \dots N + 1$$

$$w_{M+1,j} = \theta_{M+1,j} = \psi_{M+1,j} = u_{M+1,j} = v_{M+1,j} = 0$$

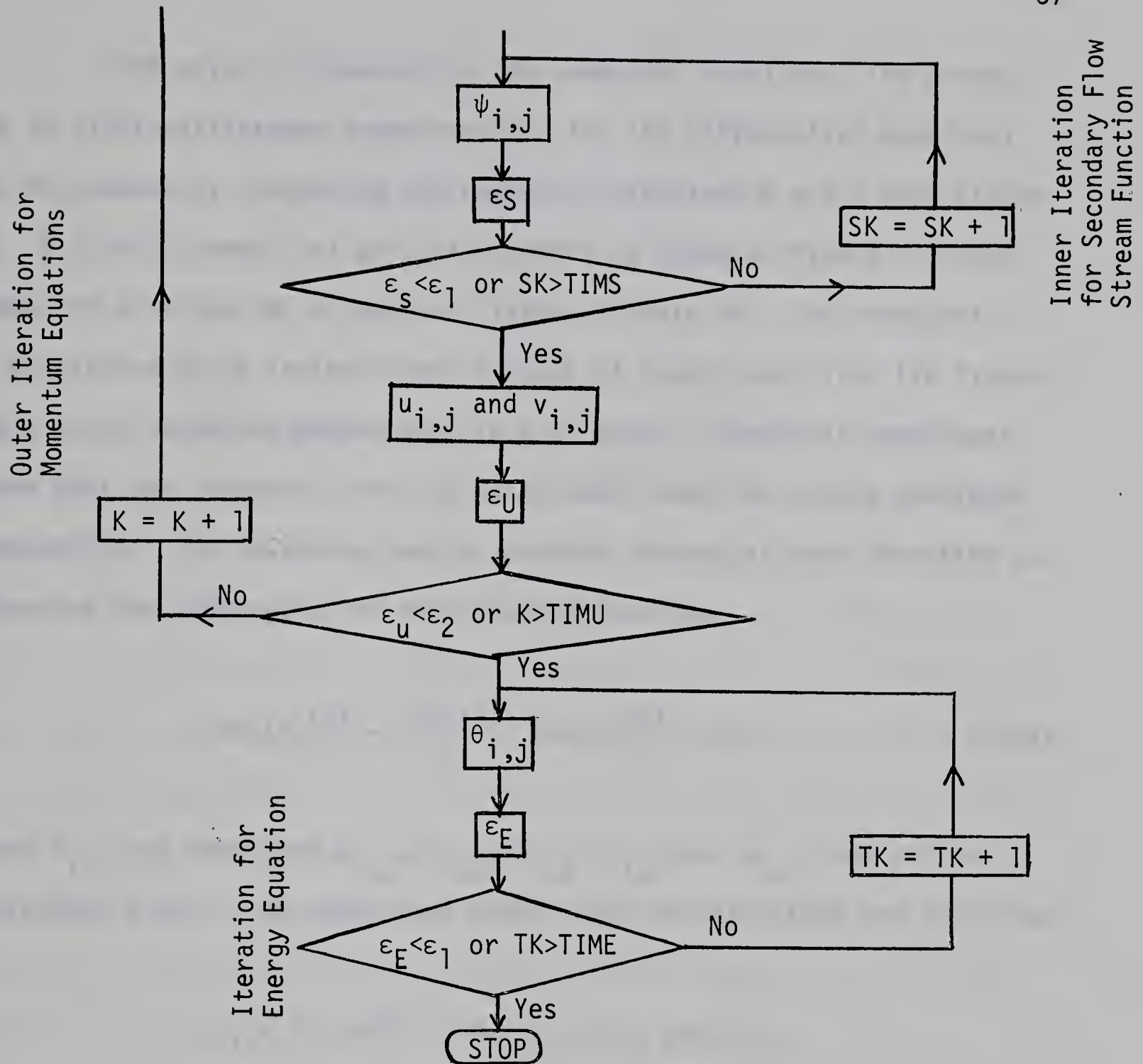
### 3.2 Iterative Method

Point successive-overrelaxation method [56] is used to solve a set of finite-difference equations (3-6), (3-9) and (3-7) and the boundary conditions. It is noted that the two momentum equations and the energy equation are not coupled. Consequently, the two momentum equations can be solved independently. The iterative procedure employed is similar to that used in references [51,53]. In order to show the procedure clearly, the schematic flow chart is presented below.



Inner Iteration  
for Axial Momentum  
Equation





where  $\epsilon_M$ ,  $\epsilon_S$  and  $\epsilon_E$  are prescribed error bounds for  $w_{i,j}$ ,  $\psi_{i,j}$  and  $\theta_{i,j}$ , respectively.  $WK$ ,  $SK$ ,  $K$ , and  $TK$  represent the number of sweeps of the inner iterations for  $w_{i,j}$ ,  $\psi_{i,j}$ , that for outer iteration for the two momentum equations and the number of iterations for the energy equation, respectively.  $TIMM$ ,  $TIMS$ ,  $TIMU$ , and  $TIME$  represent the prescribed numbers of sweeps for the corresponding iterations shown in the chart.





The error is inherent in the numerical solution. The errors due to finite-difference approximations for the differential equations can be reduced by increasing the number of divisions  $M$  and  $N$  (see Figure 1). A typical example of grid size effect is shown in Figure 2. The number of divisions  $M, N$  used are listed in Table 14. The round off is considered to be insignificant because of double precision (16 figures) and a point iterative method used in this study. Numerical experiment shows that the round-off error is quite small even for single precision computation. The following test is used at the end of each iteration to determine the convergence of the computed function.

$$\text{Max}|f_{i,j}^{(n)} - f_{i,j}^{(n-1)}| / \text{Max}|f_{i,j}^{(n)}| < \epsilon \quad (3-18)$$

where  $f_{i,j}$  may represent  $w_{i,j}, \psi_{i,j}, \theta_{i,j}, u_{i,j}$  and  $v_{i,j}$ , and  $\epsilon$  is a prescribed error. The prescribed errors used in this study are as follows.

$$\epsilon_1 = 1 \times 10^{-5} \quad \text{for } w_{i,j}, \psi_{i,j} \text{ and } \theta_{i,j}$$

$$\epsilon_2 = 5 \times 10^{-5} \quad \text{for } u_{i,j} \text{ and } v_{i,j}.$$

The above error bounds give sufficient accuracy up to a reasonably high Dean number. Specifically, the following combinations of error bounds are examined.

$$\epsilon_1 = 10^{-2}, 10^{-3}, 10^{-4}, 10^{-5}, 10^{-6}, 10^{-7}, \text{ and } 10^{-10}$$



$\epsilon_2 = 5 \times 10^{-2}, 5 \times 10^{-3}, 5 \times 10^{-4}, 5 \times 10^{-5}, 5 \times 10^{-6}, 5 \times 10^{-7}$  and  $10^{-10}$ .

Comparison of the flow and heat transfer results using  $\epsilon_1 = 1 \times 10^{-5}$ ,  $\epsilon_2 = 5 \times 10^{-5}$  and  $\epsilon_1 = 1 \times 10^{-6}$ ,  $\epsilon_2 = 5 \times 10^{-6}$ , respectively, shows that the difference in the numerical results is less than 0.03% even in high Dean number regime.

For the number of divisions,  $M, N$  used in this study (see Table 14), the flow and heat transfer results obtained by two different methods (see Section 4.1) converge to nearly the same numerical value with  $\epsilon_1 = 1 \times 10^{-5}$  and  $\epsilon_2 = 5 \times 10^{-5}$  as can be seen from Tables 2 and 14. For example, when  $\gamma = 1$ ,  $M = 32$ ,  $N = 16$  and  $c^2/r_c = 0$ , the flow and heat transfer results obtained by two different methods are off by only - 0.0083% and 0.0527% for flow and - 0.148% and 0.105% for heat transfer from the known exact values. Furthermore, when  $\gamma = 1$ ,  $M = 32$ ,  $N = 16$  and  $c^2/r_c = 1.0 \times 10^6$ , the flow and heat transfer results using two different methods are off by 0.220% and 0.222%, respectively. These examples confirm the accuracy of the numerical solutions.

The effect of grid size on computing time is shown in Figure 3. It is noted that this effect is significant and the number of divisions  $M, N$  used in this study are mainly dictated by the accuracy of the numerical results. A relation between an error bound and the computing time is also of considerable interest and is shown in Figure 4. It can be seen that the prescribed error used in this study is quite reasonable from the point of view of computing time.





For the given aspect ratio and the Prandtl number, the numerical solution starts with  $K = 0$  and proceeds gradually toward the high Dean number regime. The convergence of the iterative method is closely related to the suitable choice of relaxation factor but this problem will be considered in the next section. With the increase of the Dean number and maintaining the same prescribed errors, the numerical solution is convergent up to a reasonably high Dean number, for example, for a curved square channel; however, starting at a certain Dean number the flow pattern for the secondary flow changes from the regular two vortices to the four vortices with two additional small vortices located near the central part at the outer wall. The results of numerical experiment at high Dean number regime are shown in Figure 5 for the flow characteristics. The direction of the numerical solution for the flow is indicated by the arrow and the two numbers under the arrow represent the number of inner iterations for the axial momentum equation and the secondary flow stream function, respectively. One sees that a different combination of the number of inner iterations may lead to a different flow pattern. In Figure 5, two different flow patterns are signified by a circle (2 vortices) and a triangle (4 vortices), respectively. The results in Figure 5 seems to indicate the existence of a pair of solutions for a given Dean number in high Dean number regime. Because of uncertainties, the flow and heat transfer results for the Dean number range with this peculiar behavior will not be presented. The axial velocity and temperature profiles in the central region also indicates unusual behavior with the four





vortices for the secondary flow.

When the magnitude of the secondary velocity components exceeds  $2/h$ , the numerical results start oscillation for the solution with regular two vortices and finally the solution diverges. The above situation occurs at a certain high Dean number. One notes that the matrix is diagonally dominant when  $|u_{i,j}|$  or  $|v_{i,j}| \leq 2/h$ . On the other hand, the numerical solution with four vortices is still convergent even when the Dean number far exceeds the value indicated above for the flow pattern with two vortices. Eventually, the numerical solution with four vortices also diverges when the magnitude of the secondary velocity components  $(u,v)$  exceeds  $2/h$ .

Some example on the computing time required may be of interest. It takes about 138 minutes by IBM 360/67 to obtain a complete result up to  $c^2/r_c = 0.17 \times 10^6$  for flow and heat transfer with  $\gamma = 1$ ,  $M = 32$ ,  $N = 16$  and  $Pr = 0.71$ .

### 3.3 Point Successive-Overrelaxation Method

Since point iterative methods are well discussed elsewhere [47, 52, 55, 56, 57], the details of point successive-overrelaxation method will not be given here. To improve convergence in the process of iterations, a relaxation factor  $\omega$  is used. The value of the factor  $\omega$  usually lies between 1 and 2. A question naturally arises as to the optimum value of the factor  $\omega_{op}$  that will yield a maximum rate of convergence. Unfortunately, no general method is available for the evaluation of optimum relaxation factor for the elliptic-type partial differential equations having the non-linear terms encountered in the present



problem. However, for the low Dean number region, one would expect that the method described in [57] may be applicable.

In this study, the optimum relaxation factor  $\omega_{op}$  for linear system is used when the Dean number is zero or sufficiently small as shown in Table 14. By using  $\omega_{op} = 1.75 \sim 1.82$ , considerable computing time is saved. For the Dean number ranging from small to intermediate values, different relaxation factors for equations (3-6), (3-7) and (3-9) are used after considerable numerical experiments. For example, for a curved square channel, the relaxation factors used finally for the axial momentum equation, secondary flow stream function, and the energy equation,  $\omega_M$ ,  $\omega_S$  and  $\omega_E$ , respectively are as follows:

$c^2/r_c$	$\omega_M$	$\omega_S$	$\omega_E$
0			
0.6 x 10 <sup>5</sup> }	1.82	1.82	1.82
0.3 x 10 <sup>6</sup> }	1.60	1.60	1.60
0.5 x 10 <sup>6</sup> }	1.30	1.50	1.30
0.7 x 10 <sup>6</sup> }	1.10	1.40	1.10
0.13 x 10 <sup>7</sup> }	1.00	1.30	1.00
0.14 x 10 <sup>7</sup> }			
0.19 x 10 <sup>7</sup> }	1.00	1.00	1.00

One notes that at high Dean number region, the relaxation factor  $\omega = 1$  is found by trial and error to be the best value. The details of solving equation (3-1) and equation (3-8) by point successive-overrelaxation method is well discussed in reference [51].



## CHAPTER IV

### FLOW AND HEAT TRANSFER RESULTS

#### 4.1 Flow and Heat Transfer Characteristics

It is possible to obtain the expressions for the product of friction factor and Reynolds number,  $fRe$ , and the Nusselt number,  $Nu$ , by considering either the velocity and temperature gradients, respectively, along the channel boundary or the overall force and energy balances, respectively, for the axial length  $dZ$ .

##### (1) The Resistance Coefficient

Following the usual definition for the product of friction factor and Reynolds number, one obtains

$$\begin{aligned}(fRe) &= \frac{\bar{\tau}_W}{\frac{1}{2} \rho \bar{W}^2} \frac{D_e \bar{W}}{\nu} \\ &= \frac{2\bar{\tau}_W D_e}{\mu \bar{W}} .\end{aligned}\tag{4-1}$$

Considering the velocity gradient along the boundary, one obtains

$$\begin{aligned}\bar{\tau}_W &= \mu \left( \frac{\partial \bar{W}}{\partial n} \right)_W \\ &= \mu \frac{vc}{D_e^2} \frac{\int_S \frac{\partial w}{\partial n} dS}{S} .\end{aligned}\tag{4-2}$$







Substituting equation (4-2) into equation (4-1), one has

$$(fRe)_I = \frac{2(\frac{\partial \bar{w}}{\partial n})_W}{\bar{w}} \quad (4-3)$$

A force balance on a flow element with axial length  $dZ$  gives;

$$-\frac{\partial P_0}{\partial Z} A = \frac{\bar{\tau}_W}{S}$$

or

$$\begin{aligned} \bar{\tau}_W &= -\frac{\partial P_0}{\partial Z} \frac{A}{S} \\ &= \frac{C_1 D_e}{4} \end{aligned} \quad (4-4)$$

Consequently, one obtains

$$(fRe)_{II} = \frac{2}{\bar{w}} \quad (4-5)$$

## (2) Nusselt Number

The Nusselt number is defined by

$$Nu = \frac{\bar{h} D_e}{k} \quad (4-6)$$

where  $\bar{h}$  can be obtained in two ways. The heat flow rate through the



channel wall with axial length  $dZ$  is

$$\bar{h} T_M S dZ = - k \left| \left( \frac{\partial \bar{T}}{\partial n} \right)_W \right| S dZ$$

or

$$\bar{h} = - \frac{k \left| \left( \frac{\partial \bar{T}}{\partial n} \right)_W \right|}{T_M}$$

$$= - \frac{k c_2 \text{Pr} c}{T_M} \frac{\int_S \frac{\partial \theta}{\partial n} dS}{S} \quad (4-7)$$

where

$$T_M = \frac{\int_{-a/2}^{a/2} \int_0^{b/2} W(T - T_W) dXdY}{\int_{-a/2}^{a/2} \int_0^{b/2} W dXdY}$$

$$= (c_2 \text{Pr} D_e c) \left| \frac{(\overline{W\theta})}{\bar{W}} \right| .$$

Thus, the Nusselt number can be expressed as

$$(Nu)_I = \frac{\left| \left( \frac{\partial \theta}{\partial n} \right)_W \right| \bar{W}}{\left| (\overline{W\theta}) \right|} . \quad (4-8)$$

On the other hand, an energy balance of the bulk flow with axial length  $dZ$  yields,

$$\rho c_p \frac{\partial T}{\partial Z} \bar{W} A = \bar{h} T_M S$$



or

$$\begin{aligned}\bar{h} &= \rho c_p \frac{\partial T}{\partial Z} \bar{W} A / T_M S \\ &= \frac{\rho c_p c_2 D_e}{4} \frac{\bar{W}}{T_M} .\end{aligned}\quad (4-9)$$

Hence, one obtains

$$(Nu)_{II} = \frac{\bar{W}^2}{4 |(\bar{W}\theta)|} . \quad (4-10)$$

The single or double integrations required for the evaluation of the mean values are carried out by using Simpson's rule. For the evaluation of the first derivatives such as  $(\frac{\partial \bar{W}}{\partial n})_W$  and  $(\frac{\partial \theta}{\partial n})_W$ , five-point formula is found to be satisfactory. The foregoing two methods of evaluating  $(fRe)$  and  $Nu$  affords checking of the accuracy of the numerical results.

One notes that the parameter,  $K$ , defined by equation (2-19) can be rewritten as

$$K = \left(\frac{c}{r_c}\right)^{1/2} \bar{W} \quad (4-11)$$

and will be used in the following sections.

#### 4.2 The Effect of Dean Number on Velocity and Temperature Fields.

The order of magnitude analysis shows clearly that the important characteristic parameters for the flow and heat transfer characteristics





are Dean number and Prandtl number. In order to see the effect of Dean number on velocity and temperature fields, the dimensionless axial velocity and temperature profiles along the central horizontal axis  $Y = 0$  and the vertical axis  $X = 0$  are plotted for a curved square channel  $\gamma = 1$  with  $Pr = 0.73$  for several representative Dean numbers in Figures 6 and 7, respectively. Qualitatively, the effect of centrifugal force on the flow and temperature fields are similar to the effect of buoyancy force [51] for a given geometrical shape of channel and thermal boundary conditions at the wall. One can see clearly that the effect of the centrifugal force is to shift the location of the maximum value toward the outer wall and decrease the maximum value itself as the value of the Dean number  $K$  increases. It is also seen that when the pressure and temperature gradients in the axial direction are kept constant, the flow rate decreases and both the velocity and temperature profiles become flat in the central region of the channel as the Dean number increases. It is expected that the profiles for the velocity and temperature are similar.

Secondary flow streamlines and isothermals for a curved square channel are shown in Figure 8 for  $K = 51.9$  and  $Pr = 0.73$ . The location of the center of circulation is of interest since one can gain the general idea about the secondary flow pattern and the intensity of secondary flow. For a curved square channel, the  $X$ -coordinate of the center of circulation gradually moves from  $X/a = 0$  toward the outer wall as the Dean number increases and reaches about  $X/a = 0.1$  at  $K = 45$ . With further increase of the Dean number the center of circulation tends to move back toward the center  $X/a = 0$ . It is found that with Dean number at about 125 the



center of circulation returns to  $X/a = 0$ . On the other hand, with the increase of the Dean number the Y-coordinate of the center of circulation always moves toward the upper or lower wall indicating the increase of the intensity of secondary flow near the upper or lower wall.

The distributions of the secondary flow velocity components with the increase of the Dean number are also of considerable interest and these are shown in Figure 9. One also sees clearly the movement of the center of circulation following the broken lines with the increase of the Dean number in this figure. One notes that the intensity of the secondary flow increases as the value of the Dean number increases.

The location of the maximum velocity point for a curved square channel is also of interest. As the Dean number increases, the location of the maximum velocity gradually moves toward the outer wall. At  $K = 70$ , the maximum velocity is located at around  $X/a = .28$  and seems to remain there with further increase of the Dean number. One may add that the location of the maximum value of the temperature profile shows exactly the same trend with  $Pr = 0.73$ .

The distributions of velocity and temperature in Figures 6 and 7 suggest that boundary layer approximation is possible for both velocity and temperature fields when the Dean number is greater than say 70 or preferably 125 on the conservative side (see Figure 9). This observation is important since it confirms the applicability of the boundary layer approximation for the high Dean number region [43]. For the low Dean number region, the boundary layer approximation fails and the present numerical method is quite effective.





One can gain some insight into the flow pattern in a curved rectangular channel by considering the distribution of centrifugal forces and pressure in a cross-section. One notes that for a given radius of curvature, the centrifugal force is proportional to the square of the axial velocity at a given point and acting in a direction perpendicular to the main flow. Consequently the fluid in the central core region is subjected to a much larger centrifugal force than the region near the wall. Due to the centrifugal force, the fluid in the central core will be pushed toward the outer wall and pressure gradient arises throughout the cross-section. For a given  $Y$ -coordinate, the pressure is greatest at the outer wall and smallest at the inner wall. For a given  $X$ -coordinate to the right of the center of circulation, the pressure is greatest at  $Y = 0$  and decreases toward the upper or lower wall. By looking at the secondary flow streamlines, one can also see the distributions of pressure gradients throughout the cross-section. For example, the strong secondary flow toward the inner wall near the upper or lower wall is caused by large pressure drop. Whereas the outward flow in the core region is caused by centrifugal forces. It is well to note that the value of the dimensionless stream function at the center of circulation is proportional to the flow rate for the secondary motion. When the circulation in a cross-section is established, the main flow pattern will be distorted; due to the centrifugal force, the location of the maximum velocity will be moved toward the outer wall. For a given pressure drop in the axial direction, the volume flow rate de-





creases because of the secondary motion. Furthermore, the intensity of the secondary motion increases with the increase of the Dean number. The axial velocity distribution with the increase of the Dean number shown in Figure 6 can be understood readily by the above reasoning.

#### 4.3 The Effect of Aspect Ratio on Velocity and Temperature Fields

In order to see the effect of aspect ratio on flow and heat transfer characteristics, the aspect ratios  $\gamma = 2, 5, 0.5$  and  $0.2$  are considered in addition to a curved square channel  $\gamma = 1$ . The effect of the Dean number on velocity and temperature fields in a curved rectangular channel with various aspect ratios is generally similar to that for a curved square channel.

Consider a curved rectangular channel with long side horizontal first. Dimensionless axial velocity and temperature profiles along the central axes of the cross-section of the channel with  $\gamma = 2$  and  $Pr = 0.73$  are shown in Figures 10 and 11, respectively, for several representative Dean numbers. Nearly the same trend exists for  $\gamma = 2$  as for  $\gamma = 1$ . However, for a given value of Dean number the locations of the maximum velocity and the maximum value of the temperature profiles move closer to the outer vertical wall as compared with the case for  $\gamma = 1$ . This is due to the distribution of centrifugal forces. One notes that when the Dean number exceeds about  $K = 121.4$ , the temperature profile near the central region of the channel shows slight concave upward trend. Secondary streamlines and isothermals for  $\gamma = 2$ ,  $Pr = 0.73$  and  $K = 58.8$  are shown in Figure 12. One can see that the center of circulation is fairly close to



the outer wall and the secondary motion is very weak near the inner wall. This effect is also reflected in the isothermals. The distributions of the secondary velocity components ( $u,v$ ) are shown in Figure 13 with  $\gamma = 2$  for several Dean numbers. The loci of the center of circulation with the increase of the Dean number are also shown in the same figure. The increase of the intensity of secondary flow with the increase of the Dean number is quite evident.

For the case  $\gamma = 5$  and  $Pr = 0.73$ , graphical results for axial velocity and temperature profiles with  $K$  as a parameter, and secondary flow streamlines and isothermals for  $K = 88.1$  are shown in Figures 14 to 16. Once again one sees that secondary motion is quite strong near the outer wall and rather weak near the inner wall. This effect is again reflected in the isothermals. The locations of the maximum velocity and the maximum value of the temperature profile are much closer to the outer wall for  $\gamma = 5$  than  $\gamma = 2$  for the same Dean number.

The effect of the aspect ratio when the long side is vertical will be examined next. The velocity and temperature distributions with  $K$  as a parameter along the central axes of a curved rectangular channel with  $\gamma = 0.5$  and  $Pr = 0.73$  are shown in Figures 17 and 18, respectively. Secondary flow streamlines and isothermals for the aspect ratio  $\gamma = 0.5$ ,  $Pr = 0.73$  and  $K = 103.4$  are presented in Figure 19. The secondary flow patterns for several representative Dean numbers and the loci of the center of circulation are shown in Figure 20. One notes particularly that with the increase of the Dean number, the center of the circulation





tends to move toward the upper or lower horizontal wall; however, the center tends to move slightly toward the outer wall with the increase of the Dean number and after reaching about  $K = 70$ , tends to move toward the inner wall with further increase of the Dean number. It is expected that for the high Dean number regime, the intensity of the secondary flow will be quite strong near the upper or lower wall as compared with the central core region.

Similar graphical results for the case  $\gamma = 0.2$  are shown in Figures 21 to 23. For this case with the increase of the Dean number the center of circulation moves toward the upper or lower wall and intensive secondary flow exists only near the upper or lower wall. Consequently, for the low Dean number regime, secondary motion has less effect on the velocity and temperature distributions. Figure 23 shows that at  $K = 79.3$ , the center of the circulation is located quite close to the central vertical axis of the cross-section but slightly on the outer wall side. Although the Dean number is fairly high, the secondary flow is weak throughout the central region. It is not difficult to see the general trend for the velocity and temperature fields with further decrease of the aspect ratio, namely as  $\gamma \rightarrow 0$ . However, one notes that as  $\gamma \rightarrow 0$ , the problem leads to the instability problem discussed in reference [45].





#### 4.4 The Effect of Prandtl Number on Temperature Field

Observation of the equations of motion (2-28) and (2-29) shows that Prandtl number has no effect on the flow field. In order to understand the effect of Prandtl number on temperature field equations (2-29) and (2-30) will be rewritten as follows.

Axial Momentum Equation:

$$u \frac{\partial w}{\partial x} + v \frac{\partial w}{\partial y} = \nabla^2 w + 4$$

Energy Equation:

$$\text{Pr} \left( u \frac{\partial \theta}{\partial x} + v \frac{\partial \theta}{\partial y} \right) = \nabla^2 \theta - w$$

First, one notes immediately the similarity between the above two equations. In fact if  $\text{Pr} = 1$ , the axial velocity distribution is similar to the temperature distribution for a given Dean number. Furthermore, the effect of inertia terms in the axial momentum equation increases with the increase of the Dean number. Consequently, the effect of Prandtl number on the left-hand side of the energy equation is similar to the effect of Dean number on the left-hand side of the momentum equation. Noting the effect of the Dean number on the axial velocity distributions, one can immediately see the effect of Prandtl number on the temperature distributions. The effect of Prandtl number can be seen from Figures 24 to 26 where temperature distributions through the central axes of a curved square channel  $\gamma = 1$



with  $K$  as a parameter are shown for  $Pr = 0.1$ ,  $10^2$  and  $10^3$ , respectively. The Prandtl number effect explained above is clearly seen.

#### 4.5 Flow Resistance

The overall flow characteristics will be considered next. The ratio of the average velocity of a curved rectangular channel to that of a straight channel is plotted against Dean number for the aspect ratios  $\gamma = 0.2, 0.5, 1, 2$  and  $5$  in Figure 27. One sees that for a given axial pressure gradient, the effect of Dean number on average axial velocity is greatest for the curved square channel up to  $K \approx 100$ . One also notes that as the aspect ratio  $\gamma$  approaches zero or infinity, the Dean number effect decreases. One can see from the figure that the curves for  $\gamma = 1$  and  $2$  cross at about  $K = 100$  and similarly the curves for  $\gamma = 5$  and  $0.5$  also cross at some value of  $K$ .

The ratio of the products of friction factor and Reynolds number ( $fRe$ ) between a curved rectangular channel and a straight rectangular channel is plotted against Dean number in Figure 28 for the aspect ratios  $\gamma = 0.2, 0.5, 1, 2$  and  $5$ . Of course the product ( $fRe$ ) and the average velocity are related to each other as seen from equation (4-5). It is of interest to note that the aspect ratios  $\gamma = 0.5$  and  $2$  represent the same cross-sectional area. Similarly, the cross-sectional area is identical for the aspect ratios  $\gamma = 0.2$  and  $5$ . Comparison of the curves for  $\gamma = 2$  and  $0.5$  in Figure 28 shows that the Dean number effect is much stronger for a channel with larger aspect ratio after reaching a certain value of  $K$ . Similar remark applies for the cases  $\gamma = 5$  and  $0.2$  with the





same cross-sectional area. This fact may be of interest in design. When  $K$  is small, the centrifugal force effect is small and the inertia terms may be negligible as compared with the viscous terms; consequently, the way of placing long side horizontal or vertical has negligible effect on flow resistance. In contrast, for the high Dean number region, the effects of the centrifugal force term and the inertia terms are significant. The different effect of the aspect ratio with the same cross-sectional area may be explained from the distribution of the centrifugal forces for the high Dean number regime.

The results for the various aspect ratios presented in Figure 28 show that for the high Dean number regime, the value of  $(fRe)/(fRe)_0$  changes linearly with Dean number  $K$ ; consequently, one may write  $(fRe)/(fRe)_0 \propto K^m$  where  $m$  is a function of the aspect ratio. For example,

$$(fRe)/(fRe)_0 \approx 0.225 K^{0.39} \quad \text{for } \gamma = 1 \text{ and } 10^2 < K < 1.5 \times 10^3$$

Comparison of the result from the present analysis with the results available in the literature is of considerable interest and is shown in Figure 29. One can see that the present study covers the Dean number ranging from small to a reasonably high region where no other work is available in the literature. One numerical data at a quite high Dean number is also plotted in Figure 29 for comparison and shows a very good agreement with Ludwig's experimental data [38]. Mori and Uchida's analysis [43] using boundary layer approximation for the high Dean number





regime agrees well with Ludwig's experimental data up to a certain Dean number. Beyond that the experimental data by Ludwig are suspected to be in the turbulent region. The two curves given by Mori and Uchida represent the first and second approximations.

Observation of the result from the present numerical analysis and the results from Ludwig [38] and Mori and Uchida [43] shows clearly that a reasonable estimate can be made for the flow resistance with the Dean number ranging from 150 to 1000 where currently accurate analytical solution is not available.

#### 4.6 Heat Transfer

The overall heat transfer characteristics will be examined next. In order to see the effect of Dean number, the ratio of the average temperatures  $\bar{\theta}/(\bar{\theta})_0$  between a curved channel and a straight channel is plotted against  $K$  in Figure 30 for  $\gamma = 0.2, 0.5, 1, 2$  and  $5$  with  $Pr = 0.73$ . One notes that the Dean number effect is quite similar for  $\bar{\theta}/(\bar{\theta})_0$  as for  $\bar{w}/(\bar{w})_0$ .

In order to see the Prandtl number effect on  $\bar{\theta}/(\bar{\theta})_0$ ,  $\bar{\theta}/(\bar{\theta})_0$  is plotted against Dean number  $K$  for a curved square channel  $\gamma = 1$  in Figure 31 for  $Pr = 0.1, 0.73, 1, 10, 10^2$  and  $10^3$ . One can see that Prandtl number effect is considerable.

The graphical results for the ratio of the Nusselt number of a curved channel to that of a straight channel versus Dean number are shown in Figure 32 for the aspect ratios  $\gamma = 0.2, 0.5, 1, 2$  and  $5$  with  $Pr = 0.73$ . As can be expected, heat transfer result is similar to flow



resistance result discussed earlier. As noted earlier, the effect of Prandtl number on temperature field is considerable. This is also reflected in heat transfer result shown in Figure 33 where  $Nu/(Nu)_0$  is plotted against  $K$  for a curved square channel with  $Pr = 0, 0.1, 0.71, 0.73, 1, 10, 10^2, 10^3$  and  $10^4$ . The results in Figure 33 show clearly that an asymptotic line exists for the heat transfer result, too, in the high Dean number region with a given Prandtl number; consequently, in the high Dean number regime, the following expression may be used.

$$Nu/(Nu)_0 \approx 0.182 K^{1/2} Pr^{1/4} \quad \text{for } 1.0 \leq Pr \leq 10^4$$

$$\text{and } Nu/(Nu)_0 \geq 1.5$$

It is of interest to note that, for example, at  $Nu/(Nu)_0 = 1.6$  the distance between two neighboring curves decreases slightly as  $Pr$  increases by the same factor.

Again it is of considerable interest to compare the heat transfer result from the present analysis with the result from Mori and Uchida [43] for a curved square channel  $\gamma = 1$ . Mori and Uchida [43] show the first and second approximations for the ratio of Nusselt numbers for  $Pr = 0.71$  and  $\infty$ . The comparison of the heat transfer results is shown in Figure 34. A data from numerical solution at  $K = 460$  is also shown in the figure for comparison. Concentrating on the case  $Pr = 0.71$ , one sees that the present result is very reasonable up to a fairly high Dean number and suggests clearly that a reasonable estimate can be made for





the Dean number ranging from  $K = 150$  to  $1000$ . The estimated line is shown in Figure 34 as a broken line. One notes the asymptotic nature of the heat transfer result for the high Dean number regime.

Mori and Uchida's work [43] shows that an asymptotic value exists for the ratio  $Nu/(Nu)_0$  as  $Pr \rightarrow \infty$ ; however, this behavior of the effect of Prandtl number is difficult to comprehend in view of the energy equation (2-30). The numerical result for heat transfer from this study shows that an asymptotic line for  $Pr = \infty$  will not be reached at least up to the range ( $Pr = 10^4$ ) studied in this work. Furthermore, in reference [30] it is stated that the Nusselt number ratio approaches the asymptotic value with the increasing Prandtl number for a similar problem in curved pipes. Based on the result of this work, it appears that an asymptotic value does not exist at least up to  $Pr = 10^4$ . On the other hand, an asymptotic value does exist as  $Pr \rightarrow 0$ .

It is known that as the Dean number increases, the effect of the convective terms in the energy equation (2-30) increases for a given Prandtl number. As the Prandtl number increases, the effect of the convective terms also increases for a given Dean number. One can see that the Nusselt number increases with the increase of the Prandtl number even if the Dean number is held constant. The effect of the Prandtl number is equivalent to the effect of the Dean number. For example, at  $Nu/(Nu)_0 = 1.6$ , as the Prandtl number increases from  $10$  to  $10^3$ , the Dean number changes from  $K = 20$  to  $K = 2$ .

In addition to the graphical results shown above, the numerical





results are tabulated in Tables 1 to 15. One may be particularly interested in the numerical results based on two different methods of obtaining flow and heat transfer results discussed in Section 4.1. It can be seen from Tables 2 and 14 that the results from the two methods are off by only 0.4% at most for all the cases considered. This confirms the accuracy of the numerical solutions. The numerical values given in Tables 3 to 13 are obtained by using equations (4-3) and (4-8). Comparisons of equation (4-3) with equation (4-5) and equation (4-8) with equation (4-10) show that

$$\left(\frac{\partial \bar{w}}{\partial n}\right)_W = 1 \quad \text{and} \quad \left|\frac{\partial \theta}{\partial n}\right|_W = \frac{\bar{w}}{4}$$

The numerical results in Table 15 also confirms the accuracy of the numerical solutions.



## CHAPTER V

### CONCLUDING REMARKS

1. Numerical solution by point successive-overrelaxation is obtained for the fully developed laminar forced convection problem in curved rectangular channels with various aspect ratios under the thermal boundary conditions of constant heat flux per unit axial length with a uniform wall temperature for the conducting surfaces at each cross-section. The limitation of the numerical method is encountered at a reasonably high Dean number. The difficulty seems to come from the non-linear terms in the governing equations. In spite of this difficulty, the numerical method has definite advantage over the perturbation method.

2. Forced convection problems in rotating, bent, and heated horizontal tubes are known to be similar and characterized by the secondary flow acting in a cross-section normal to the main flow. Buoyancy force effects on forced-convection flow and heat transfer in horizontal rectangular channels with various aspect ratios are studied in references [51,52]. The aspect ratios considered in this study are identical to those in references [51,52] and the direct comparison is possible since the thermal boundary conditions are also identical. Comparison of the results shows that a striking similarity exists between the centrifugal force effect and the buoyancy force effect on the flow and heat transfer characteristics within the range studied by the references [51,52], namely,  $Pr = 0.71$  and  $7$ ,  $(fRe)/(fRe)_0 < 1.18$  and  $Nu/(Nu)_0 < 1.3$ . One is





impressed with this similarity in view of the fact that for the forced convection problem with buoyancy effect the momentum equations for the main flow and the secondary flow are coupled with the energy equation whereas for the forced convection problem in a curved channel, the two momentum equations and the energy equation are uncoupled. It is noted that the effect of the secondary flow caused by Coriolis force on forced convective heat transfer in a rotating channel is recently studied in reference [58].

3. By using  $\omega = 1$  for the relaxation factor at the high Dean number region and at the sacrifice of the computing time, the range of the numerical solution in terms of the ratios  $(fRe)/(fRe)_0$  and  $Nu/(Nu)_0$  is further extended beyond the range studied by the reference [51]. One may note that the range of the numerical solution in reference [51] may be extended by using the relaxation factor similar to the one employed in this study. The relaxation factor used in reference [51] is an optimum value based on linear system. For the low Dean number region, the relaxation factor,  $1.5 \sim < \omega < 1.82$ , based on linear equation may be used. For a curved rectangular channel with  $\gamma = 2$  the numerical solution is obtained up to the ratios  $(fRe)/(fRe)_0 = 1.8$  and  $Nu/(Nu)_0 = 2.2$ , respectively. One sees clearly that the range of applicability of the present numerical solution far exceeds that of the perturbation method [34].

4. The result of the present numerical analysis shows clearly that boundary-layer approximation around the wall for the high Dean





number regime is possible and it clarifies the assumption that at high Dean number a flow field may be divided into a core region occupying most of the cross-section where the viscous stress may be neglected and the boundary layer region adjacent to the wall where the viscous stress cannot be neglected. The numerical method is effective for the flow regime with Dean number ranging from small to a reasonably high value and complements the boundary layer technique [43].

5. Because of geometrical symmetry, two vortices with opposite sense are formed for the secondary flow. For a given aspect ratio of the curved rectangular channel, the intensity of secondary motion increases with the increase of the Dean number. The secondary motion is independent of the Prandtl number. For a given Prandtl number, the effects of Dean number on axial velocity and temperature profiles are similar as can be seen from the axial momentum equation and the energy equation. As the Dean number increases, the center of circulation always tends to move toward the upper or lower wall. The center of circulation gradually moves toward the outer wall with the increase of the Dean number and after reaching a certain Dean number tends to move toward the inner wall. The location of the center of circulation is of special interest since this gives some insight into the secondary flow pattern. For a given Dean number, the effect of aspect ratio is considerable. Even for the same cross-sectional area, the secondary flow pattern changes considerably depending on whether the long side is horizontal or vertical. This fact is of considerable interest in design.



The numerical results show an asymptotic nature for both  $(fRe)/(fRe)_0$  and  $Nu/(Nu)_0$  in the high Dean number regime.

6. The effect of Prandtl number on heat transfer result is significant. The role of the Prandtl number can be seen clearly from the energy equation. Considering the convective terms in the energy equation, one sees that the effect of the Prandtl number is equivalent to the effect of Dean number. It is pointed out in references [30,43] that the Nusselt number ratio  $Nu/(Nu)_0$  approaches the asymptotic value as the Prandtl number approaches infinity. In view of the above reasoning and the numerical results obtained in this study at high Prandtl number, it appears that the heat transfer results for  $Pr = \infty$  shown in references [30,43] are incorrect. In reference [30], the heat transfer results obtained from boundary-layer approximation for  $Pr = \infty$  are shown to agree with the experimental results obtained by Seban and McLaughlin [28] for  $Pr \approx 400$ . It is believed that the use of the analytical results for  $Pr = \infty$  presented in references [30,43] will lead to serious error in heat transfer prediction when  $Pr > 400$ . On the other hand, as  $Pr$  approaches zero, the heat transfer result approaches the asymptotic value as shown in Figures 33 and 34. One may note that the boundary-layer approximation cannot be used as  $Pr \rightarrow 0$ .

7. Comparison of the results from this analysis and the results available in the literature [38,43] for a curved square channel shows that a reasonable estimate can be made for the flow and heat transfer results for the Dean number ranging from 150 to 1000 where currently







accurate solutions are not available.

8. The order of magnitude analysis establishes the conditions under which the present analysis may apply. Specifically, it shows under what conditions the buoyancy force effect and the Coriolis force effect may be neglected for the forced convection problem in a curved rectangular channel.

9. The result of the present analysis confirms the known fact that the local heat transfer coefficient is higher at the outer wall of the curved channel than at the inner wall.



## REFERENCES

1. Reid, W.H., "On the Stability of Viscous Flow in a Curved Channel", Proceedings of Royal Society, Series A, No. 244, 1958, pp. 186-198.
2. Uchida, Y., "Studies on Forced Convective Heat Transfer with Secondary Flow in Channels", Ph.D. Thesis, Tokyo Institute of Technology, Tokyo, Japan, 1968.
3. Taylor, G.I., "Stability of a Viscous Liquid Contained Between Two Rotating Cylinders", Philosophical Trans. A, Vol. 233, 1923, pp. 289-343.
4. Ostrach, S., "Laminar Flow with Body Forces", in Theory of Laminar Flows, Moore, F.K. editor, Princeton University Press, Princeton, N.J., 1964, pp. 528-718.
5. Mori, M., Nakayama, W., and Uchida, Y., "Convective Heat Transfer in Ducts with Secondary Flow", Journal of the Japan Society of Mechanical Engineers, Vol. 70, No. 583, 1967, pp. 1188-1196.
6. Thomson, J., "On the Origin of Windings of Rivers in Alluvial Plains, with Remarks on the Flow of Water Round Bends in Pipes", Proceedings of Royal Society, Series A, Vol. 25, 1876, pp. 5-8.
7. Eustice, J., "Experiments on Stream-Line Motion in Curved Pipes", Proceedings of Royal Society, Series A, Vol. 85, 1911, pp. 119-131.
8. Eustice, J., "Flow of Fluids in Curved Passages", Engineering, Nov. 13, 1925, pp. 604-605.



9. White, C.M., "Streamline Flow Through Curved Pipes", Proceedings of Royal Society, Series A, Vol. 123, 1929, pp. 645-663.
10. Taylor, G.I., "The Criterion for Turbulence in Curved Pipes", Proceedings of Royal Society, Series A, Vol. 124, 1929, pp. 243-249.
11. Yarnell, D.L., and Nagler, F.A., "Flow of Water Around Bends in Pipes", Proceedings of the American Society of Civil Engineers, Vol. 60, 1934, pp. 783-797.
12. Dean, W.R., "Note on the Motion of Fluid in a Curved Pipe", Philosophical Magazine and Journal of Science, Series 7, Vol. 4, 1927, pp. 208-223.
13. Dean, W.R., "The Stream-Line Motion of Fluid in a Curved Pipe", Philosophical Magazine and Journal of Science, Series 7, Vol. 5, No. 30, 1928, pp. 673-695.
14. Adler, M., "Strömung in gekrümmten Rohren", Zeitschrift für angewandte Mathematik und Mechanik, Vol. 14, No. 4, 1934, pp. 257-275.
15. Barua, S.N., "On Secondary Flow in Stationary Curved Pipes", Quarterly Journal of Mechanics and Applied Mathematics, Vol. 16, Pt. 1, 1963, pp. 61-77.
16. Itō, H., "Friction Factors for Turbulent Flow in Curved Pipes", Journal of Basic Engineering, Transactions of the American Society of Mechanical Engineers, Series D, Vol. 81, 1959, pp. 123-134.





17. Itō, H., "Theory of Friction Resistance for Laminar Flow in Curved Pipes", Paper presented at the 45th General Meeting, Paper No. 832, The Japan Society of Mechanical Engineers, No. 194, ('68-4), 1968, pp. 121-124.
18. Weske, J.R., "Investigations of the Flow in Curved Ducts at Large Reynolds Numbers", Journal of Applied Mechanics, Trans. of ASME, Vol. 15, 1948, pp. 344-348.
19. Cuming, H.G., "The Secondary Flow in Curved Pipes", Aeronautical Research Council, Reports and Memoranda, No. 2880, Feb., 1952.
20. Topakoglu, H.C., "Steady Laminar Flows of an Incompressible Viscous Fluid in Curved Pipes", Journal of Mathematics and Mechanics, Vol. 16, No. 12, 1967, pp. 1321-1337.
21. Dean, W.R., and Hurst, J.M., "Note on the Motion of Fluid in a Curved Pipe", Mathematika, Vol. 6, 1959, pp. 77-85.
22. Hawthorne, W.R., "Secondary Circulation in Fluid Flow", Proceedings of Royal Society, Series A, Vol. 206, 1951, pp. 374-387.
23. Detra, R.W., "The Secondary Flow in Curved Pipes", Mitteilungen aus dem Institut für Aerodynamik, An der eidgenössischen technischen Hochschule in Zürich, Nr. 20, 1953.
24. McAdams, W.H., "Heat Transmission", 3rd Edition, McGraw-Hill Book Co., Inc., N.Y., 1954, p. 228.
25. Hawes, W.B., "Some Sidelights on the Heat Transfer Problem", Transactions of Institution of Chemical Engineers, London, Vol. 10, 1932, pp. 161-167.



26. Pratt, N.H., "The Heat Transfer in a Reaction Tank Cooled by Means of a Coil", Transactions of Institution of Chemical Engineers, Vol. 25, 1947, pp. 163-180.
27. Ede, A.J., "The Effect of a Right-Angled Bend on Heat Transfer in a Pipe", International Developments in Heat Transfer, 1961, pp. 634-642.
28. Seban, R.A., and McLaughlin, E.F., "Heat Transfer in Tube Coils with Laminar and Turbulent Flow", International Journal of Heat and Mass Transfer, Vol. 6, 1963, pp. 387-395.
29. Rogers, G.F.C., and Mayhew, Y.R., "Heat Transfer and Pressure Loss in Helically Coiled Tubes with Turbulent Flow", International Journal of Heat and Mass Transfer, Vol. 7, 1964, pp. 1207-1216.
30. Mori, Y., and Nakayama, W., "Study on Forced Convective Heat Transfer in Curved Pipes (1st Report, Laminar Region)", International Journal of Heat and Mass Transfer, Vol. 8, 1965, pp. 67-82.
31. Mori, Y., and Nakayama, W., "Study on Forced Convective Heat Transfer in Curved Pipes (2nd Report, Turbulent Region)", International Journal of Heat and Mass Transfer, Vol. 10, 1967, pp. 37-59.
32. Mori, Y., and Nakayama, W., "Study on Forced Convective Heat Transfer in Curved Pipes (3rd Report, Theoretical Analysis Under Condition of Uniform Wall Temperature and Practical Formulae)", International Journal of Heat and Mass Transfer, Vol. 10, 1967, pp. 681-695.







33. Kubair, V., and Kuloor, N.R., "Heat Transfer to Newtonian Fluids in Coiled Pipes in Laminar Flow", International Journal of Heat and Mass Transfer, Vol. 9, 1966, pp. 63-75.
34. Özisik, M.N., and Topakoglu, H.C., "Heat Transfer for Laminar Flow in a Curved Pipe", Journal of Heat Transfer, Transactions of the American Society of Mechanical Engineers, Series C, Vol. 90, 1968, pp. 313-318.
35. Clegg, D.B., and Power, G., "Flow of a Bingham Fluid in a Slightly Curved Tube", Applied Scientific Research, Section A, Vol. 12, 1963, pp. 199-212.
36. Jones, J.R., "Flow of a Non-Newtonian Liquid in a Curved Pipe", Quarterly Journal of Mechanics and Applied Mathematics, Vol. 13, 1960, pp. 428-443.
37. Itō, H., "Theory on Laminar Flows Through Curved Pipes of Elliptic and Rectangular Cross-Sections", The Reports of the Institute of High Speed Mechanics, Tōhoku University, Sendai, Japan, Vol. 1, 1951, pp. 1-16.
38. Ludwig, H., "Die ausgebildete Kanalströmung in einem rotierenden System", Ingenieur - Archiv Vol. 19, 1951, pp. 296-308.
39. Kapur, J.N., Tyagi, V.P. and Srivastava, R.C., "Streamline Flow Through a Curved Annulus", Applied Scientific Research, Section A, Vol. 14, 1964, pp. 253-267.
40. Eichenberger, H.P., "Secondary Flow Within a Bend", Journal of Mathematics and Physics, Vol. 32, 1953, pp. 34-42.



41. Wattendorf, F.L., "A Study of the Effect of Curvature on Fully Developed Turbulent Flow", Proceedings of Royal Society, Vol. 148, 1935, pp. 565-598.
42. Eskinazi, S., and Yeh, H., "An Investigation on Fully Developed Turbulent Flows in a Curved Channel", Journal of the Aeronautical Sciences, Vol. 23, 1956, pp. 23-34 and p. 75.
43. Mori, Y., and Uchida, Y., "Study on Forced Convective Heat Transfer in Curved Square Channel (1st Report, Theory of Laminar Region)", Transactions of Japan Society of Mechanical Engineers, Vol. 33, No. 255, 1967, pp. 1836-1846.
44. Kreith, F., "The Influence of Curvature on Heat Transfer to Incompressible Fluids", Transactions of the American Society of Mechanical Engineers, Vol. 77, 1955, pp. 1247-1256.
45. Mori, Y., and Uchida, Y., "Forced Convective Heat Transfer in a Curved Channel", JSME 1967 Semi-International Symposium, Heat and Mass Transfer, Thermal Stress, Vol. 1, pp. 181-190.
46. Ustimenko, B.P., Zhurgembaev, K.A. and Nusupbekova, D.A., "Calculation of Convective Heat Transfer for an Incompressible Liquid in Complex-Configuration Channels", Proceedings of the Second All-Soviet Union Conference on Heat and Mass Transfer, Vol. 1, 1966.
47. Churchill, S.W., "The Prediction of Natural Convection", Proceedings of the Third International Heat Transfer Conference, A.I.Ch.E., Vol. 6, 1966, pp. 15-30.





48. Wilkes, J.O., and Churchill, S.W., "The Finite-Difference Computation of Natural Convection in a Rectangular Enclosure", A.I.Ch.E. Journal, Vol. 12, No. 1, 1966, pp. 161-166.
49. Samuels, M.R., and Churchill, S.W., "Stability of a Fluid in a Rectangular Region Heated from Below", A.I.Ch.E. Journal, Vol. 13, No. 1, 1967, pp. 77-85.
50. Barakat, H.Z., and Clark, J.A., "Analytical and Experimental Study on the Transient Laminar Natural Convection Flows in Partially Filled Liquid Containers", Proceedings of the Third International Heat Transfer Conference, A.I.Ch.E., Vol. 2, 1966, pp. 152-162.
51. Hwang, Gwang-Jyh, "Numerical Solution for Combined Free and Forced Laminar Convection in Horizontal Rectangular Channels", M.Sc. thesis, Department of Mechanical Engineering, University of Alberta, April, 1968.
52. Cheng, K.C., and Hwang, Guang-Jyh, "Numerical Solution for Combined Free and Forced Laminar Convection in Horizontal Rectangular Channels", to be published in Journal of Heat Transfer, Transactions of the American Society of Mechanical Engineers, 1969.
53. DeVahl, Davis G., "Laminar Natural Convection in an Enclosed Rectangular Cavity", International Journal of Heat and Mass Transfer, Vol. 11, 1968, pp. 1675-1693.
54. Forsythe, G.E., and Wasow, W.R., "Finite-Difference Methods for Partial Differential Equations", John Wiley & Sons, Inc., N.Y., 1967.





55. Takada, M., "Finite-Difference Methods for Boundary Value Problems in Differential Equations", Journal of Japan Society of Mechanical Engineers, Vol. 71, No. 594, 1968, pp. 927-939.
56. Varga, R.S., "Matrix Iterative Analysis", Prentice-Hall Inc., Englewood Cliffs, New Jersey, 1965.
57. Young, D., "The Numerical Solution of Elliptic and Parabolic Partial Differential Equations", in Survey of Numerical Analysis, Todd, J., editor, McGraw-Hill Book Company, Inc., New York, N.Y., 1962, pp. 380-438.
58. Mori, Y., Uchida, Y., and Cheng, K.C., "Forced Convective Heat Transfer in a Rotating Channel. (Effect of the secondary flow caused by Coriolis force)", Dept. of Mechanical Engineering, Univ. of Alberta, 1969, unpublished.



## APPENDIX

## FORTRAN PROGRAM

---

A '\*' IN COL. 6 INDICATES THAT THIS  
LINE IS A PART OF THE PREVIOUS CARD

---

```

      DOUBLE PRECISION      ERR,FM,FN,H,H2,H4,H3,H4,H6,H8,H9
*      ,H24,H72,
      1W(81,43),T(81,43),S(81,43),U(81,43),V(81,43),
      2GAMMA,PR,CON,DI,REF,WM,TM,TW,FRE,TB,NU,ER1,VTEST,COW2J
*      ,COWMJ,
      3WA,WN,WD,WER,TA,TN,TD,HA,TER,RCT,SA,SN,SER,VN,UN,UD,VD
*      ,
      4SH(81,43),TG(81,43),SUM,SUT,SUM1,SUT1,SHM,TGM,HB,VER,S
*      D,
      5B1,B2,B3,B4,B5,B6,B7,B8,B9,B10,B11,B12,B13,DK,RC,NUE,F
*      REM,
      6W1,W2,W3,U1,U2,U3,U4,U5,V1,V2,V3,V4,V5, OMEM,OMES,OMEE
*      ,
      7H10,H23,H40,H80,H120,H144,H240,H144C,B40,B80
      INTEGER TIMM,TIMS,TIMU,TIME,WK,TK,SK
      COMMON M1,N3
C      M IS THE NUMBER OF DIVISIONS IN THE X DIRECTION BETWEE
*      N 0 AND A.
C      N IS THE NUMBER OF DIVISIONS IN THE Y DIRECTION BETWEE
*      N 0 AND B12.
C      GAMMA IS THE ASPECT RATIO OF A RECTANGULAR CHANNEL
C      OMEM,OMES AND OMEE ARE THE RELAXATION FACTORS
C      FOR Z_MOMENTUM,STREAM FUNCTION AND THE ENERGY EQUATION,
C      RESPECTIVLY.
C      ERR IS THE PRESCRIBED ALLOWABLE ERROR
C      TIMM, TIMS, TIMU AND TIME ARE THE PRESCRIBED
C      NUMBERS OF SWEEPS FOR Z_MOMENTUM, STREAM FUNCTION,
C      THE VELOCITY COMPONENTS OF THE SECONDARY FLOW AND THE
C      ENERGY EQUATION, RESPECTIVELY.
      READ(5,45) M,N,OMEM,OMES,OMEE,ERR,TIMM,TIMS,TIMU,TIME
      M1=M+1
      M1=M-1

```





```

      MJ=M-2
      MK=M-3
      N1=N+1
      N2=N+2
      N3=N+3
      NI=N-1
      FM=DBLE(FLOAT(M))
      FN=DBLE(FLOAT(N))
C      U,V AND W ARE THE DIMENSIONLESS VELOCITY COMPORNENTS I
*      N THE X, Y A
C      Z DIRECTIONS.
C      T IS THE DIMENSIONLESS TEMPERATURE
C      S IS THE STREAM FUNCTION
C      I AND J ARE THE SPACE SUBSCRIPTS OF GRID POINTS IN THE
C      X AND Y DIRECTIONS.
      DO 1 I=1,M1
      DO 1 J=1,N3
      W(I,J)=0D0
      T(I,J)=0D0
      S(I,J)=0D0
      U(I,J)=0D0
1     V(I,J)=0D0
      CALL DATA (W,T,S,U,V)
555  CONTINUE
C      K IS THE NUMBER OF SWEEPS OF U AND V.
C      PR IS THE PRANDTL NUMBER.
C      CON IS THE RATIO OF THE SQUARE OF PRESSURE GADIENT,C,
*      TO
C      THE RADIOUS OF THE CURVETURE,RC.
C      OF CURVETURE,RC.
C      H IS THE DIMENSIONLESS GRID SPACING IN THE X AND Y DIP
*      ECTIONS.
      K=1
      READ(5,46) GAMMA,PR,CON
      IF(GAMMA) 600,1000,600
600  B1=4D-1
      B2=1D-1
      B3=-B2
      B5=-5D-2
      B40=25D-3
      B80=5D-1*B40
      H=(GAMMA+1D0)/(2D0*FM)
      H2=H*H
      H3=H**3D0
      H4=H2*25D-2
      H8=H/8D0
      H10=H*B2
      H23=H3*2D-1/3D0
      H40=H*B40
      H120=H3/12D1
      WRITE(6,49) M,N, ERR,GAMMA,PR,CON
C
C

```



```

C
C   ITERATION PROCEDURE
C
C
C   THE START OF ITERATIONS
C   WK IS THE NUMBER OF SWEEPS OF MOMENTUM EQUATION FOR CO
*   MPUTATION OF
C   VELOCITY PROFILE WITH RESPECT TO THE AXIAL,Z,DIRECTION
*   .
24 WK=1
   WRITE(6,64)
7   DI=0D0
   REF=0D0
   DO 4 I=2,M
     II=I+1
     II=I-1
     DO 4 J=2,N1
       JI=J+1
       JI=J-1
       U1=U(I,J)*H8
       V1=V(I,J)*H8
C   THE VELOCITY WITH RESPECT TO THE AXIAL DIRECTION, WA,
*   IS
       WA=W(II,J)*(25D-2-U1)+W(II,J)*(25D-2+U1)
1       +W(I,J1)*(25D-2-V1)+W(I,J1)*(25D-2+V1)
1       +H2
       WN=OMEM*(WA-W(I,J))+W(I,J)
       IF(J.LT.N.OR.J.GT.N) GO TO 5
       W(I,N2)=WN
5   WD=DABS(WN-W(I,J))
C   DI IS THE MAXIMUM DIFFERENCE BETWEEN THE VALUE JUST OB
*   TAINED AND P
C   VALUE
   DI=DMAX1(DI,WD)
C   REF IS THE MAXIMUM ABSOLUTE VALUE
   REF=DMAX1(REF,WN)
4   W(I,J)=WN
   WER=DI/REF
   WRITE(6,51) WK,WER,OMEM
   IF(WER.LE.ERR.OR.WK.GE.TIMM) GO TO 6
   WK=WK+1
   GO TO 7
6   CONTINUE
C   SK IS THE NUMBER OF SWEEPS OF THE VORTICITY ( STREAM F
*   UNCTION )
C   EQUATION USING THE OBTAINED W TO COMPUTE STREAM FUNCTI
*   ON
   SK=1
   WRITE(6,65)
16  DI=0D0
   REF=0D0
   DO 12 I=3,MI

```





```

I1=I+1
I2=I+2
II=I-1
IJ=I-2
DO 12 J=3,N
J1=J+1
J2=J+2
JI=J-1
JJ=J-2
W2=H23*CON*W(I,J)
W3=H120*CON*W(I,J)
COW=W2*(W(I,J1)-W(I,JI))-W3*(W(I,J2)-W(I,JJ))
U3=U(I,J)*H10
U4=U(I,J)*H40
V3=V(I,J)*H10
V4=V(I,J)*H40
SA=S(I1,J)*(B1-U3)+S(I,J1)*(B1-V3)+S(II,J)*(B1+U3)
1 +S(I,JI)*(B1+V3)+S(I1,J1)*(B3+U4+V4)+S(II,J1)*(B3+V
* 4-U4)
2 +S(II,J1)*(B3-U4-V4)+S(I1,JI)*(B3+U4-V4)+S(I,JJ)*(B
* 5-V4)
3 +S(IJ,J)*(B5-U4)+S(I2,J)*(B5+U4)+S(I,J2)*(B5+V4)-CO
* W
SN=OMES*(SA-S(I,J))+S(I,J)
IF(J.LT.NI.OR.J.GT.N) GO TO 14
IF(J.EQ.NI) GO TO 25
S(I,N2)=-SN
GO TO 14
25 S(I,N3)=-SN
14 SD=DABS(SN-S(I,J))
DI=DMAX1(DI,SD)
HA=DABS(SN)
REF=DMAX1(REF,HA)
12 S(I,J)=SN
SER=DI/REF
WRITE(6,81) SK,SER,OMES
IF(SER.LE.ERR.OR.SK.GE.TIMS) GO TO 15
SK=SK+1
DO 27 J=3,N
S(2,J)=(S(3,J)*(B1-U3)+S(2,J1)*(B1-V3)
1 +S(2,JI)*(B1+V3)+S(3,J1)*(B3+U4+V4)+S(3,JI)*(B3
* +U4-V4)
2 +S(2,JJ)*(B5-V4)+S(4,J)*(B5+U4)+S(2,J2)*(B5+V4)
3 -COW)/(100+B5-U4)
27 S(M,J)=(S(M,J1)*(B1-V3)+S(MI,J)*(B1+U3)+S(M,JI)*(B1+V3
* )
1 +S(MI,J1)*(B3+V4-U4)+S(MI,JI)*(B3-U4-V4)+S(M,JJ
* )*(B5-V4)
2 +S(MJ,J)*(B5-U4)+S(M,J2)*(B5+V4)
3 -COW)/(100+B5+U4)
DO 28 I=3,MI
COWI2=CON*W(I,2)*H120*(W(I,5)-6D0*W(I,4)+18D0*
1 W(I,3)-10D0*W(I,2))

```





```

      COWI2=CON*W(I,2)*(H80*W(I,3)-H240*W(I,4)
1      -H144*W(I,2)+H1440*W(I,5))
28 S(I,2)=(S(I1,2)*(B1-U3)+S(I,3)*(B1-V3)+S(I1,2)*(B1+U3)
1      +S(I1,3)*(B3+U4+V4)+S(I1,3)*(B3+V4-U4)+S(IJ,2)*
*      (B5-U4)
2      +S(I2,2)*(B5+U4)+S(I,4)*(B5+V4)
3      -COWI2)/(1D0+B5-V4)
      S(2,2)=(S(3,2)*(B1-U3)+S(2,3)*(B1-V3)+S(3,3)*(B3+U4+V4
*      )
1      +S(4,2)*(B5+U4)+S(2,4)*(B5+V4)
2      -COWI2)/(1D0+2D0*B5-U4-V4)
      S(M,2)=(S(M,3)*(B1-V3)+S(MI,2)*(B1+U3)+S(MI,3)*(B3+V4-
*      U4)
1      +S(MJ,2)*(B5-U4)+S(M,J)*(B5+V4)
2      -COWI2)/(1D0+2D0*B5+U4-V4)
      GO TO 16
15 CONTINUE
C USING STREAM FUNCTION TO FIND U AND V
  WRITE(6,66)
  DI=0D0
  REF=0D0
  DO 17 J=2,N1
    J1=J+1
    J2=J+2
    JI=J-1
    JJ=J-2
    DO 17 I=2,M
      I1=I+1
      I2=I+2
      II=I-1
      IJ=I-2
      IF(J.EQ.2) GO TO 18
      UN=(S(I,JJ)-8D0*S(I,JI)+8D0*S(I,J1)-S(I,J2))/(12D0*H)
      GO TO 19
18 UN=(S(I,5)-6D0*S(I,4)+18D0*S(I,3)-10D0*S(I,2))/(12D0*H
*      )
19 IF(I.EQ.2) GO TO 20
   IF(I.EQ.M) GO TO 21
   VN=(S(I2,J)-8D0*S(I1,J)+8D0*S(II,J)-S(IJ,J))/(12D0*H)
   GO TO 22
20 VN=(S(5,J)-6D0*S(4,J)+18D0*S(3,J)-10D0*S(2,J))/(-12D0*
*      H)
   GO TO 22
21 VN=(S(MK,J)-6D0*S(MJ,J)+18D0*S(MI,J)-10D0*S(M,J))/(12D
*      0*H)
22 VD=DABS(VN-V(I,J))
   UD=DABS(UN-U(I,J))
   DI=DMAX1(DI,UD,VD)
   HA=DABS(UN)
   HB=DABS(VN)
   REF=DMAX1(REF,HA,HB)
   U(I,J)=UN
17 V(I,J)=VN

```



```

VER=DI/REF
WRITE(6,82) K,VER
IF(VER.GE.VTEST.AND.VER.GE.5D-2.AND.K.GE.500) CALL EXI
*   T
VTEST=VER
ER1=ERR*2D0
IF(VER.LE.ER1.OR.K.GE.TIMU) GO TO 23
K=K+1
GO TO 24
23 CONTINUE
C   THE TEMPERATURE PROFILE,T,( THE ENERGY EQUATION )
C   USING THE OBTAINED W AND U,V
TK=1
WRITE(6,67)
11 DI=0D0
REF=0D0
DO 8 I=2,M
  I1=I+1
  I1=I-1
  DO 8 J=2,N1
    J1=J+1
    J1=J-1
    W1=H4*W(I,J)
    U2=U(I,J)*H8*PR
    V2=V(I,J)*H8*PR
    TA=T(I1,J)*(25D-2-U2 )+T(I1,J)*(25D-2+U2 )
    1  +T(I,J1)*(25D-2-V2 )+T(I,J1)*(25D-2+V2 )
    1  -W1
    TN=OMEE*(TA-T(I,J))+T(I,J)
    IF(J.LT.N.OR.J.GT.N) GO TO 9
    T(I,N2)=TN
9  TD=DABS(TN-T(I,J))
  DI=DMAX1(DI,TD)
  HA=DABS(TN)
  REF=DMAX1(REF,HA)
8  T(I,J)=TN
  TER=DI/REF
  WRITE(6,80) TK,TER,OMEE
  IF(TER.LE.ERR.OR.TK.GE.TIME) GO TO 10
  TK=TK+1
  GO TO 11
10 CONTINUE
  WRITE(6,49) M,N,      ERR,GAMMA,PR,CON
  WRITE(6,50)
  WRITE (6,51) WK,WER,OMEM
  WRITE (6,52) ((W(I,J),I=2,M1),J=2,N1)
  WRITE (6,53)
  WRITE(6,80) TK,TER,OMEE
  WRITE(6,52)((T(I,J),I=2,M1),J=2,N1)
  WRITE(6,55)
  WRITE(6,81) SK,SER,OMES
  WRITE(6,52)((S(I,J),I=2,M1),J=2,N1)
  WRITE(6,54)

```







```

WRITE(6,82) K,VER
WRITE(6,52)((U(I,J),I=2,M1),J=2,N1)
WRITE(6,70)
WRITE(6,52)((V(I,J),I=2,M1),J=2,N1)

```

```

C
C
C THE END OF ITERATIONS
C
C
C

```

```

C CALCULATION OF FLOW AND HEAT TRANSFER
C
C

```

```

C WM IS MEAN VELOCITY

```

```

C TM IS THE MEAN TEMP.

```

```

C BT IS THE MIXED MEAN TEMP.

```

```

C TO CALCULATE MEAN, MEAN TEMP., MIXED MEAN TEMP., MEAN S

```

```

* HEAR

```

```

C STRESS AND MEAN TEMP. GRADIENT BY APPLYING SIMPSON RUL

```

```

* E

```

```

42 WM=0D0

```

```

TM=0D0

```

```

TW=0D0

```

```

DO 34 I=2,M,2

```

```

WM=WM+2D0*W(I,N1)

```

```

TM=TM+2D0*T(I,N1)

```

```

34 TW=TW+2D0*W(I,N1)*T(I,N1)

```

```

DO 35 I=3,M1,2

```

```

WM=WM+W(I,N1)

```

```

TM=TM+T(I,N1)

```

```

35 TW=TW+W(I,N1)*T(I,N1)

```

```

DO 36 J=2,N,2

```

```

DO 37 I=2,M,2

```

```

WM=WM+W(I,J)*8D0

```

```

TM=TM+T(I,J)*8D0

```

```

37 TW=TW+W(I,J)*T(I,J)*8D0

```

```

DO 36 I=3,M1,2

```

```

WM=WM+W(I,J)*4D0

```

```

TM=TM+T(I,J)*4D0

```

```

36 TW=TW+W(I,J)*T(I,J)*4D0

```

```

DO 38 J=3,N1,2

```

```

DO 39 I=2,M,2

```

```

WM=WM+W(I,J)*4D0

```

```

TM=TM+T(I,J)*4D0

```

```

39 TW=TW+W(I,J)*T(I,J)*4D0

```

```

DO 38 I=3,M1,2

```

```

WM=WM+W(I,J)*2D0

```

```

TM=TM+T(I,J)*2D0

```

```

38 TW=TW+W(I,J)*T(I,J)*2D0

```

```

WM=WM*2D0/(9D0*FM*FN)

```



```

TM=TM*2D0/(9D0*FM*FN)
TW=TW*2D0/(9D0*FM*FN)
WRITE(6,56)
WRITE(6,68)
DO 500 J=1,N1
  SH(1,J)=(4D0*W(2,J)-3D0*W(3,J)+4D0*W(4,J)/3D0
1      -W(5,J)/4D0)/H
  TG(1,J)=(4D0*T(2,J)-3D0*T(3,J)+4D0*T(4,J)/3D0
1      -T(5,J)/4D0)/H
  SH(M1,J)=(4D0*W(M,J)-3D0*W(MI,J)+4D0*W(MJ,J)/3D0
1      -W(MK,J)/4D0)/H
  TG(M1,J)=(4D0*T(M,J)-3D0*T(MI,J)+4D0*T(MJ,J)/3D0
1      -T(MK,J)/4D0)/H
500 CONTINUE
DO 501 I=1,M1
  SH(I,1)=(4D0*W(I,2)-3D0*W(I,3)+4D0*W(I,4)/3D0
1      -W(I,5)/4D0)/H
  TG(I,1)=(4D0*T(I,2)-3D0*T(I,3)+4D0*T(I,4)/3D0
1      -T(I,5)/4D0)/H
501 CONTINUE
103 DO 104 J=1,N1
  WRITE(6,57) J,SH(1,J),SH(M1,J),TG(1,J),TG(M1,J)
104 CONTINUE
  WRITE(6,58)
  WRITE(6,69)
  DO 105 I=1,M1
  WRITE(6,59) I,SH(I,1),TG(I,1)
105 CONTINUE
  SHM=SH(1,1)+SH(M1,1)+SH(1,N1)+SH(M1,N1)
  TGM=TG(1,1)+TG(M1,1)+TG(1,N1)+TG(M1,N1)
  SUM=0D0
  SUT=0D0
  DO 30 J=2,N,2
  SUM=SUM+SH(1,J)+SH(M1,J)
  SUT=SUT+TG(1,J)+TG(M1,J)
30 CONTINUE
  SHM=SHM+4D0*SUM
  TGM=TGM+4D0*SUT
  SUM=0D0
  SUT=0D0
  DO 31 J=3,N1,2
  SUM=SUM+SH(1,J)+SH(M1,J)
  SUT=SUT+TG(1,J)+TG(M1,J)
31 CONTINUE
  SHM=(SHM+2D0*SUM)*H
  TGM=(TGM+2D0*SUT)*H
  SUM=0D0
  SUT=0D0
  DO 32 I=2,M,2
  SUM=SUM+SH(I,1)
  SUT=SUT+TG(I,1)
32 CONTINUE
  SHM=SHM+SUM*4D0*H

```





```

TGM=TGM+SUT*4D0*H
SUM=0D0
SUT=0D0
DO 33 I=3,MI,2
SUM=SUM+SH(I,1)
SUT=SUT+TG(I,1)
33 CONTINUE
SHM=(SHM+2D0*H*SUM)*2D0*GAMMA/(3D0*(GAMMA+1D0)**2)
TGM=(TGM+2D0*H*SUT)*2D0*GAMMA/(3D0*(GAMMA+1D0)**2)
C FRE IS THE PRODUCT OF FRICTION FACTOR AND REYIVOLDS NO
* .
C NU IS THE NUSSELT NO.
DK=CON**5D-1*WM
TB=PR*TW/WM
FRE=2D0*SHM/WM
FREM=2D0/WM
NU=WM*TGM/TW
NUE=WM**2/(4*TW)
WRITE(6,60) SHM,TGM,WM,TM,TW,TB
WRITE(6,61) FRE,FREM,NU,NUE,DK
CALL PRINT(W,T,S,U,V)
GO TO 555
45 FORMAT(3X,I2,2X,I3,4D10.3,4I5)
46 FORMAT(5X,D25.16,2D10.3)
49 FORMAT('1'3X,2HM=,I2,3X,2HN=,I2,5X,4HERR=,D10.3,
15X,6HGAMMA=,D15.4,5X,3HPR=,D10.3,5X,4HCON=,D10.3)
50 FORMAT('0'10X,17HMOMENTUM EQUATION)
51 FORMAT(10X,6HSWEEP=,I3,10X,7HMAXERR=,D13.6,10X,5HOMEM=
* ,D13.6)
52 FORMAT(1X,8D13.5)
53 FORMAT('0'10X,15HENERGY EQUATION)
54 FORMAT('0'10X,10HVELOCITY,U)
55 FORMAT('0'10X,15HSTREAM FUNCTION)
56 FORMAT('0'10X,30HSHEARING STRESS OF Y-RIRECTION,12X,
135HTEMPERATURE GRADIENT OF Y-DIRECTION)
57 FORMAT(10X,2HJ=,I3,5X,,2(D13.5,7X),10X,2(D13.5,7X))
58 FORMAT('0'10X,30HSHEARING STRESS OF X-RIRECTION,12X,
135HTEMPERATURE GRADIENT OF X-DIRECTION)
59 FORMAT(10X,2HI=,I3,5X,D13.5,7X,30X,D13.5)
60 FORMAT(10X,4HSHM=,D13.5,3X,4HTGM=,D13.5,4X,
13HWM=,D13.5,4X,3HTM=,D13.5,4X,3HTW=,D13.5,4X,3HTB=,D13.
* .5)
61 FORMAT(10X,4HFRE=,D13.5,2X,5HFREM=,D13.5,4X,3HNU=,D13.
* 5,3X,
14HNUE=,D13.5,4X,3HDK=,D13.5)
64 FORMAT('0'10X,25HERROR OF AXIAL VELOCITY,W)
66 FORMAT('0'10X,29HERROR OF SECONDARY FLOW,U & V)
65 FORMAT('0'10X,24HERROR OF STREAM FUNCTION)
67 FORMAT('0'10X,19HERROR OF TEMPERATUR)
68 FORMAT(20X,3HI=1,17X,4HI=M1,24X,3HI=1,17X,4HI=M1)
69 FORMAT(20X,3HJ=1,45X,3HJ=1)
70 FORMAT('0'10X,10HVELOCITY,V)
80 FORMAT(10X,6HSWEEP=,I3,10X,7HMAXERR=,D13.6,10X,5HOMEE=
* ,D13.6)

```





```
81 FORMAT(10X,6HSWEEP=,I3,10X,7HMAXERP=,D13.6,10X,5HOMES=  
* ,D13.6)  
82 FORMAT(10X,6HSWEEP=,I3,10X,7HMAXERR=,D13.6)  
1000 STOP  
END
```



```
SUBROUTINE PRINT (W,T,S,U,V)
DOUBLE PRECISION W(81,43),T(81,43),S(81,43),U(81,43),V
* (81,43)
COMMON M1,N3
WRITE (7,71) ((W(I,J),I=1,M1),J=1,N3)
WRITE(7,71)((T(I,J),I=1,M1),J=1,N3)
WRITE(7,71)((S(I,J),I=1,M1),J=1,N3)
WRITE(7,71)((U(I,J),I=1,M1),J=1,N3)
WRITE(7,71)((V(I,J),I=1,M1),J=1,N3)
RETURN
71 FORMAT(10A8)
END
```





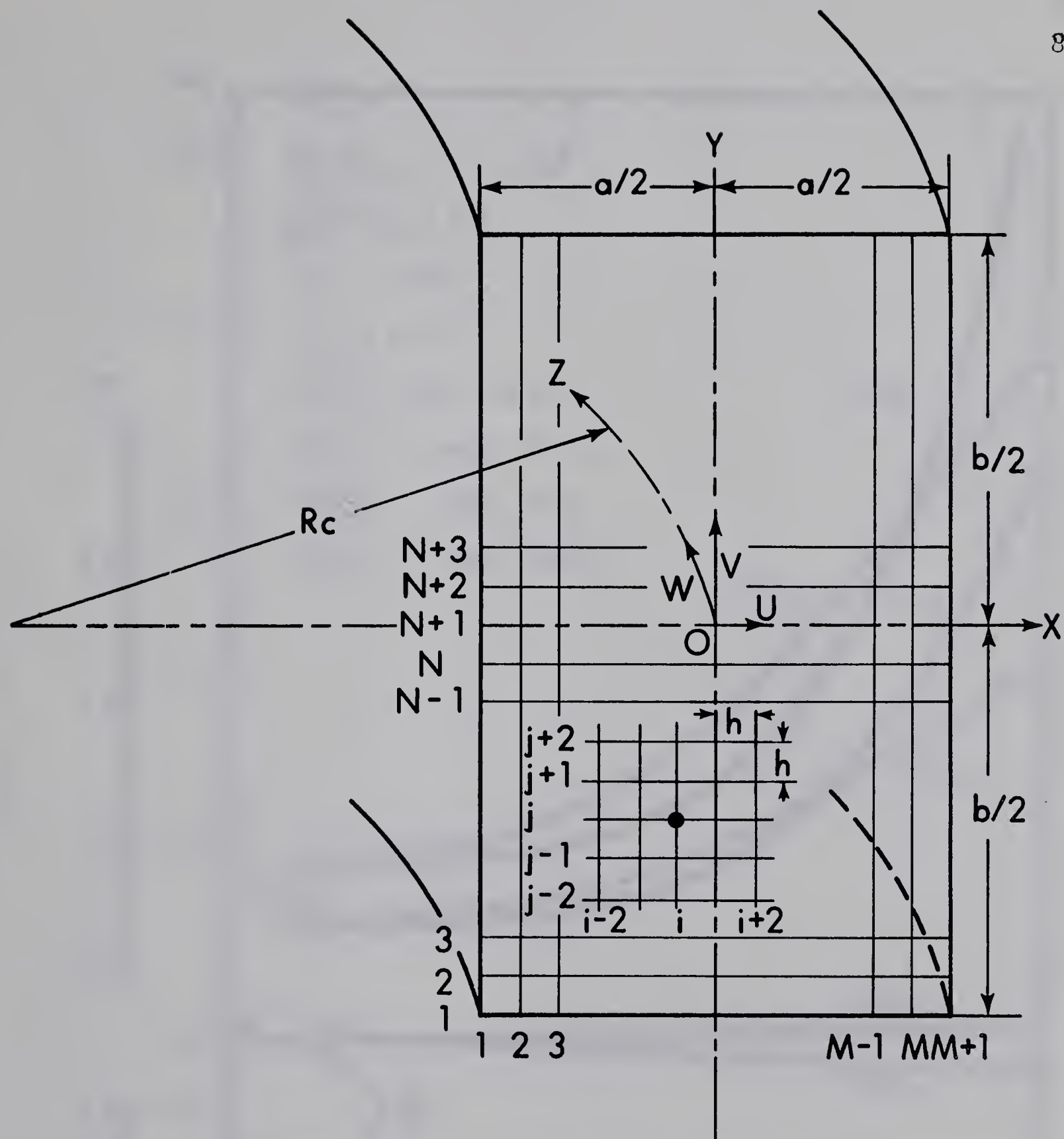


Fig. 1 Coordinate system and numerical grid for a curved rectangular channel







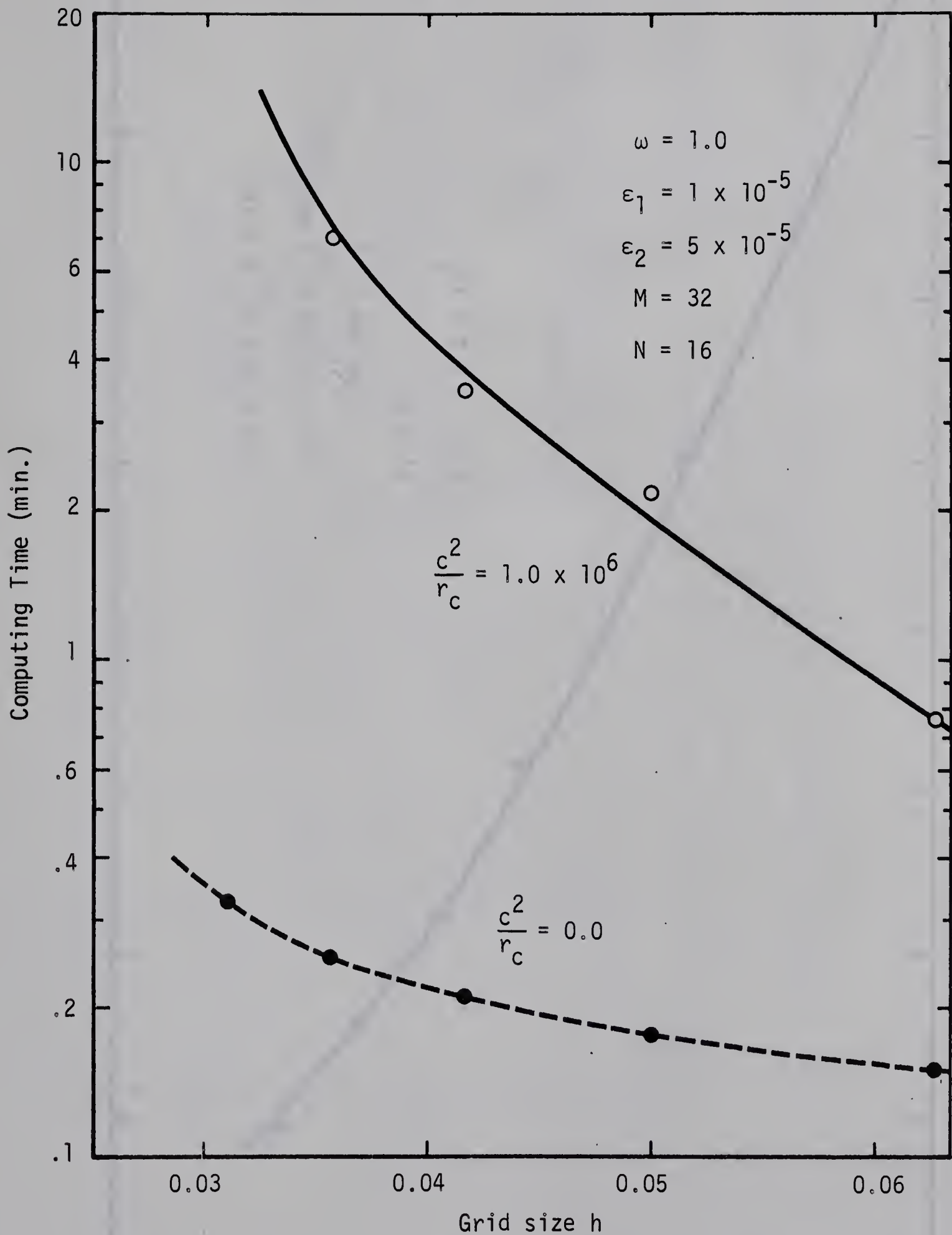


Fig. 3 Effect of grid size on computing time for a curved square channel ( $\gamma = 1$ ) with  $Pr = 0.73$





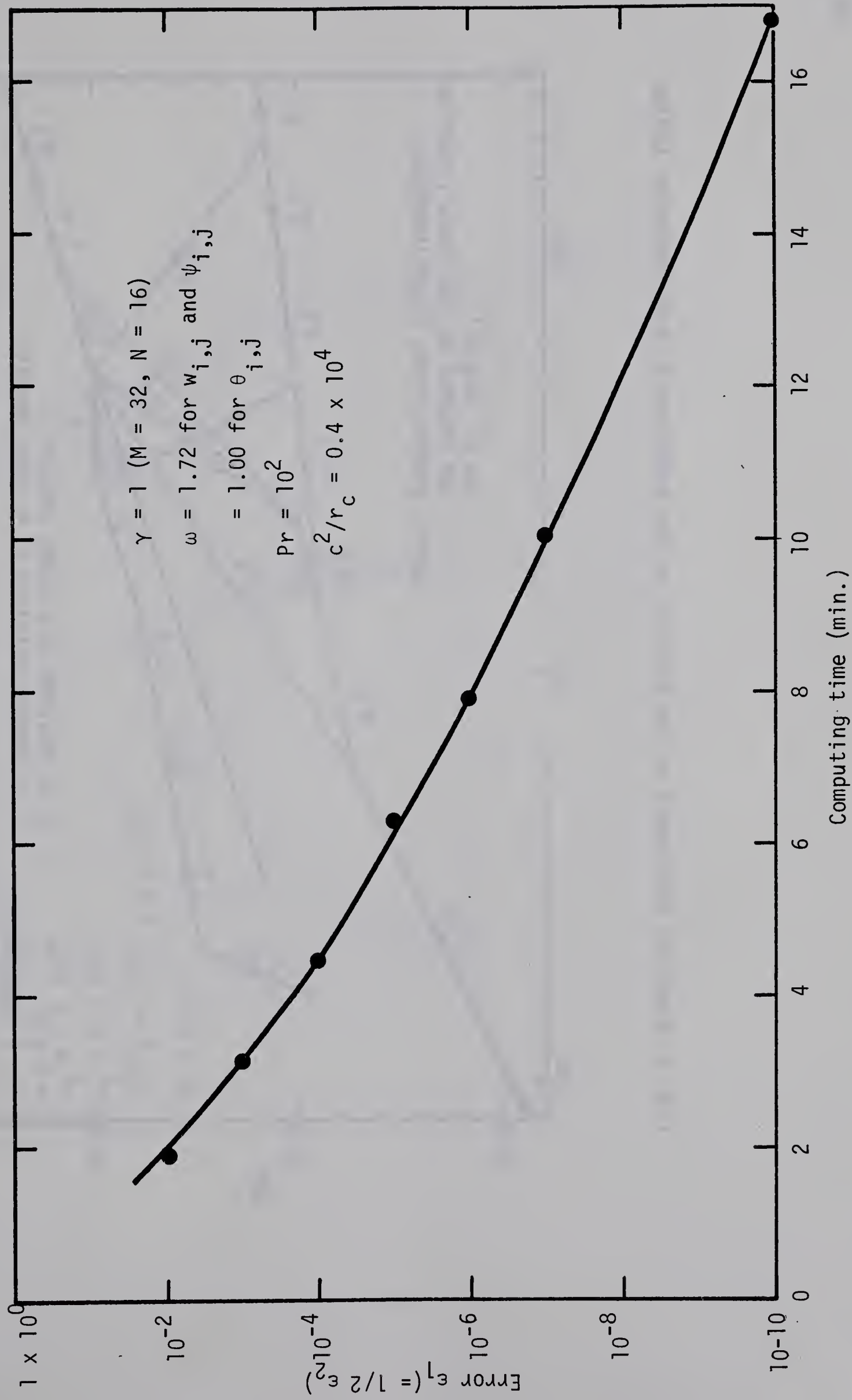


Fig. 4 A relation between error  $\epsilon_1$  and computing time for a curved square channel  $\gamma = 1$  with  $Pr = 10^2$



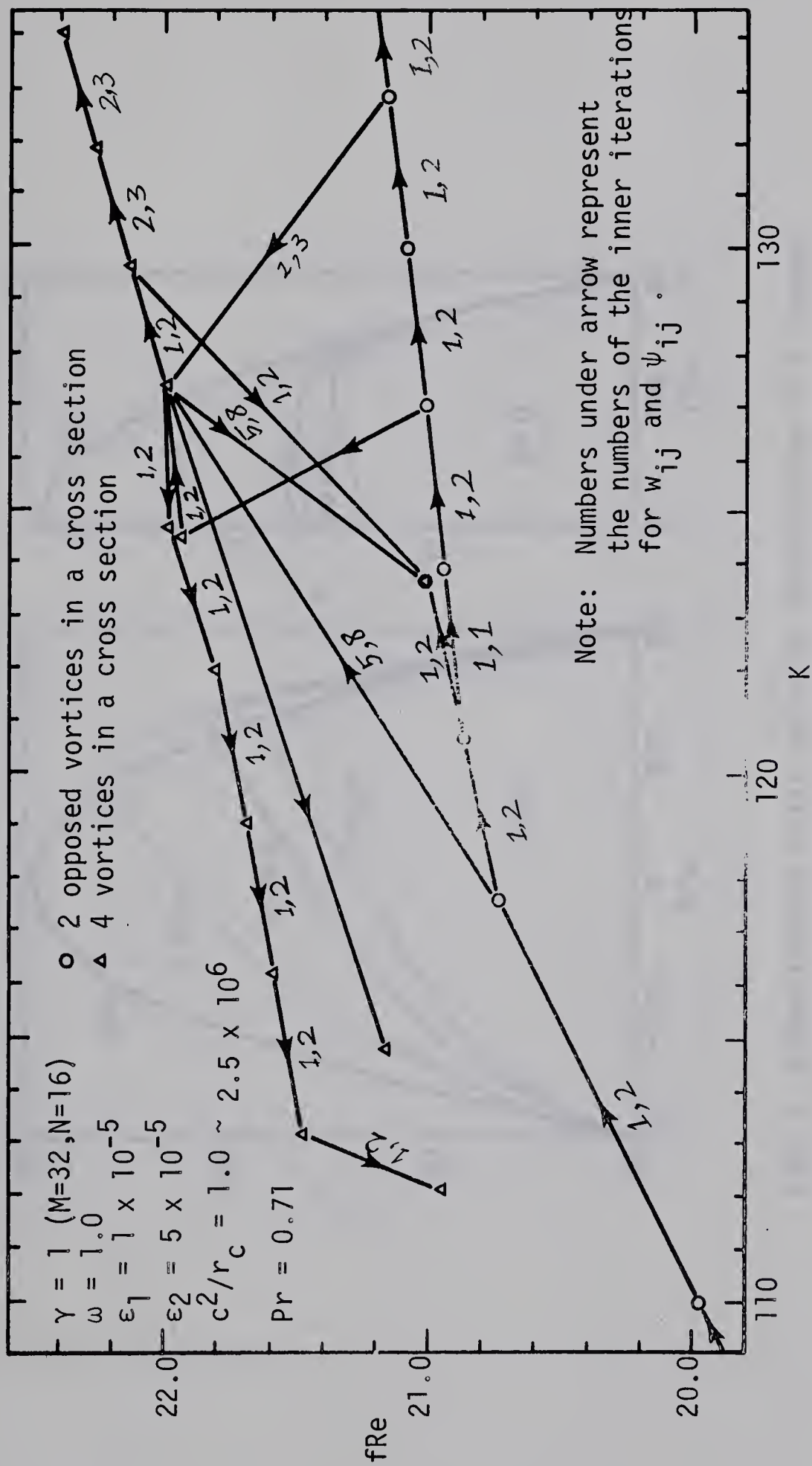


Fig. 5 Numerical experiment on the behavior of the equations at high parameter regime





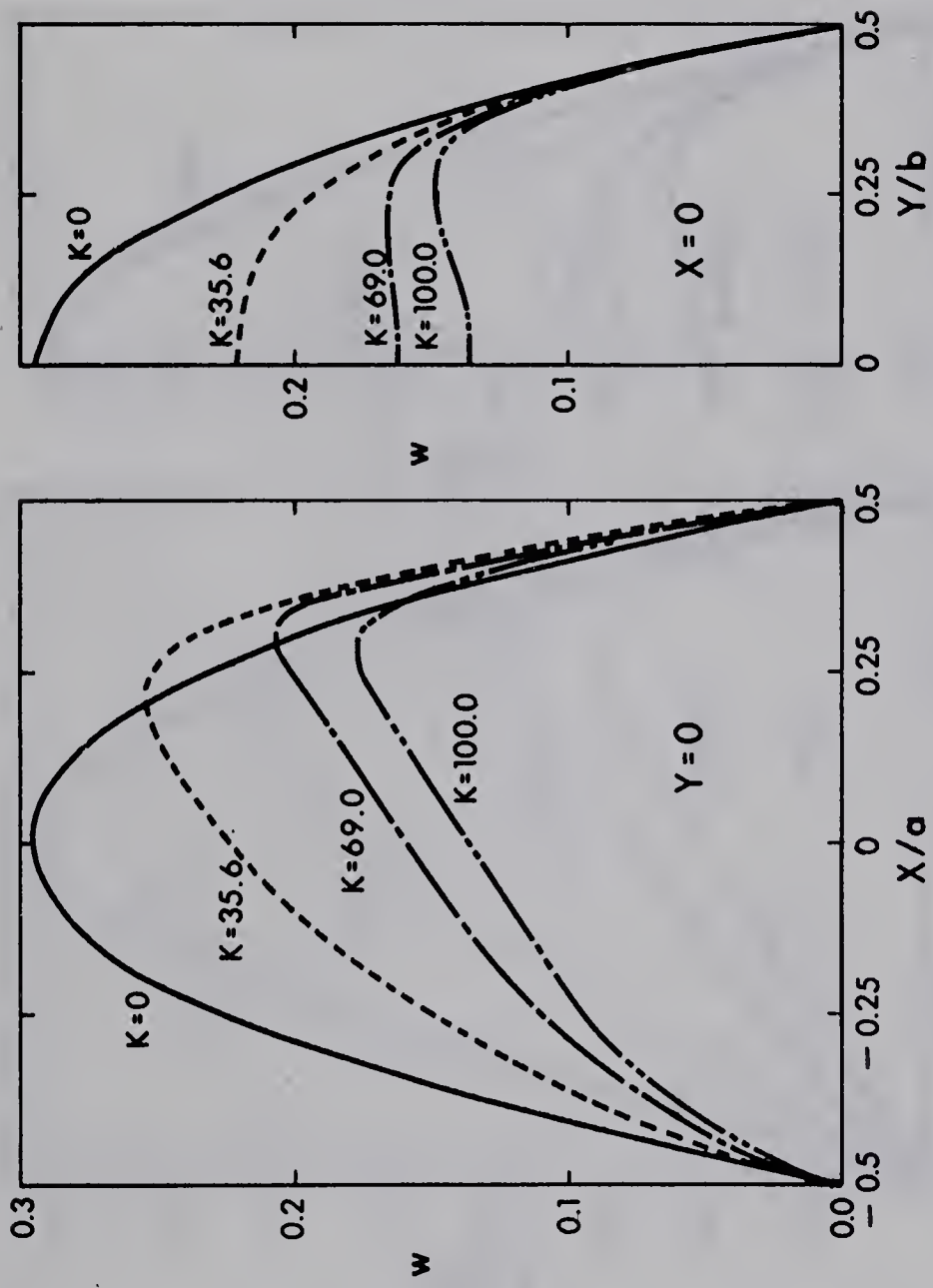


Fig. 6 Dimensionless axial velocity distribution in a curved square channel  $\gamma = 1$  with  $K$  as a parameter



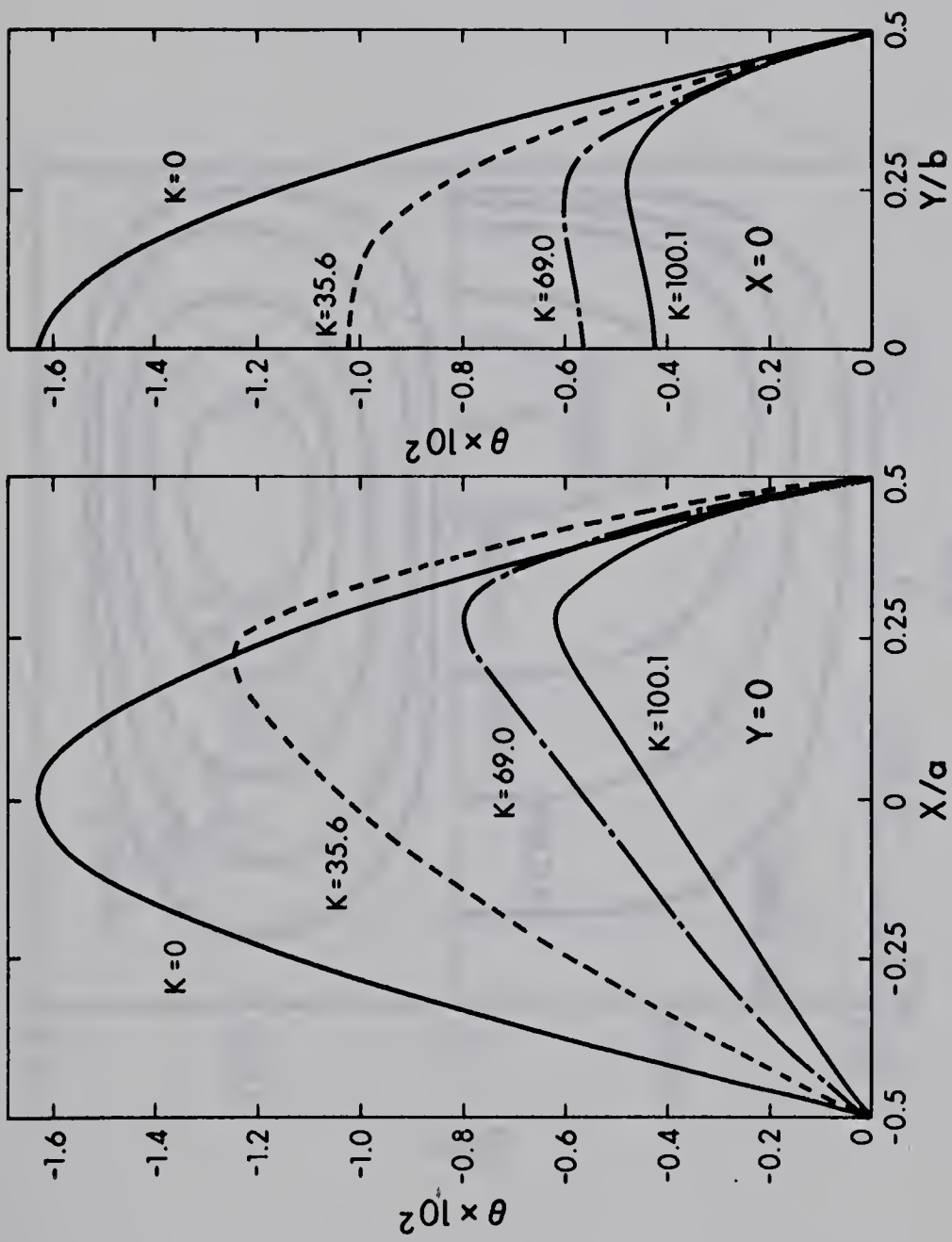


Fig. 7 Dimensionless temperature distribution in a curved square channel  $\gamma = 1$  and  $Pr = 0.73$  with  $K$  as a parameter



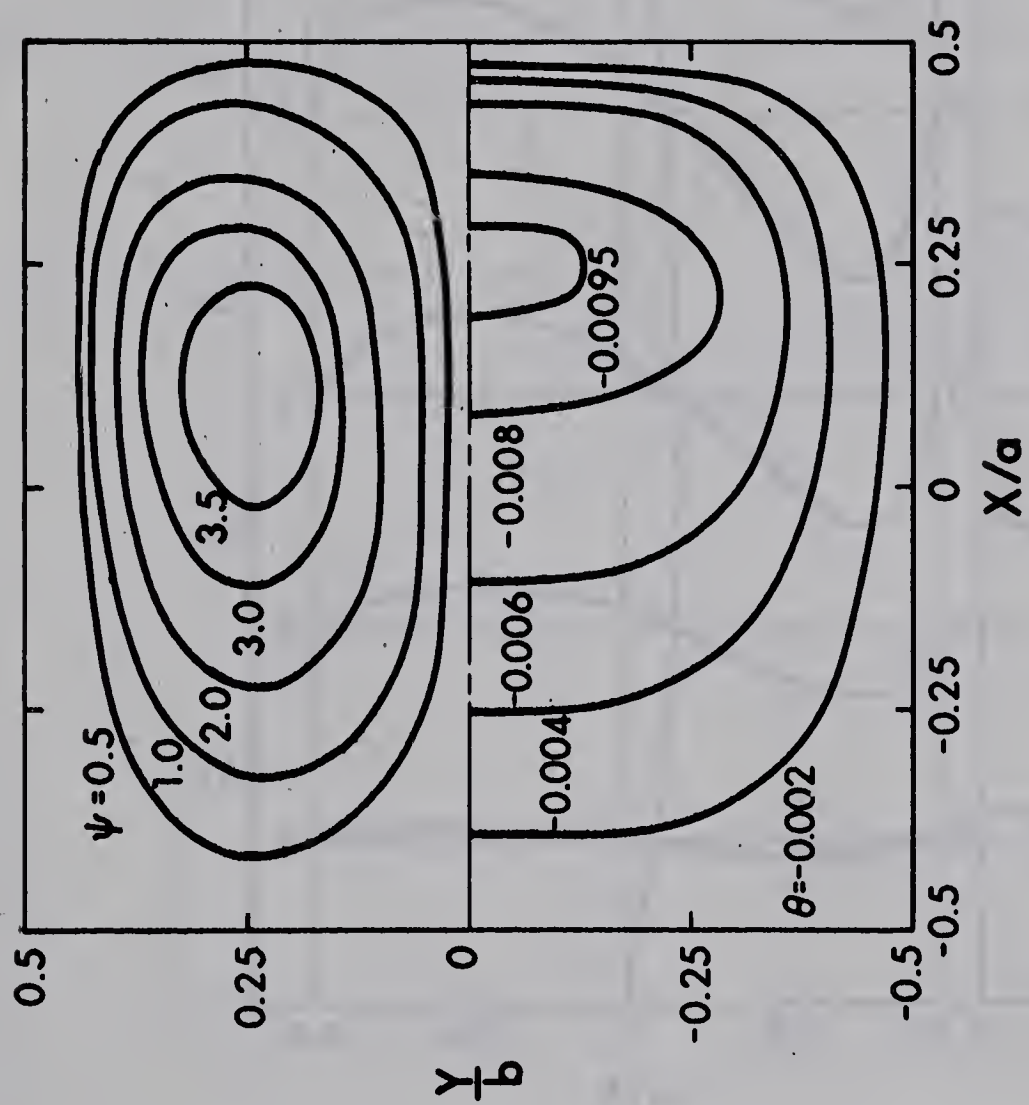


Fig. 8 Secondary flow streamlines and dimensionless isothermals for a curved square channel  $\gamma = 1$  with  $K = 51.9$  and  $Pr = 0.73$





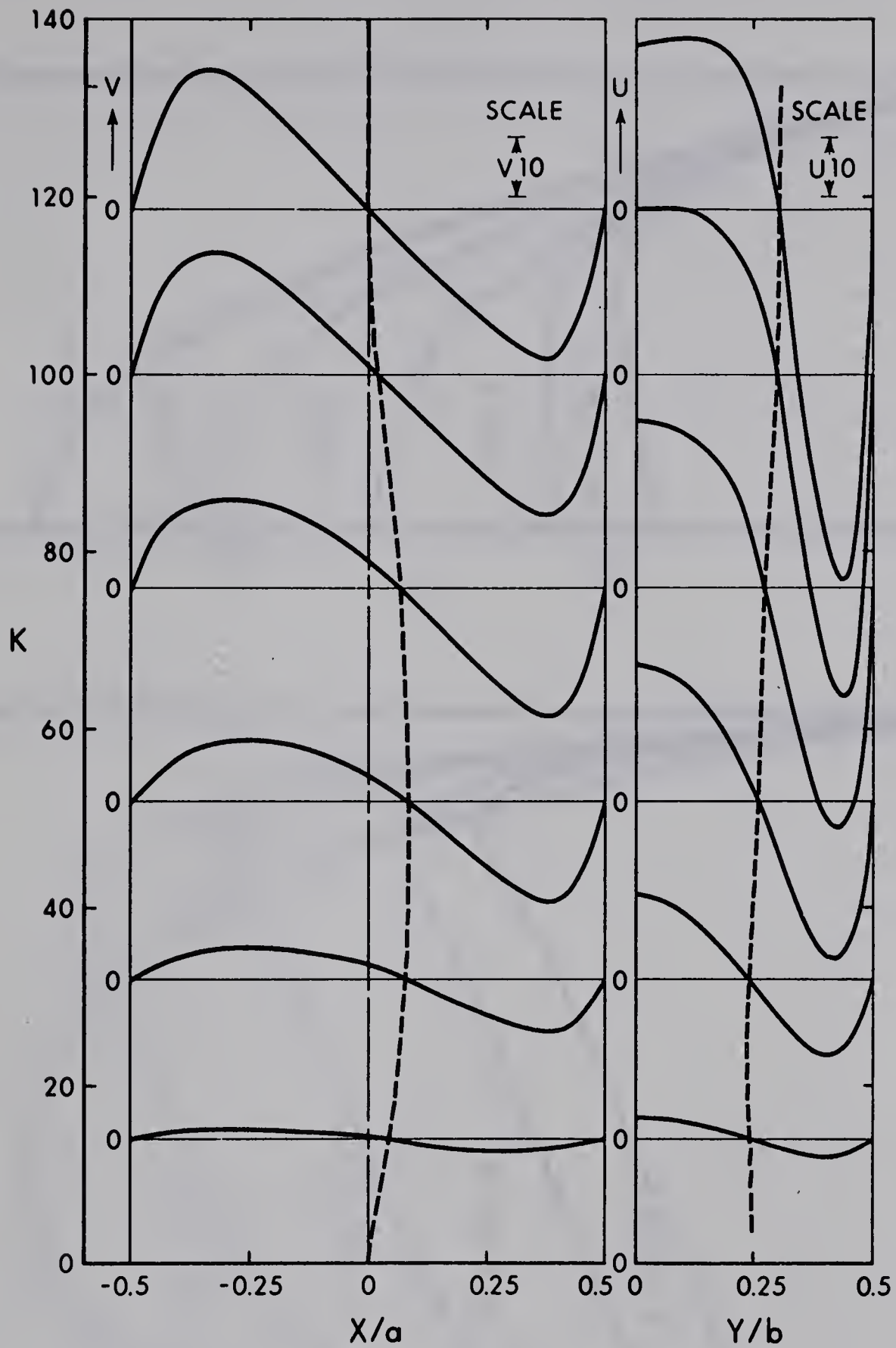


Fig. 9 Distribution of dimensionless secondary velocity components  $(u, v)$  in two directions  $(X$  and  $Y)$  passing through the center of circulation for a curved square channel  $(\gamma = 1)$  with  $K$  as a parameter



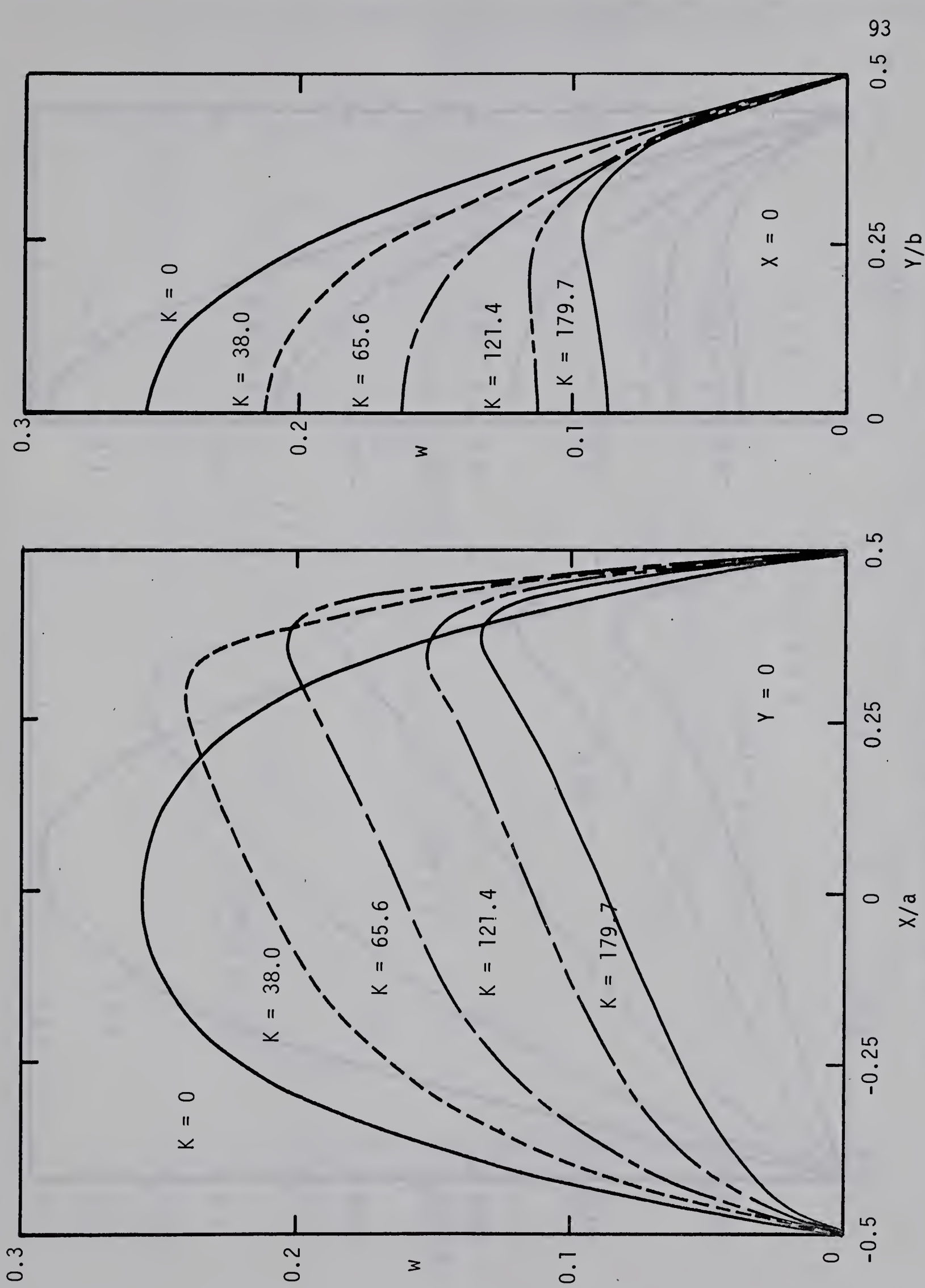


Fig. 10 Dimensionless axial velocity distribution in a curved rectangular channel  $\gamma = 2$  with  $K$  as a parameter





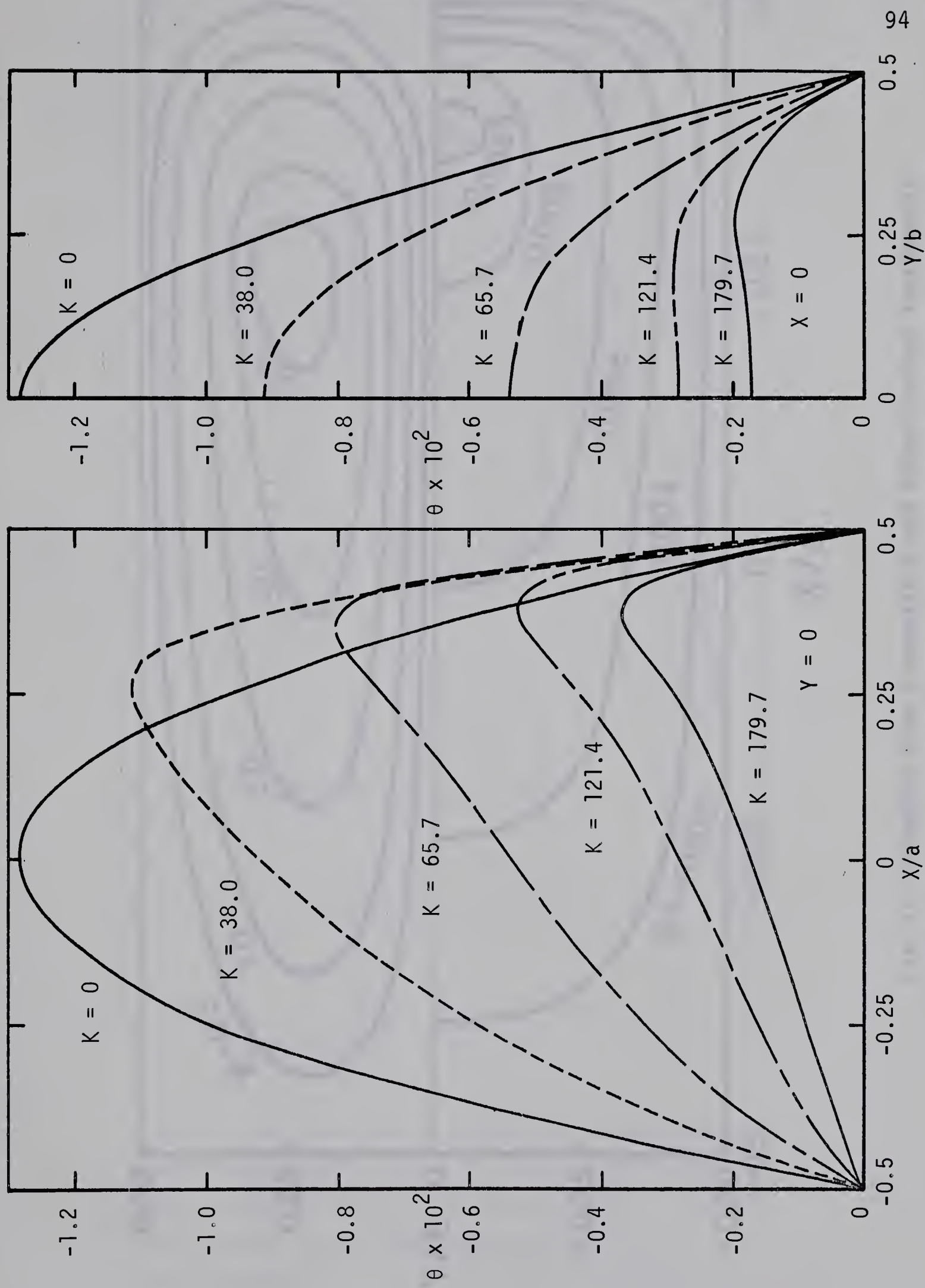


Fig. 11 Dimensionless temperature distribution in a curved rectangular channel  $\gamma = 2$  and  $Pr = 0.73$  with  $K$  as a parameter



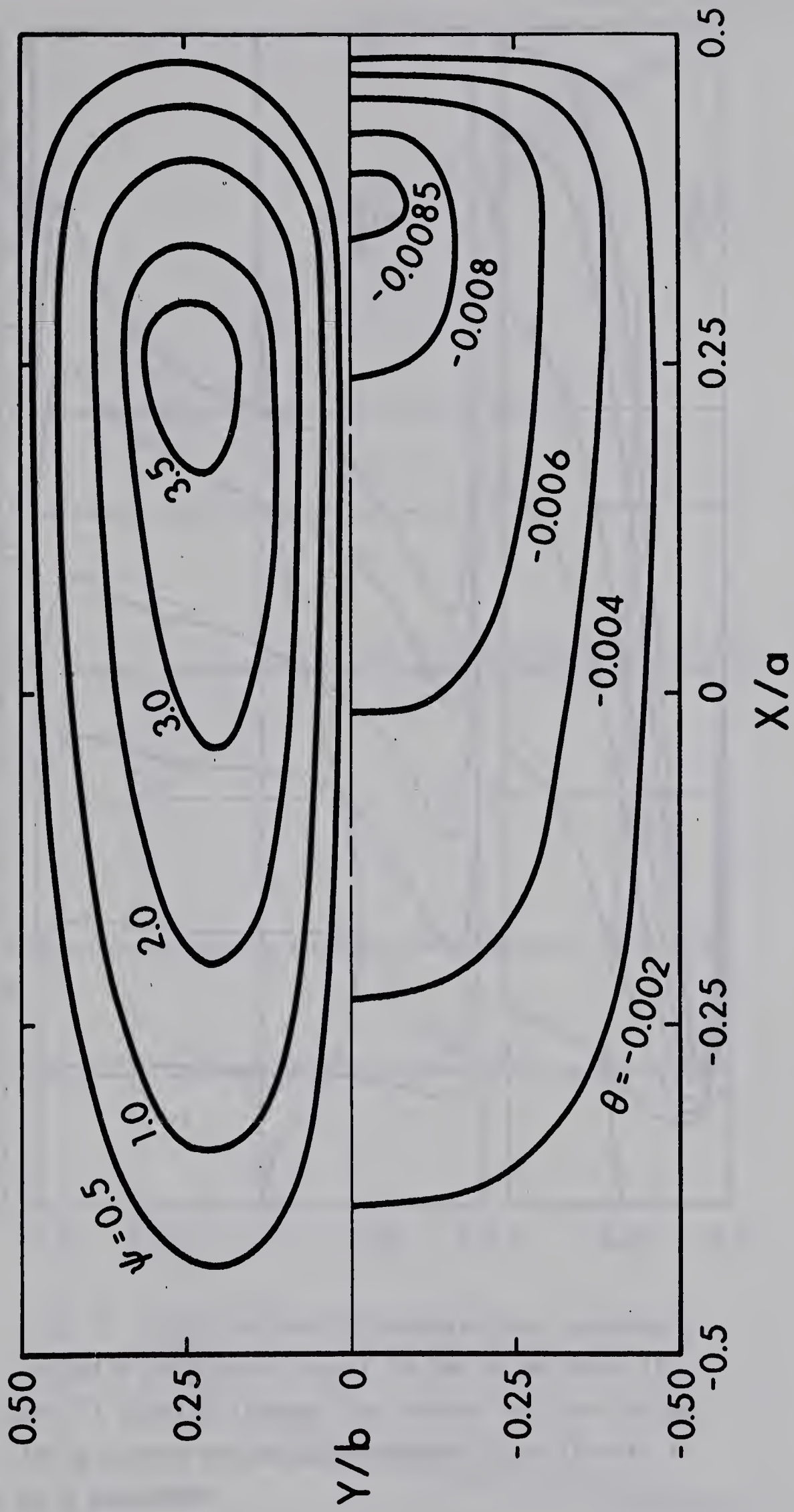


Fig. 12 Secondary flow streamlines and dimensionless isothermals for a curved rectangular channel  $\gamma = 2$  with  $K = 58.8$  and  $Pr = 0.73$





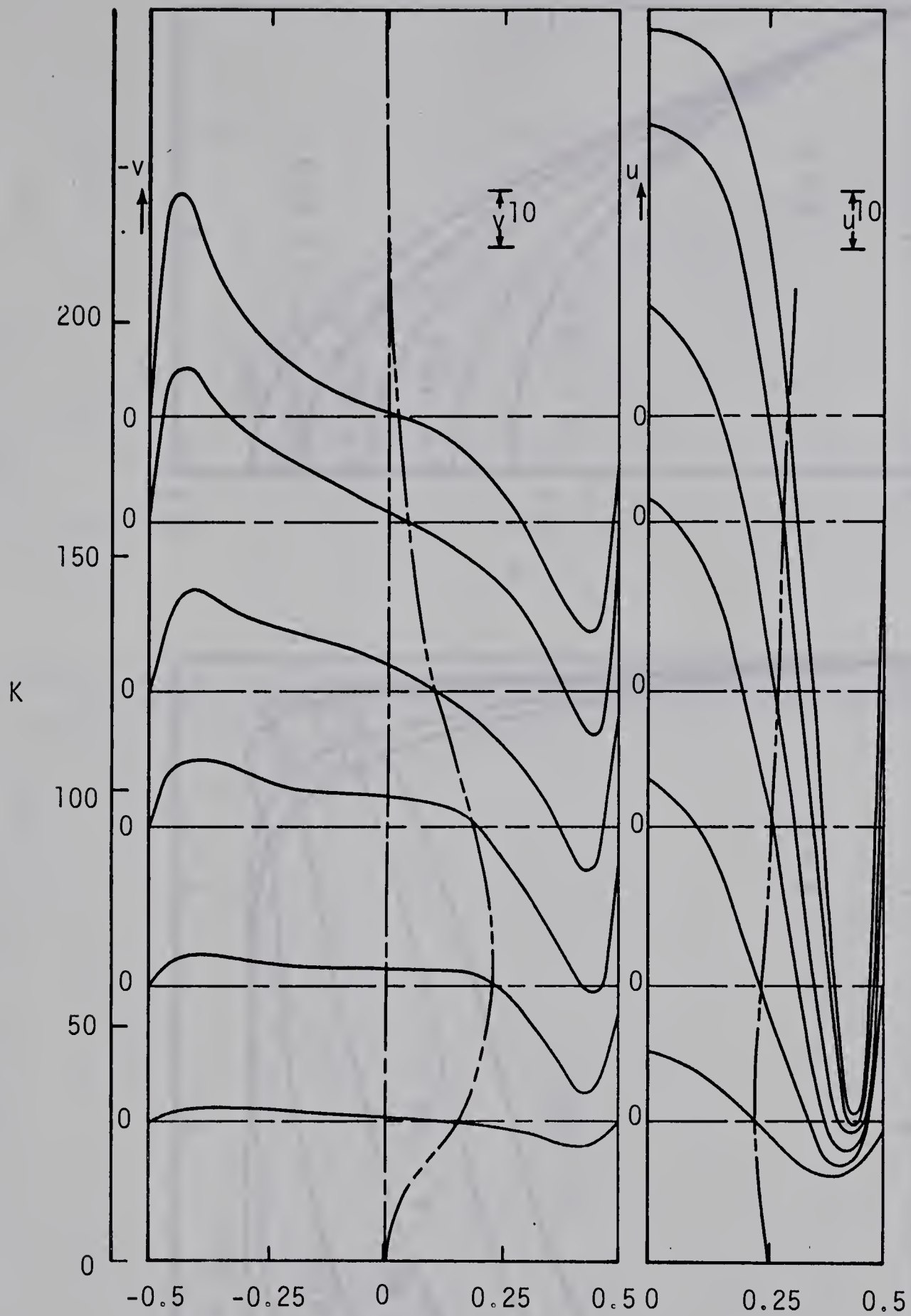


Fig. 13 Distribution of dimensionless secondary velocity components ( $u, v$ ) in two directions ( $X$  and  $Y$ ) passing through the center of circulation for a curved rectangular channel ( $\gamma = 2$ ) with  $K$  as a parameter





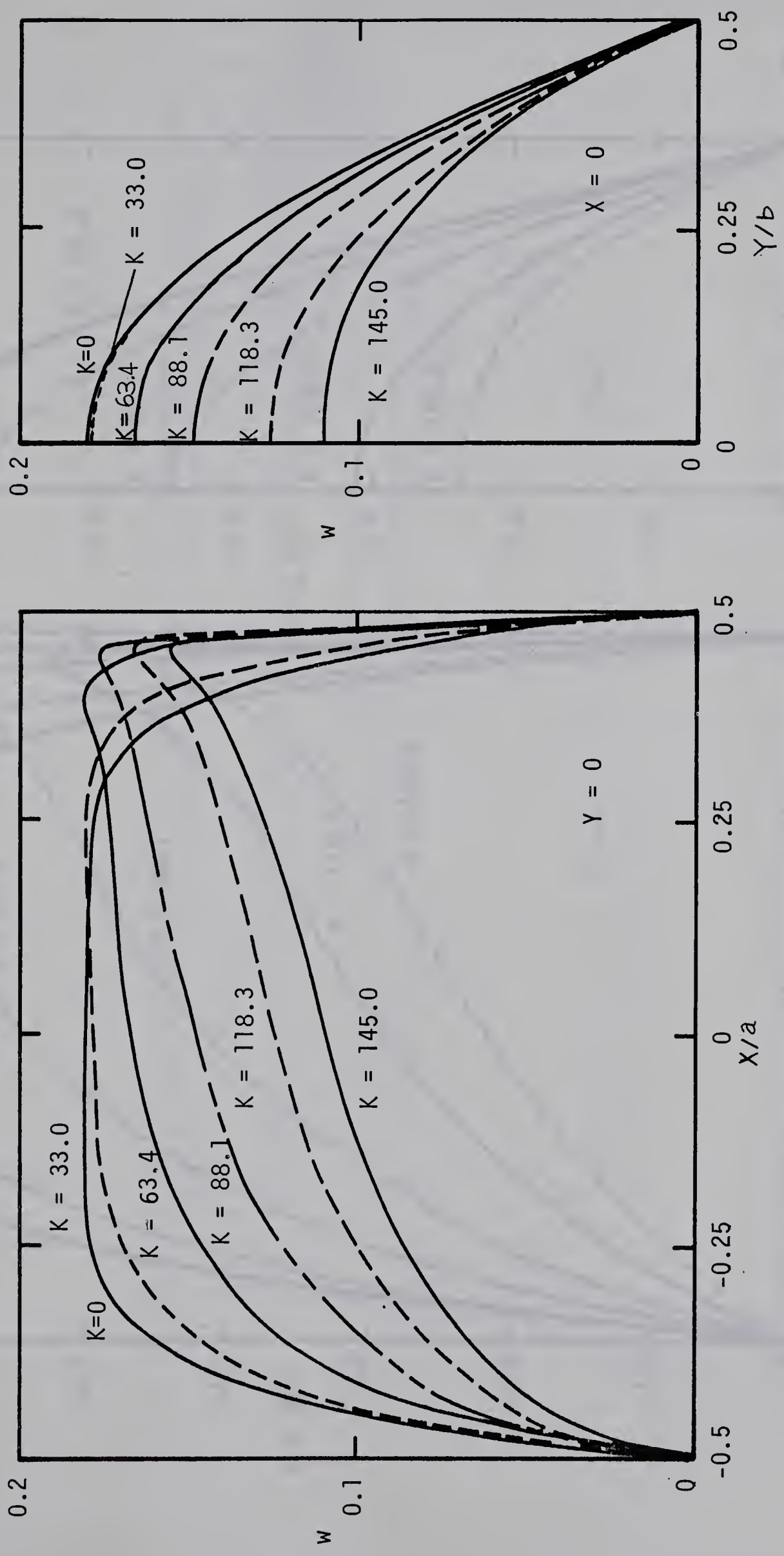


Fig. 14 Dimensionless axial velocity distribution in a curved rectangular channel  $\gamma = 5$  with  $K$  as a parameter



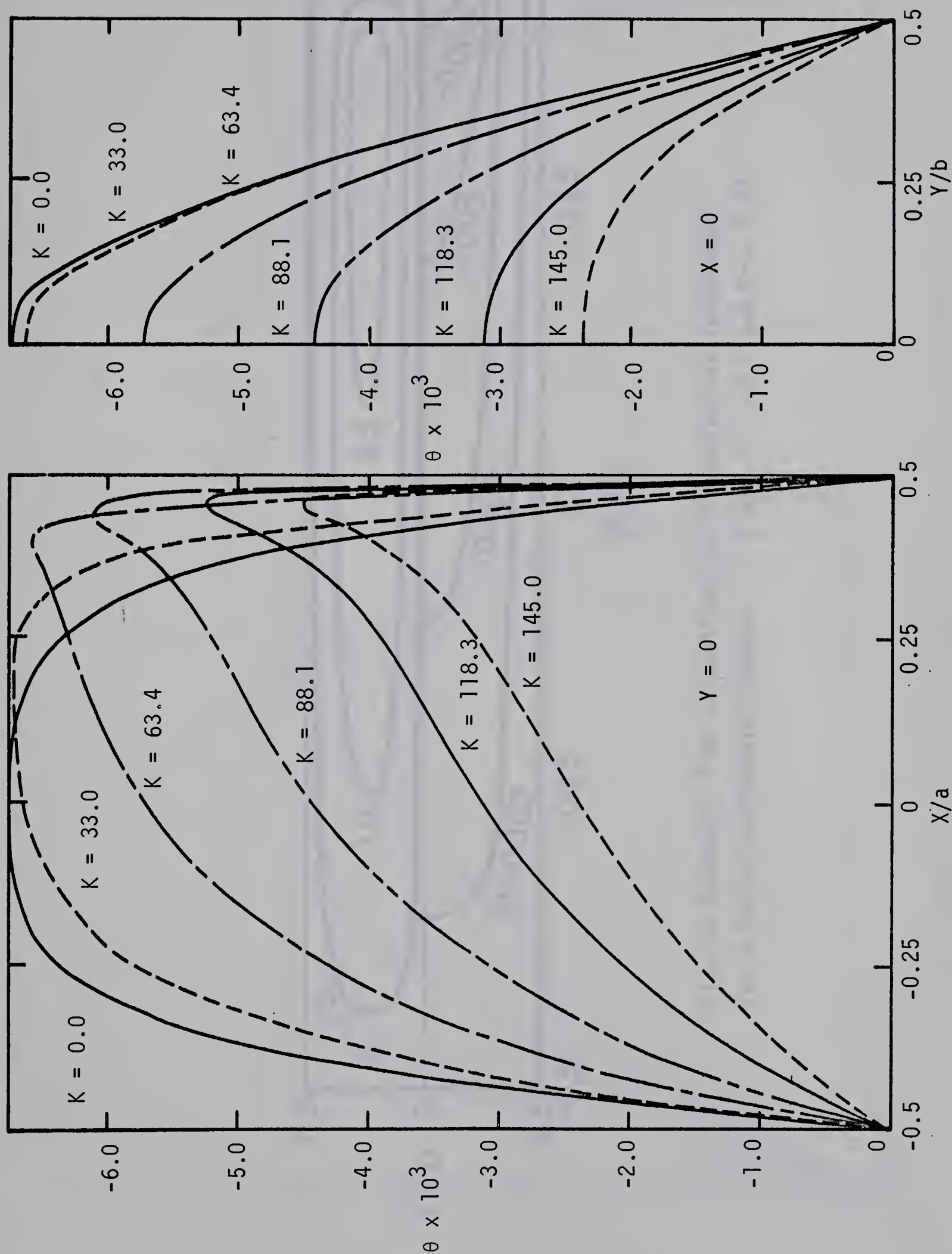


Fig. 15 Dimensionless temperature distribution in a curved rectangular channel  $\gamma = 5$  and  $Pr = 0.73$  with  $K$  as a parameter





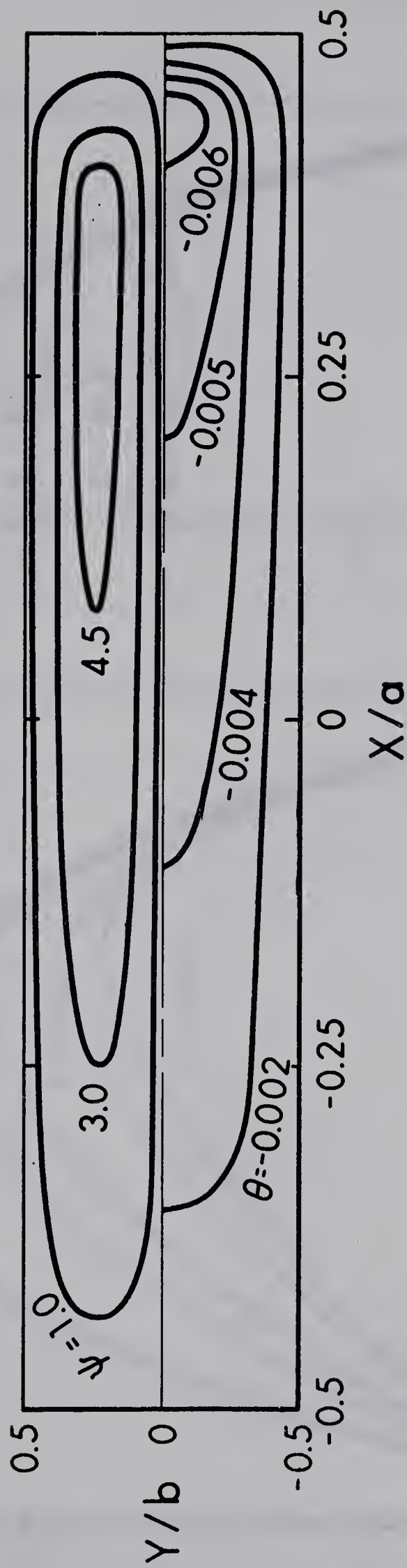


Fig. 16 Secondary flow streamlines and dimensionless isothermals for a curved rectangular channel  $\gamma = 5$  with  $K = 88.1$  and  $Pr = 0.73$



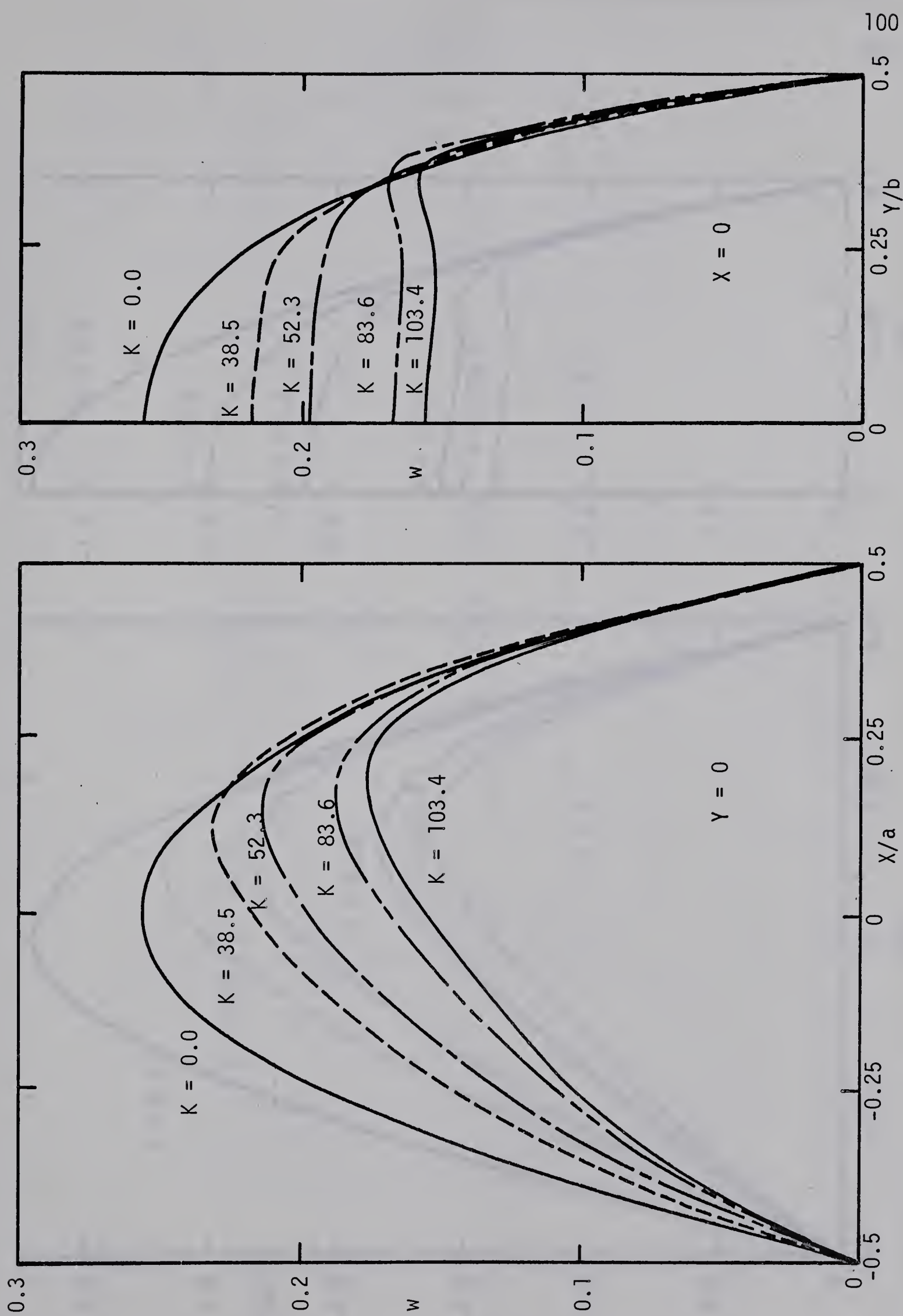


Fig. 17 Dimensionless axial velocity distribution in a curved rectangular channel  $\gamma = 0.5$  with  $K$  as a parameter



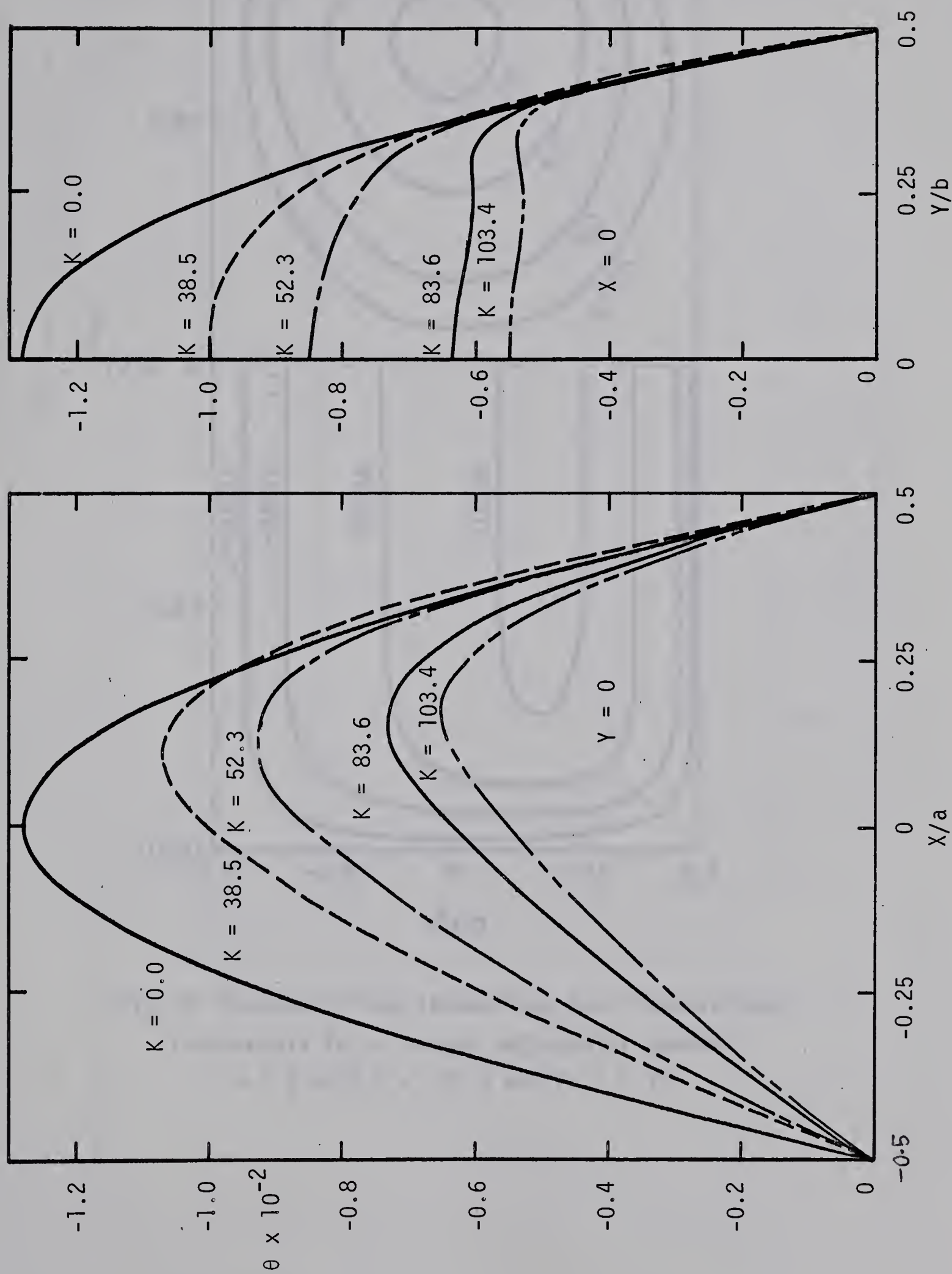


Fig. 18 Dimensionless temperature distribution in a curved rectangular channel  $\gamma = 0.5$  and  $Pr = 0.73$  with  $K$  as a parameter





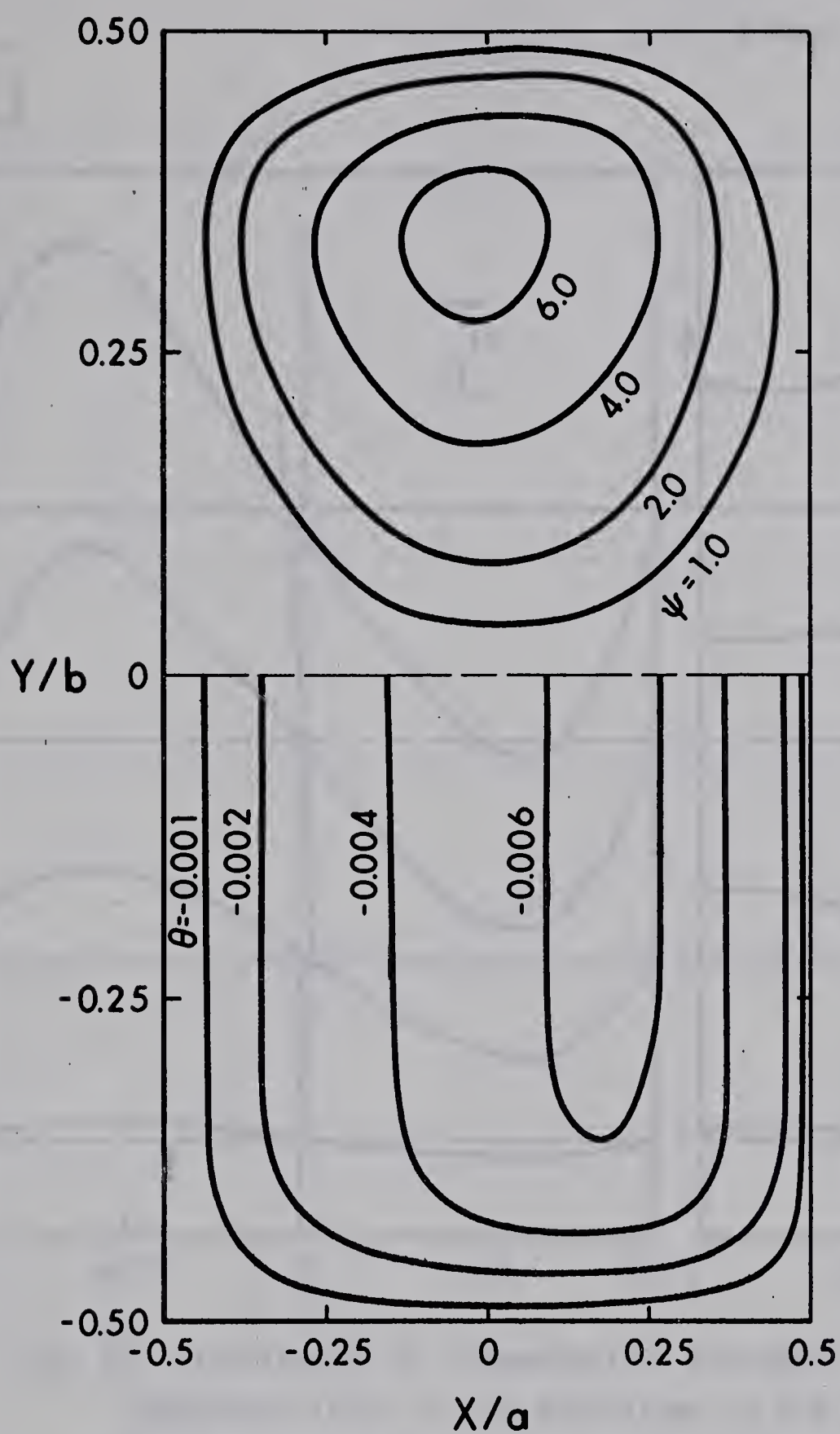


Fig. 19 Secondary flow streamlines and dimensionless isotherms for a curved rectangular channel  $\gamma = 0.5$  with  $K = 103.4$  and  $Pr = 0.73$



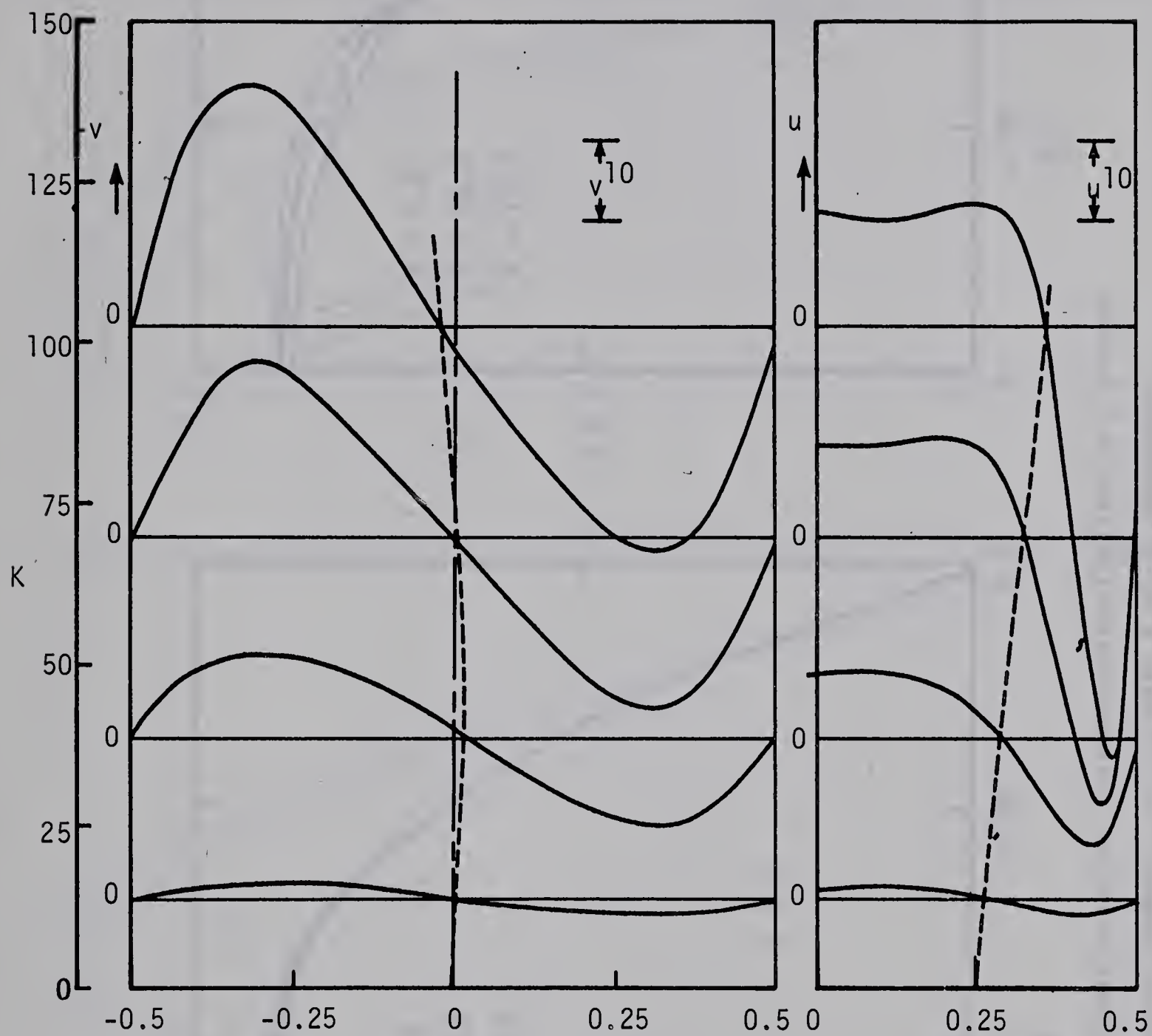


Fig. 20 Distribution of dimensionless secondary velocity components ( $u, v$ ) in two directions ( $X$  and  $Y$ ) passing through the center of circulation for a curved rectangular channel ( $\gamma = 0.5$ ) with  $K$  as a parameter





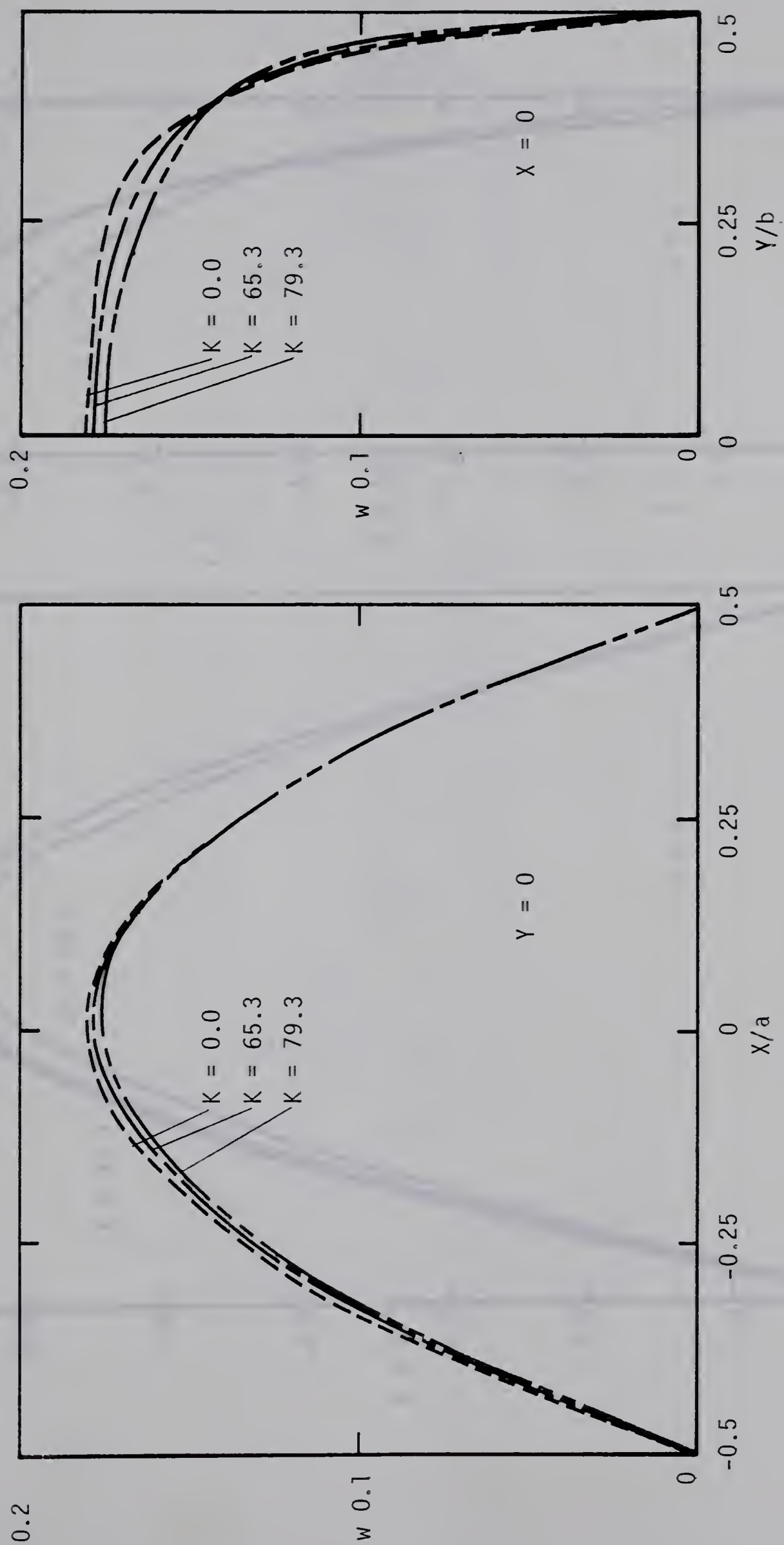


Fig. 21 Dimensionless axial velocity distribution in a curved rectangular channel  $\gamma = 0.2$  with  $K$  as a parameter



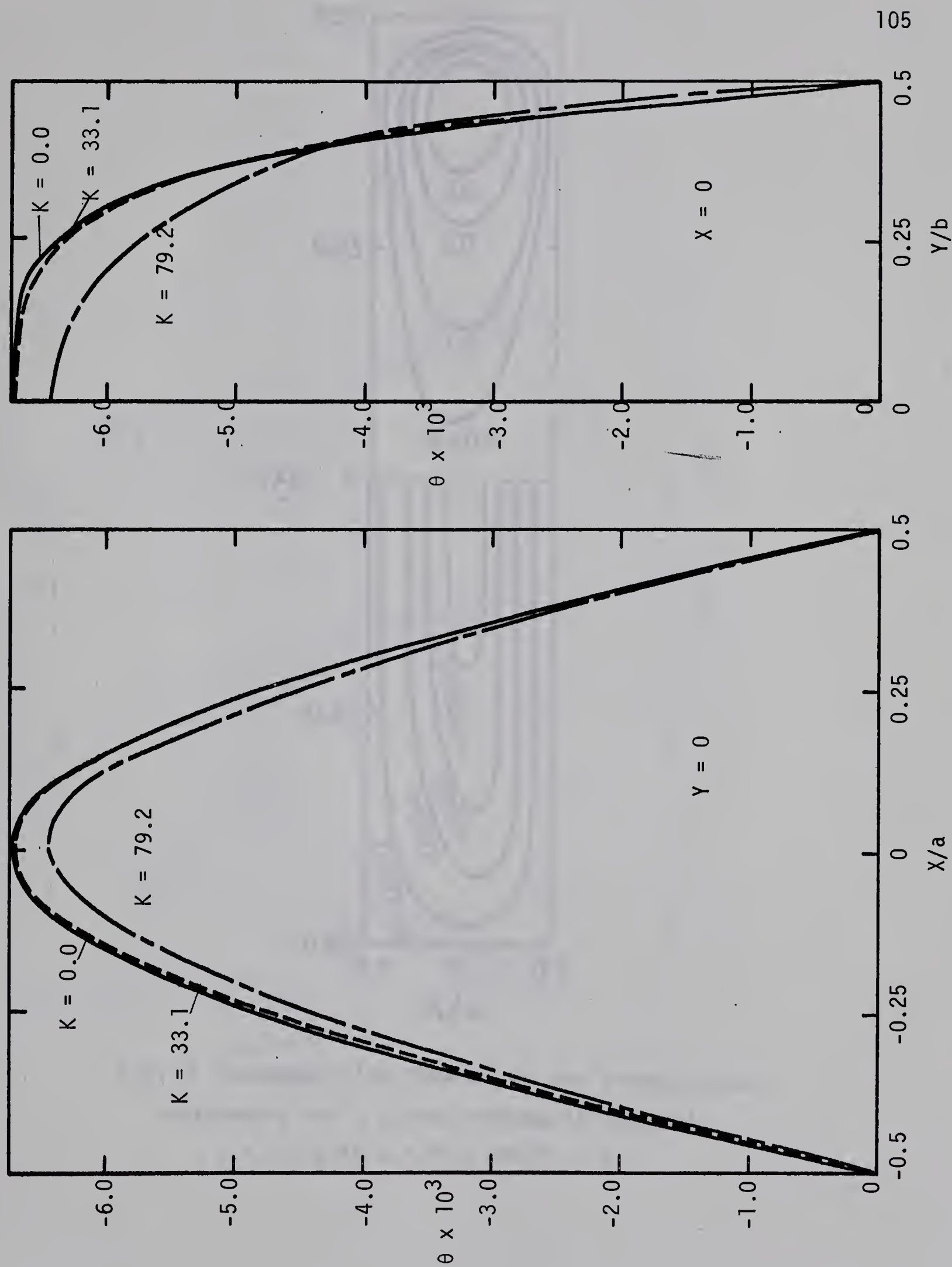


Fig. 22 Dimensionless temperature distribution in a curved rectangular channel  $\gamma = 0.2$  and  $Pr = 0.73$  with  $K$  as a parameter



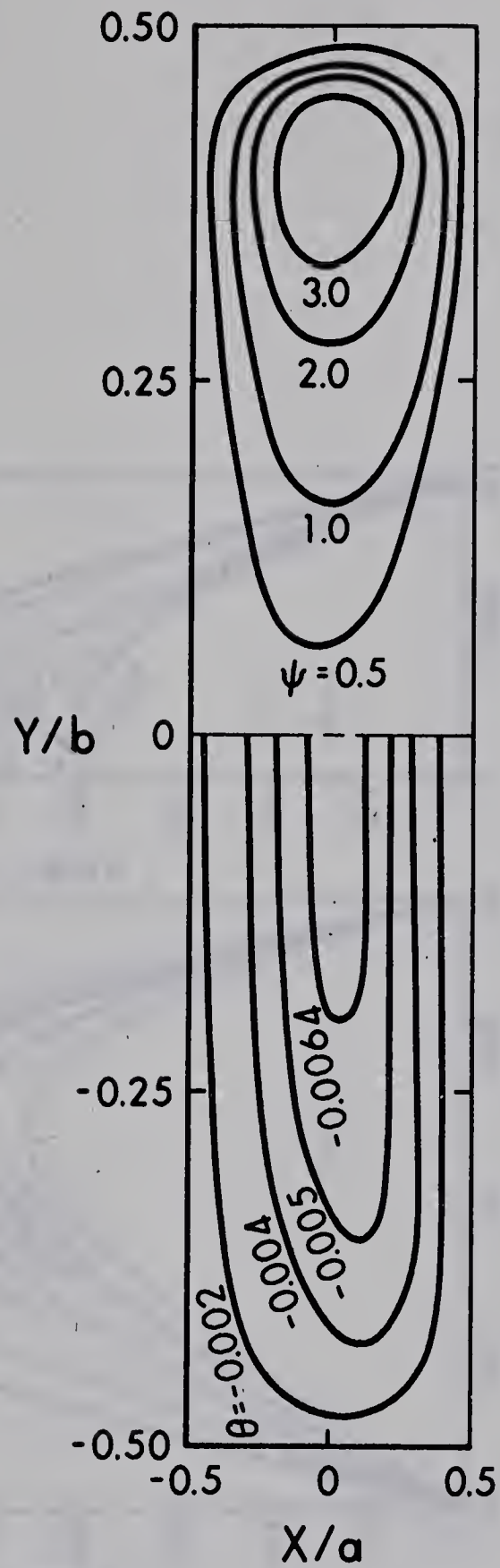


Fig. 23 Secondary flow streamlines and dimensionless isotherms for a curved rectangular channel  
 $\gamma = 0.2$  with  $K = 79.3$  and  $Pr = 0.73$





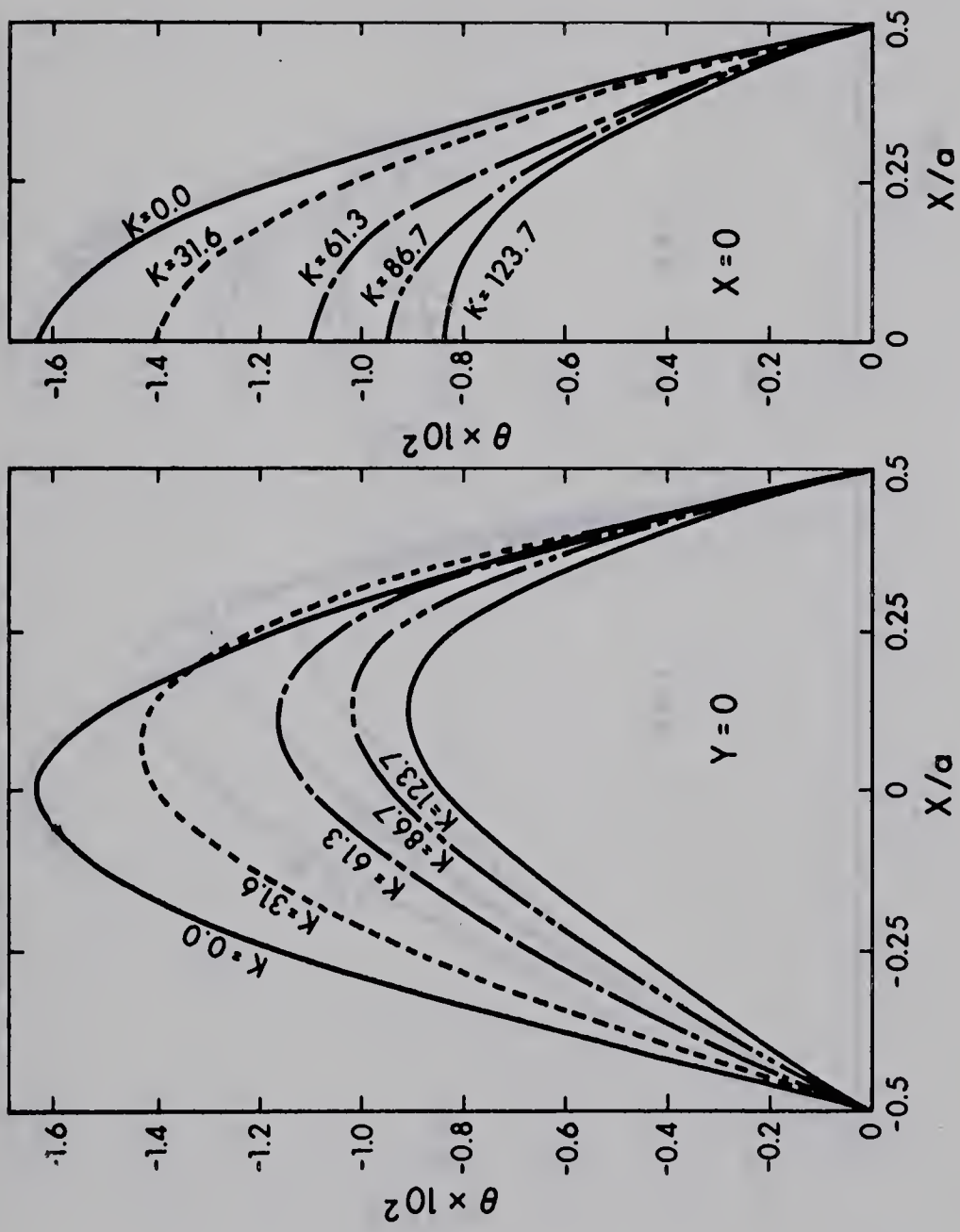


Fig. 24 Dimensionless temperature distribution in a curved square channel  $\gamma = 1$  with  $K$  as a parameter and  $Pr = 0.1$



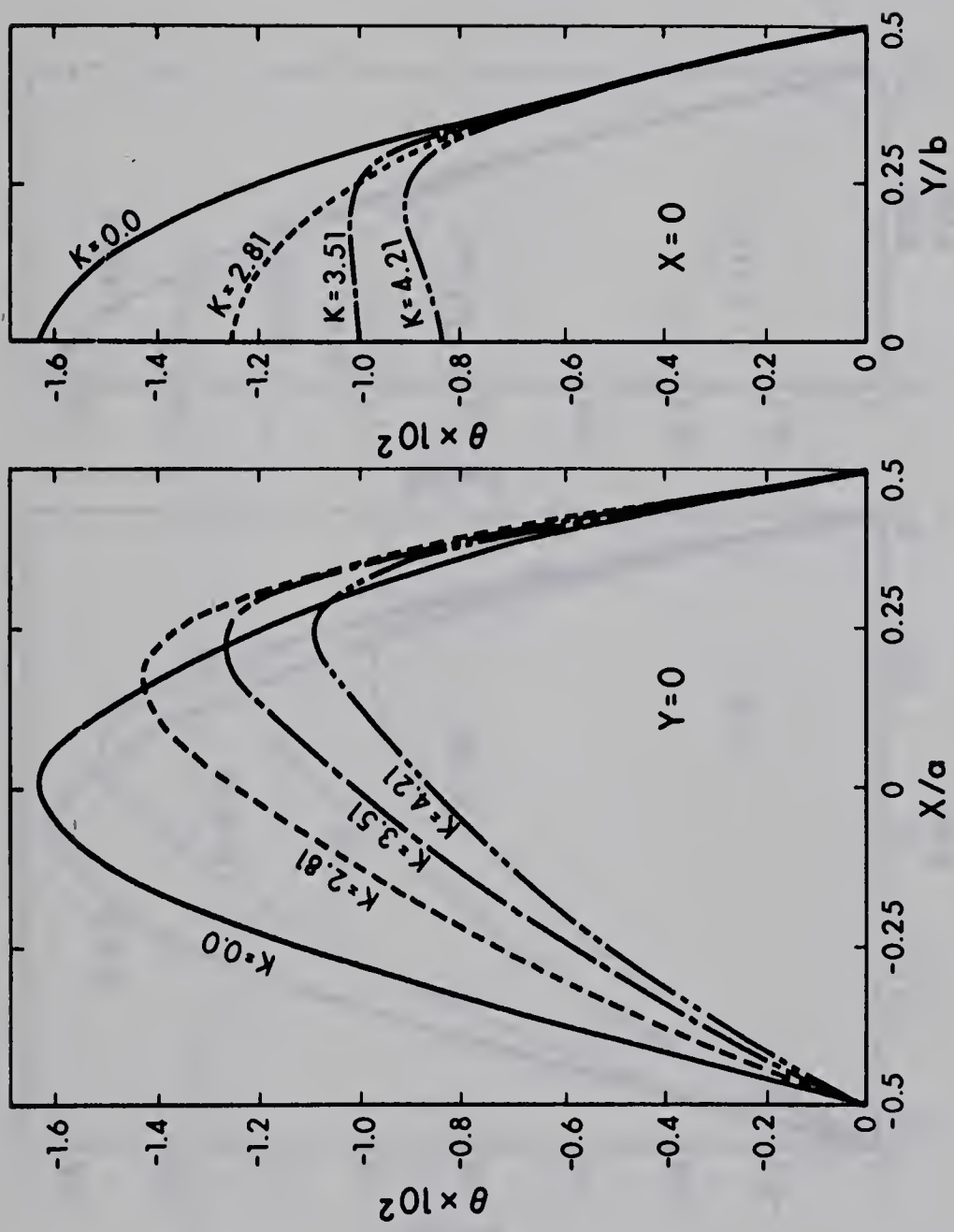


Fig. 25 Dimensionless temperature distribution in a curved square channel  $\gamma = 1$  with  $K$  as a parameter and  $Pr = 10^2$





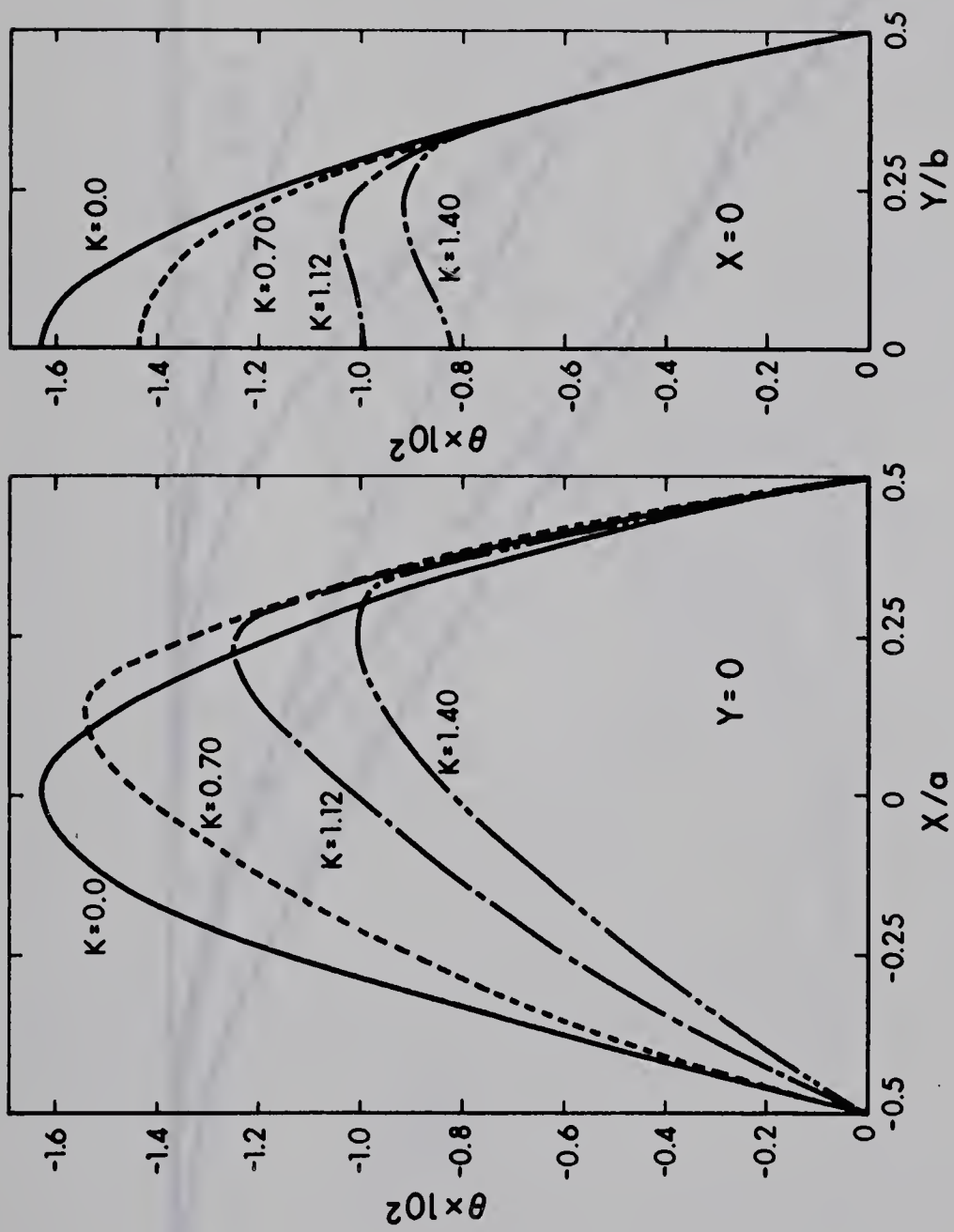


Fig. 26 Dimensionless temperature distribution in a curved square channel  $\gamma = 1$  with  $K$  as a parameter and  $Pr = 10^3$



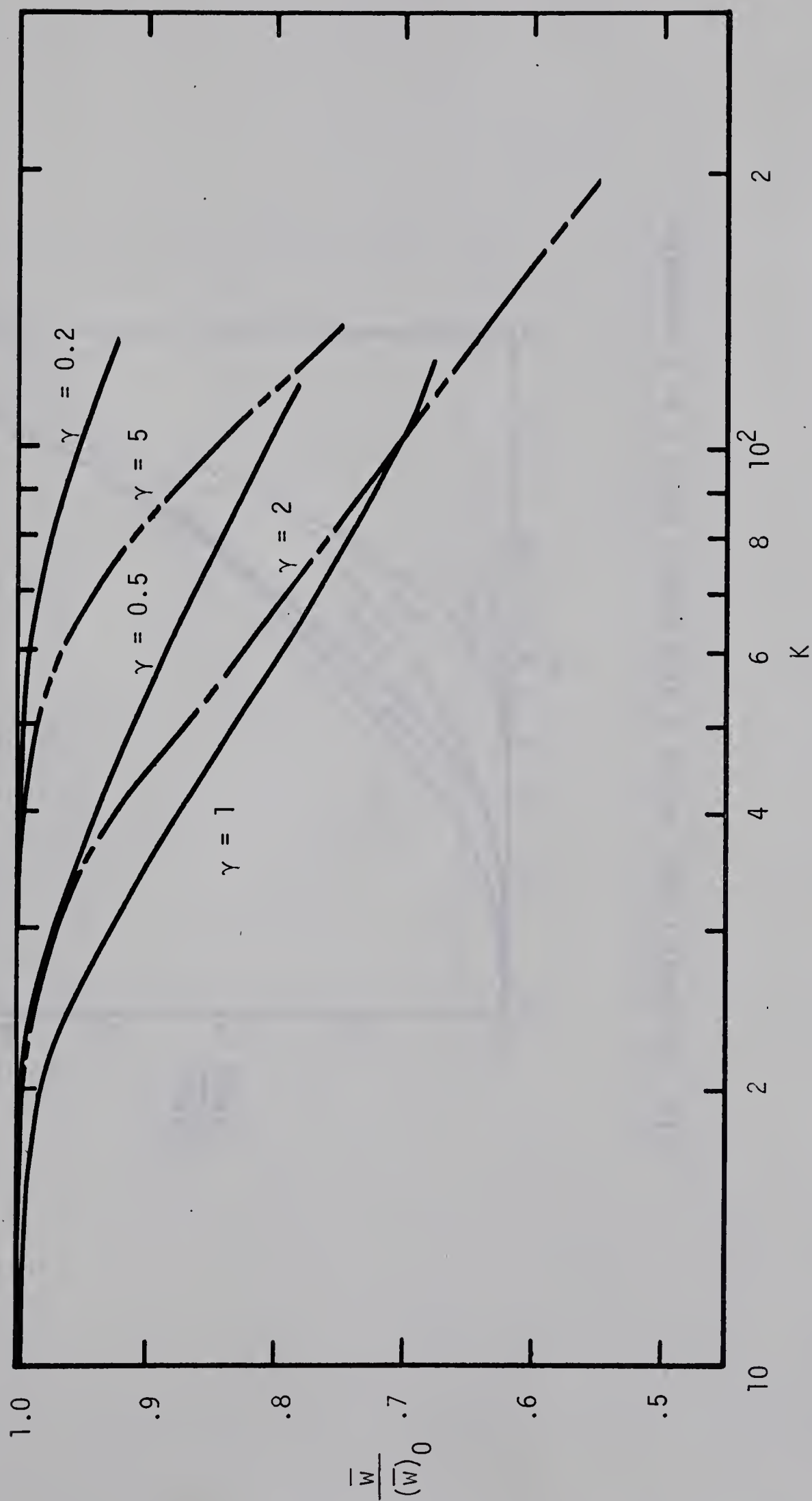


Fig. 27  $\bar{w}/(\bar{w})_0$  versus  $K$  with aspect ratio  $\gamma$  as a parameter



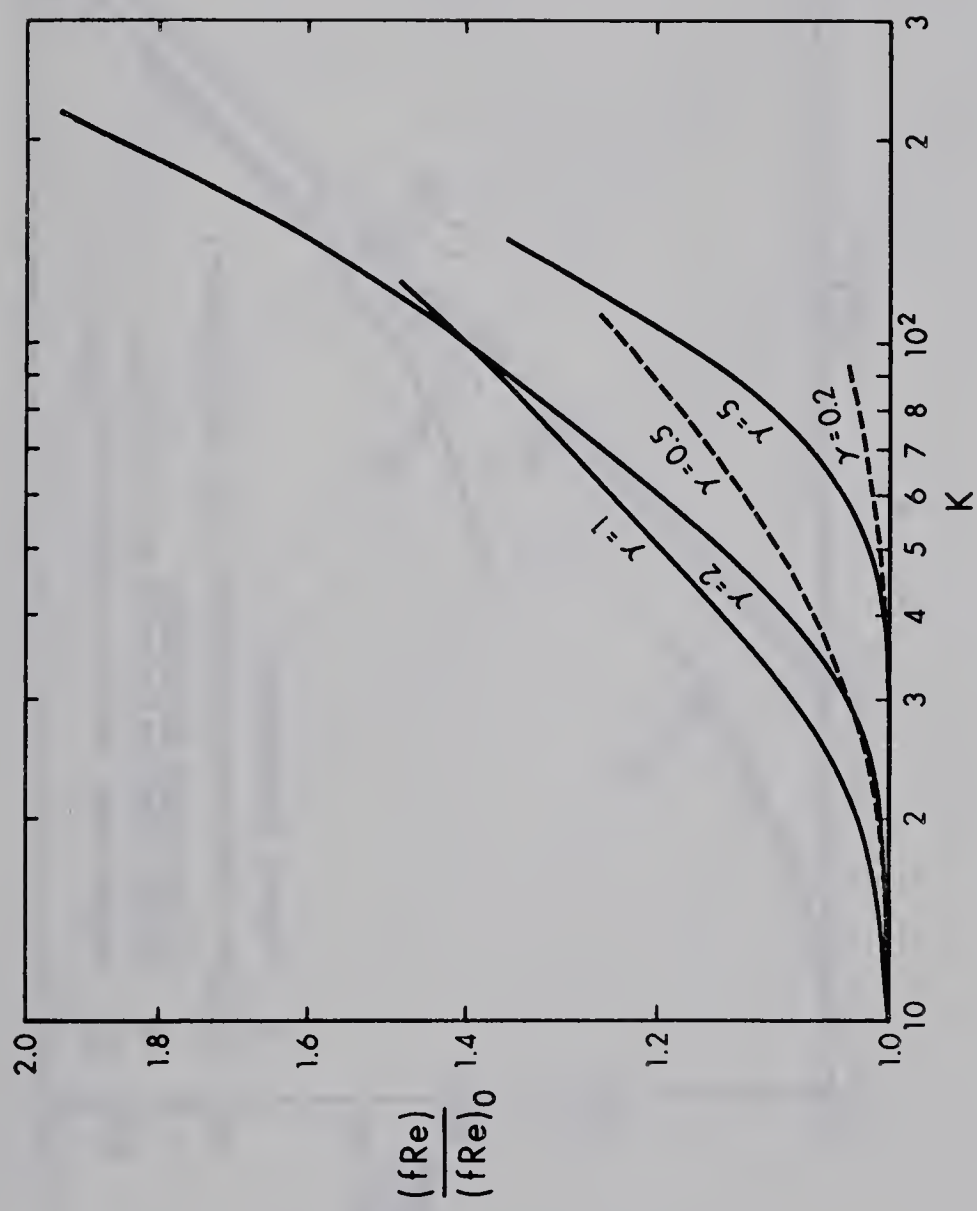


Fig. 28  $(fRe)/(fRe)_0$  versus  $K$  with aspect ratio  $\gamma$  as a parameter





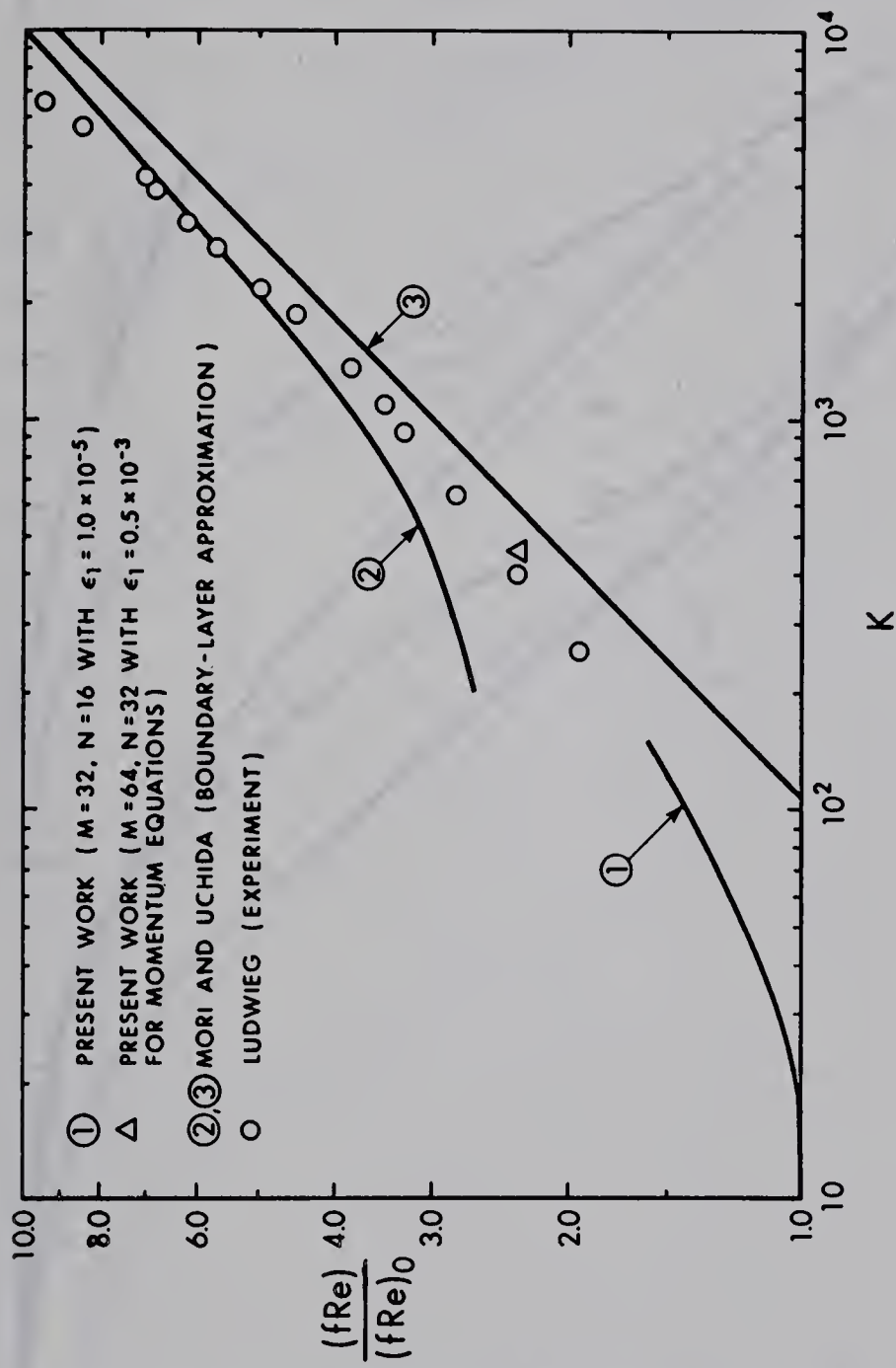


Fig. 29 Comparison of the results for friction factor from this work with the theoretical and experimental results available in literature



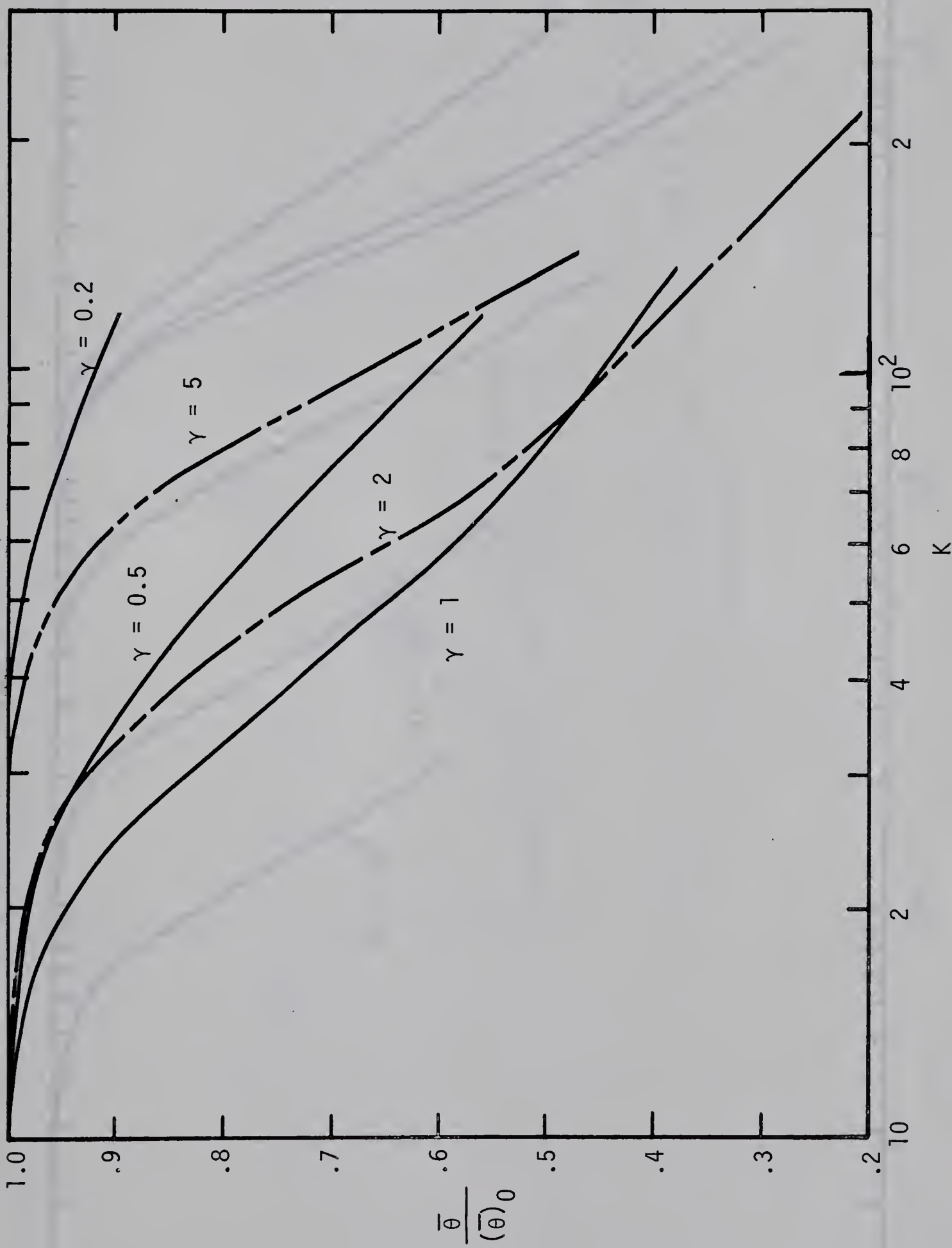


Fig. 30  $\bar{\theta}/(\bar{\theta})_0$  versus  $K$  with aspect ratio  $\gamma$  as a parameter and  $Pr = 0.73$





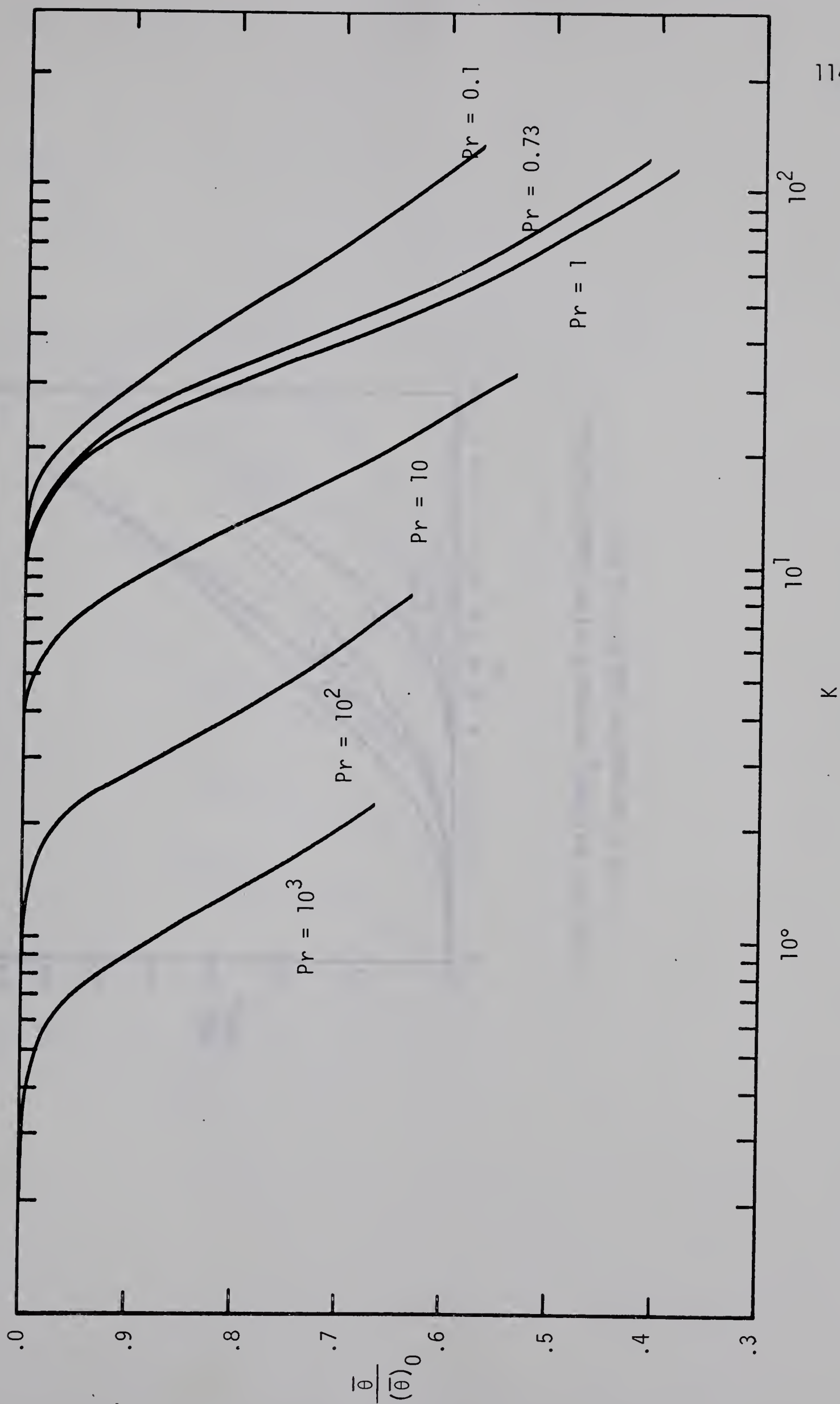


Fig. 31  $\bar{\theta}/(\bar{\theta})_0$  versus  $K$  with Prandtl number  $Pr$  as a parameter in a curved square channel  $\gamma = 1$



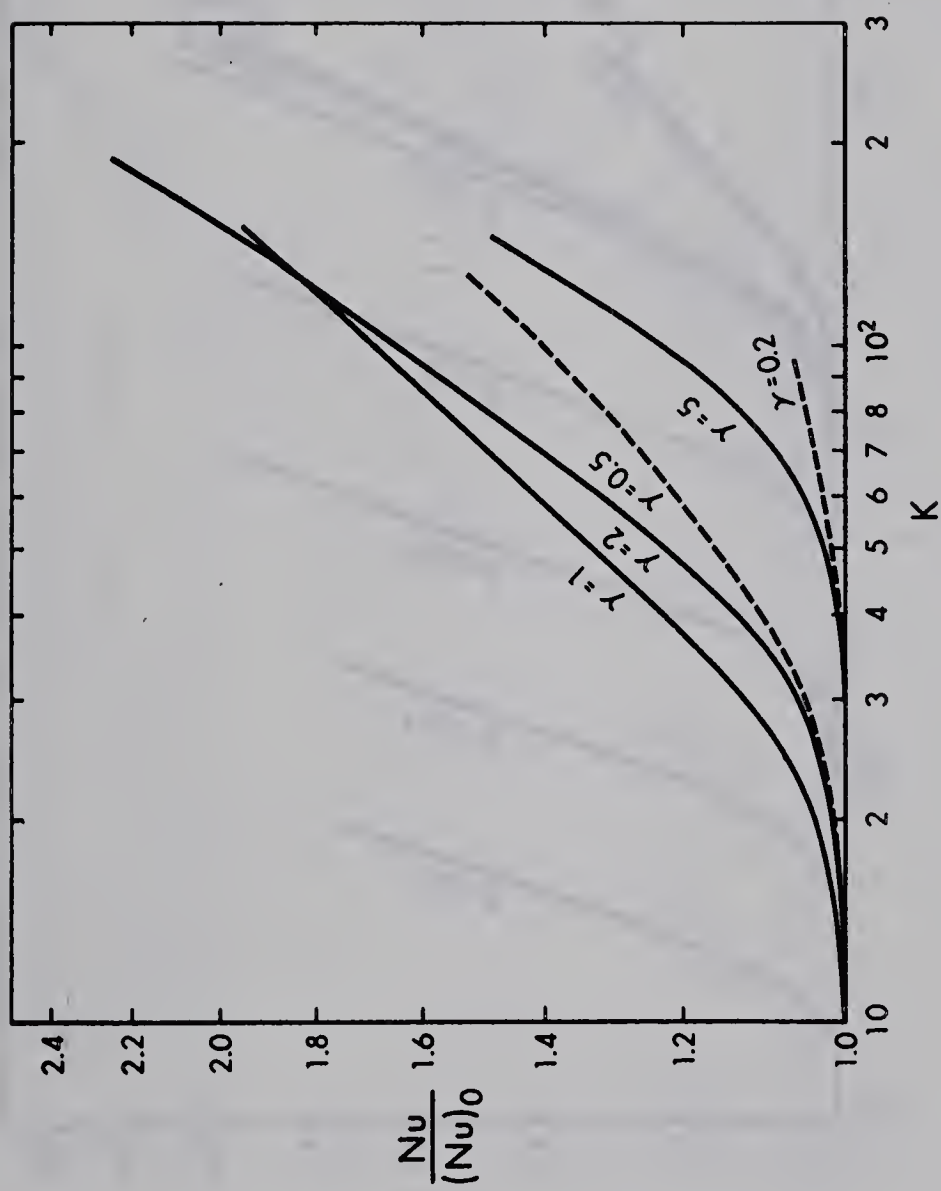


Fig. 32  $Nu/(Nu)_0$  versus  $K$  with aspect ratio  $\gamma$   
as a parameter and  $Pr = 0.73$



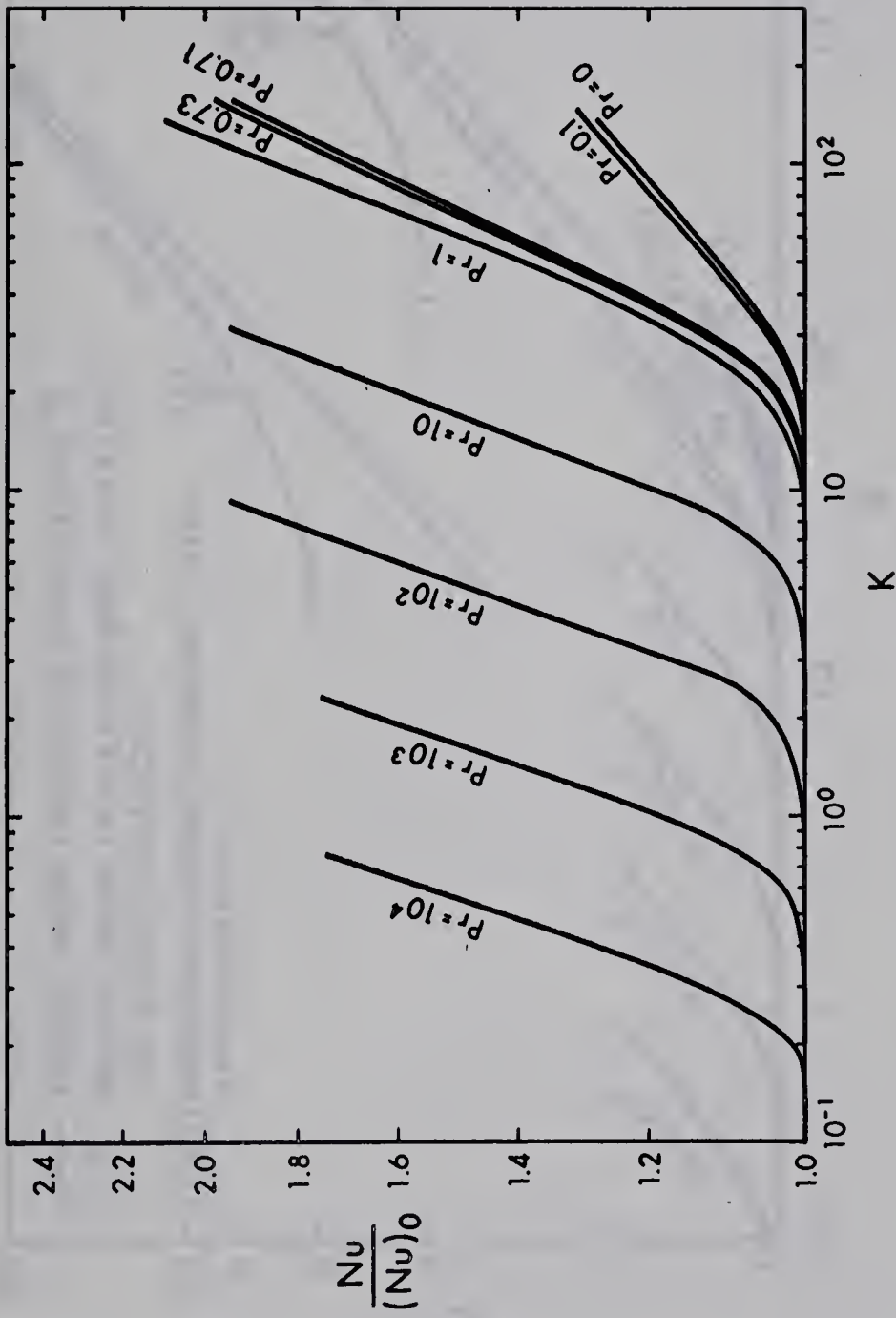


Fig. 33  $Nu/(Nu)_0$  versus  $K$  with Prandtl number  $Pr$  as a parameter in a curved square channel  $\gamma = 1$





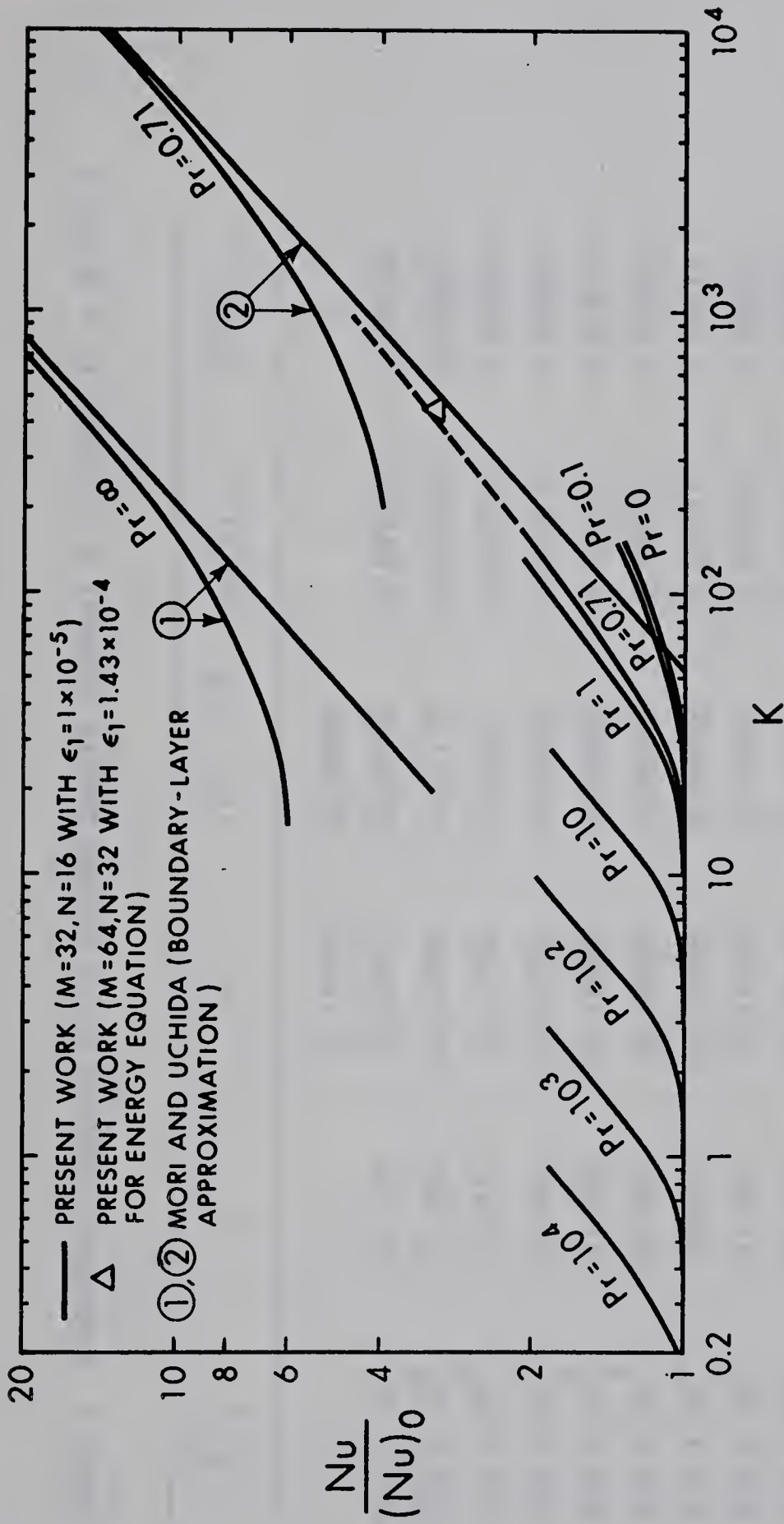


Fig. 34 Comparison of heat transfer results from this work with theoretical results available in literature



Table 1 Numerical Results for a Curved Square Channel  $\gamma = 1$  with  $Pr = 0.73(1)$

$c^2/r_c$	K	$\overline{w}$	$ \overline{\theta}  \times 10^2$	$\overline{w}/(\overline{w})_0$	$\overline{\theta}/(\overline{\theta})_0$
0	0	0.14045	0.68098	1	1
$0.8 \times 10^4$	12.510	0.13987	0.67488	0.99590	0.99100
$0.1 \times 10^5$	13.950	0.13956	0.67110	0.99366	0.98551
$0.2 \times 10^5$	19.442	0.13748	0.64827	0.97892	0.95203
$0.4 \times 10^5$	26.564	0.13282	0.59832	0.94578	0.87862
$0.6 \times 10^5$	31.585	0.12895	0.55820	0.91812	0.81970
$0.8 \times 10^5$	35.625	0.12595	0.52812	0.89682	0.77553
$0.1 \times 10^6$	39.050	0.12349	0.50402	0.87921	0.74014
$0.2 \times 10^6$	51.887	0.11602	0.43496	0.82603	0.63873
$0.4 \times 10^6$	68.974	0.10906	0.37624	0.77654	0.55250
$0.6 \times 10^6$	81.394	0.10508	0.34544	0.74827	0.50727
$0.8 \times 10^6$	91.499	0.10230	0.32492	0.72845	0.47714
$0.1 \times 10^7$	100.12	0.10012	0.30937	0.71296	0.45430
$0.15 \times 10^7$	117.64	0.09605	0.28189	0.68396	0.41395





Table 2 Numerical Results for a Curved Square Channel  $\gamma = 1$  with  $Pr = 0.73$  (2)

K	$(fRe)_I$	$\frac{(fRe)_I}{(fRe)_{OI}}$	$(fRe)_{II}$	$\frac{(fRe)_{II}}{(fRe)_{OII}}$	$(Nu)_I$	$\frac{(Nu)_I}{(Nu)_{OI}}$	$(Nu)_{II}$	$\frac{(Nu)_{II}}{(Nu)_{OII}}$
0	14.204	1	14.240	1	3.6099	1	3.6083	1
12.510	14.264	1.0042	14.299	1.0047	3.6318	1.0061	3.6266	1.0051
13.950	14.296	1.0065	14.331	1.0070	3.6436	1.0093	3.6381	1.0083
19.442	14.512	1.0217	14.548	1.0222	3.7245	1.0317	3.7187	1.0306
26.564	15.020	1.0574	15.058	1.0580	3.9216	1.0863	3.9155	1.0851
31.585	15.470	1.0891	15.510	1.0898	4.1037	1.1380	4.0971	1.1355
35.625	15.839	1.1151	15.879	1.1157	4.2578	1.1795	4.2500	1.1778
39.050	16.154	1.1373	16.196	1.1380	4.3924	1.2168	4.3843	1.2151
51.887	17.190	1.2102	17.238	1.2112	4.8503	1.3436	4.8412	1.3417
68.974	18.286	1.2874	18.339	1.2886	5.3501	1.4821	5.3391	1.4797
81.394	18.972	1.3357	19.033	1.3373	5.6630	1.5687	5.6511	1.5661
91.499	19.481	1.3715	19.550	1.3737	5.8934	1.6326	5.8817	1.6300
100.01	19.922	1.4026	19.976	1.4036	6.0834	1.6852	6.0699	1.6822
117.64	20.722	1.4589	20.822	1.4630	6.4389	1.7837	6.4343	1.7831



Table 3 Numerical Results for Aspect Ratio  $\gamma = 0.2$  with  $Pr = 0.73$

$c^2/r_c$	K	$\overline{w}$	$\overline{w}/(\overline{w})_0$	$ \overline{\theta}  \times 10^2$	$\overline{\theta}/(\overline{\theta})_0$	fRe	$\frac{(\text{fRe})}{(\text{fRe})_0}$	Nu	$\frac{Nu}{(Nu)_0}$
0	0	0.10482	1	0.35053	1	19.046	1	5.7414	1
$0.1 \times 10^4$	3.3148	0.10480	0.99998	0.35049	1.00000	19.046	1.0000	5.7415	1.0000
$0.1 \times 10^6$	33.096	0.10466	0.99847	0.34933	0.99658	19.075	1.0015	5.7568	1.0027
$0.2 \times 10^6$	46.627	0.10426	0.99466	0.34643	0.98830	19.148	1.0056	5.7948	1.0093
$0.3 \times 10^6$	56.843	0.10378	0.99008	0.34291	0.97826	19.236	1.0100	5.8403	1.0172
$0.4 \times 10^6$	65.328	0.10329	0.98540	0.33935	0.96810	19.326	1.0147	5.8864	1.0253
$0.5 \times 10^6$	72.708	0.10282	0.98092	0.33594	0.95838	19.413	1.0193	5.9308	1.0330
$0.6 \times 10^6$	79.298	0.10237	0.97663	0.33268	0.94908	19.498	1.0237	5.9734	1.0404
$0.7 \times 10^6$	85.276	0.10192	0.97233	0.32951	0.94003	19.583	1.0282	6.0156	1.0478





Table 4 Numerical Results for Aspect Ratio  $\gamma = 0.5$  with  $Pr = 0.73$

$c^2/r_c$	K	$\bar{w}$	$\bar{w}/(\bar{w})_0$	$ \bar{\theta}  \times 10^2$	$\bar{\theta}/(\bar{\theta})_0$	fRe	$\frac{(fRe)}{(fRe)_0}$	Nu	$\frac{Nu}{(Nu)_0}$
0	0	0.12851	1	0.55792	1	15.517	1	4.1264	1
$0.1 \times 10^5$	12.832	0.12832	0.99852	0.55604	0.99663	15.540	1.0015	4.1366	1.0025
$0.2 \times 10^5$	18.075	0.12781	0.99455	0.55099	0.98758	15.602	1.0055	4.1645	1.0092
$0.3 \times 10^5$	22.014	0.12710	0.98903	0.54394	0.97494	15.689	1.0111	4.2024	1.0184
$0.4 \times 10^5$	25.258	0.12629	0.98273	0.53599	0.96069	15.789	1.0175	4.2501	1.0300
$0.5 \times 10^5$	28.056	0.12547	0.97634	0.52795	0.94628	15.892	1.0242	4.2979	1.0416
$0.6 \times 10^5$	30.537	0.12467	0.97011	0.52012	0.93225	15.995	1.0308	4.3456	1.0531
$0.7 \times 10^5$	32.779	0.12389	0.96404	0.51268	0.91891	16.094	1.0372	4.3922	1.0644
$0.8 \times 10^5$	34.800	0.12316	0.95837	0.50568	0.90637	16.184	1.0430	4.4532	1.0791
$0.1 \times 10^6$	38.544	0.12189	0.94849	0.49359	0.88470	16.360	1.0543	4.5182	1.0949
$0.2 \times 10^6$	52.307	0.11696	0.91012	0.44863	0.80411	17.047	1.0986	4.8415	1.1733
$0.4 \times 10^6$	70.422	0.11135	0.86647	0.40081	0.71840	17.899	1.1535	5.2336	1.2683
$0.6 \times 10^6$	83.575	0.10790	0.83962	0.37324	0.66898	18.462	1.1900	5.4845	1.3291
$0.8 \times 10^6$	94.232	0.10536	0.81986	0.35385	0.63421	18.893	1.2176	5.6726	1.3747
$0.1 \times 10^7$	103.36	0.10336	0.80430	0.33900	0.60761	19.247	1.2404	5.8246	1.4115





Table 5 Numerical Results for Aspect Ratio  $\gamma = 2$  with  $Pr = 0.73$

$c^2/r_c$	K	$\bar{w}$	$\bar{w}/(\bar{w})_0$	$ \bar{\theta}  \times 10^2$	$\bar{\theta}/(\bar{\theta})_0$	fRe	$\frac{(fRe)}{(fRe)_0}$	Nu	$\frac{Nu}{(Nu)_0}$
0	0	0.12851	1	0.55792	1	15.517	1	4.1264	1
$0.1 \times 10^4$	4.0637	0.12851	1.0000	0.55790	0.99996	15.517	1.0000	4.1266	1.0000
$0.1 \times 10^5$	12.834	0.12840	0.99914	0.55612	0.99677	15.537	1.0013	4.1359	1.0023
$0.2 \times 10^5$	18.086	0.12789	0.99518	0.55096	0.98753	15.593	1.0049	4.1627	1.0088
$0.4 \times 10^5$	25.259	0.12629	0.98273	0.53419	0.95747	15.788	1.0175	4.2531	1.0307
$0.6 \times 10^5$	30.440	0.12427	0.96701	0.51343	0.92026	16.044	1.0340	4.3660	1.0581
$0.8 \times 10^5$	34.558	0.12218	0.95074	0.49279	0.88326	16.315	1.0514	4.4828	1.0864
$0.1 \times 10^6$	38.007	0.12019	0.93526	0.47373	0.84910	16.582	1.0686	4.5958	1.1138
$0.2 \times 10^6$	50.287	0.11245	0.87503	0.40441	0.72485	17.703	1.1409	5.0651	1.2275
$0.3 \times 10^6$	58.818	0.10739	0.83565	0.36273	0.65015	18.518	1.1934	5.4084	1.3107
$0.4 \times 10^6$	65.681	0.10382	0.80787	0.33490	0.60027	19.140	1.2335	5.6133	1.3603
$0.6 \times 10^6$	76.655	0.09896	0.77006	0.29995	0.53762	20.063	1.2930	6.0706	1.4712
$0.8 \times 10^6$	85.571	0.09567	0.74446	0.27818	0.49860	20.735	1.3363	6.3653	1.5426
$0.1 \times 10^7$	93.220	0.09322	0.72539	0.26137	0.46847	21.268	1.3706	6.5951	1.5983
$0.2 \times 10^7$	121.46	0.08591	0.66850	0.21775	0.39029	23.052	1.4856	7.3739	1.7870
$0.4 \times 10^7$	156.63	0.07831	0.60937	0.17756	0.31825	25.440	1.6395	8.3662	2.0275
$0.6 \times 10^7$	179.74	0.07338	0.57101	0.15305	0.27432	27.553	1.7757	9.1541	2.2184



Table 6 Numerical Results for Aspect Ratio  $\gamma = 5$  with  $Pr = 0.73$

$c^2/r_c$	K	$\overline{w}$	$\overline{w}/(\overline{w})_0$	$ \overline{\theta}  \times 10^2$	$\overline{\theta}/(\overline{\theta})_0$	fRe	$\frac{(\text{fRe})}{(\text{fRe})_0}$	Nu	$\frac{Nu}{(Nu)_0}$
0	0	0.10482	1	0.35053	1	19.046	1	5.7414	1
$0.1 \times 10^4$	3.3148	0.10482	1.0000	0.35053	1.0000	19.046	1.0000	5.7415	1.0000
$0.1 \times 10^6$	33.041	0.10448	0.99676	0.34766	0.99181	19.107	1.0032	5.7732	1.0055
$0.2 \times 10^6$	46.279	0.10348	0.98722	0.33959	0.96879	19.289	1.0128	5.8574	1.0202
$0.3 \times 10^6$	55.870	0.10200	0.97310	0.32813	0.93895	19.561	1.0270	5.9719	1.0401
$0.4 \times 10^6$	63.447	0.10032	0.95707	0.31552	0.90012	19.879	1.0437	6.0992	1.0623
$0.5 \times 10^6$	69.736	0.09862	0.94085	0.30315	0.86483	20.209	1.0611	6.2290	1.0849
$0.6 \times 10^6$	75.152	0.09702	0.92559	0.29168	0.83211	20.534	1.0781	6.3558	1.1070
$0.7 \times 10^6$	79.912	0.09551	0.91118	0.28116	0.80210	20.848	1.0946	6.4781	1.1283
$0.8 \times 10^6$	84.184	0.09412	0.89792	0.27162	0.77488	21.148	1.1104	6.5946	1.1486
$0.9 \times 10^6$	88.082	0.09285	0.88580	0.26305	0.75044	21.431	1.1252	6.7046	1.1678
$0.1 \times 10^7$	91.673	0.09167	0.87455	0.25529	0.72830	21.703	1.1395	6.8015	1.1846
$0.15 \times 10^7$	106.58	0.08703	0.83028	0.22578	0.64411	22.856	1.2000	7.2552	1.2637
$0.20 \times 10^7$	118.31	0.08366	0.79813	0.20568	0.58677	23.809	1.2501	7.6163	1.3266
$0.25 \times 10^7$	128.11	0.08102	0.77294	0.19079	0.54429	24.632	1.2933	7.9253	1.3804
$0.30 \times 10^7$	136.57	0.07885	0.75224	0.17906	0.51083	25.375	1.3323	8.2009	1.4284







Table 7 Numerical Results for a Curved Square Channel  $\gamma = 1$  with  $Pr = 0.1$

$c^2/r_c$	K	$\overline{w}$	$\overline{w}/(\overline{w})_0$	$ \overline{\theta}  \times 10^2$	$\overline{\theta}/(\overline{\theta})_0$	fRe	$\frac{(fRe)}{(fRe)_0}$	Nu	$\frac{Nu}{(Nu)_0}$
0	0	0.14045	1	0.68098	1	14.204	1	3.6099	1
$0.2 \times 10^5$	19.442	0.13748	0.97885	0.66139	0.97123	14.512	1.0217	3.6559	1.0127
$0.6 \times 10^5$	31.574	0.12890	0.91776	0.60622	0.89022	15.472	1.0892	3.7967	1.0517
$0.3 \times 10^6$	61.276	0.11187	0.79651	0.49841	0.73190	17.830	1.2553	4.1453	1.1483
$0.7 \times 10^6$	86.670	0.10359	0.73756	0.44781	0.65760	19.243	1.3548	4.3497	1.2049
$0.17 \times 10^7$	123.65	0.09484	0.67526	0.39750	0.58372	20.980	1.4770	4.5637	1.2642



Table 8 Numerical Results for a Curved Square Channel  $\gamma = 1$  with  $Pr = 0.71$

$c^2/r_c$	K	$\bar{w}$	$\bar{w}/(\bar{w})_0$	$ \bar{\theta}  \times 10^2$	$\bar{\theta}/(\bar{\theta})_0$	fRe	$\frac{(fRe)}{(fRe)_0}$	Nu	$\frac{Nu}{(Nu)_0}$
0	0	0.14045	1	0.68098	1	14.204	1	3.6099	1
$0.6 \times 10^4$	10.853	0.14012	0.99765	0.67733	0.99464	14.239	1.0025	3.6223	1.0034
$0.8 \times 10^4$	12.510	0.13987	0.99587	0.67462	0.99066	14.264	1.0042	3.6313	1.0059
$0.1 \times 10^5$	13.950	0.13956	0.99366	0.67130	0.98579	14.300	1.0068	3.6380	1.0078
$0.2 \times 10^5$	19.442	0.13748	0.97885	0.64888	0.95286	14.512	1.0217	3.7208	1.0307
$0.4 \times 10^5$	26.564	0.13282	0.94567	0.62363	0.91578	15.020	1.0574	3.8155	1.0570
$0.6 \times 10^5$	31.585	0.12895	0.91812	0.56004	0.82240	15.470	1.0891	4.0040	1.1092
$0.8 \times 10^5$	35.625	0.12595	0.89676	0.53023	0.77823	15.839	1.1151	4.2399	1.1745
$0.1 \times 10^6$	39.050	0.12349	0.87925	0.50627	0.74344	16.154	1.1373	4.3715	1.2110
$0.2 \times 10^6$	51.887	0.11602	0.82606	0.43739	0.64229	17.190	1.2102	4.8213	1.3356
$0.4 \times 10^6$	68.974	0.10906	0.77650	0.37860	0.55596	18.286	1.2874	5.3134	1.4719
$0.6 \times 10^6$	81.389	0.10570	0.75258	0.34769	0.51057	18.975	1.3359	5.6227	1.5576
$0.8 \times 10^6$	91.501	0.10230	0.72837	0.32715	0.48041	19.481	1.3715	5.8488	1.6202
$0.1 \times 10^7$	100.12	0.10012	0.71285	0.31160	0.45758	19.901	1.4011	6.0318	1.6709
$0.15 \times 10^7$	117.64	0.096054	0.68390	0.28407	0.41715	20.722	1.4589	6.3842	1.7685





Table 9 Numerical Results for a Curved Square Channel  $\gamma = 1$  with  $Pr = 1$

$c^2/r_c$	K	$\bar{w}$	$\bar{w}/(\bar{w})_0$	$ \bar{\theta}  \times 10^2$	$\bar{\theta}/(\bar{\theta})_0$	fRe	$\frac{(fRe)}{(fRe)_0}$	Nu	$\frac{Nu}{(Nu)_0}$
0	0	0.14045	1	0.68098	1	14.204	1	3.6099	1
$0.2 \times 10^4$	6.2795	0.14041	0.99972	0.68043	0.99919	14.209	1.0004	3.6122	1.0006
$0.4 \times 10^4$	8.8734	0.14030	0.99893	0.67879	0.99678	14.220	1.0011	3.6187	1.0023
$0.6 \times 10^4$	10.853	0.14012	0.99765	0.67610	0.99283	14.239	1.0025	3.6292	1.0053
$0.8 \times 10^4$	12.500	0.13987	0.99587	0.67251	0.98756	14.270	1.0046	3.6460	1.0100
$0.1 \times 10^5$	13.953	0.13958	0.99381	0.66809	0.98107	14.310	1.0075	3.6750	1.0180
$0.3 \times 10^5$	23.401	0.13511	0.96198	0.60807	0.89293	14.766	1.0396	3.9222	1.0865
$0.5 \times 10^5$	29.240	0.13076	0.93101	0.55499	0.81499	15.256	1.0740	4.1897	1.1606
$0.3 \times 10^6$	61.276	0.11187	0.79651	0.37295	0.54767	17.830	1.2553	5.5505	1.5376
$0.7 \times 10^6$	86.667	0.10359	0.73756	0.31050	0.45596	19.243	1.3548	6.2918	1.7429
$0.1 \times 10^7$	100.12	0.10012	0.71285	0.28635	0.42050	19.901	1.4011	6.6402	1.8394
$0.15 \times 10^7$	117.64	0.09605	0.68387	0.25948	0.38104	20.722	1.4589	7.0737	1.9595
$0.2 \times 10^7$	127.39	0.09008	0.64137	0.22626	0.33226	21.983	1.5477	7.7029	2.1338





Table 10 Numerical Results for a Curved Square Channel  $\gamma = 1$  with  $Pr = 10$

$c^2/r_c$	K	$\overline{w}$	$\overline{w}/(\overline{w})_0$	$ \overline{\theta}  \times 10^2$	$\overline{\theta}/(\overline{\theta})_0$	fRe	$\frac{(\text{fRe})}{(\text{fRe})_0}$	Nu	$\frac{\text{Nu}}{(\text{Nu})_0}$
0	0	0.14045	1	0.68098	1	14.204	1	3.6099	1
$0.1 \times 10^3$	1.4045	0.14045	1.0000	0.68065	0.99951	14.205	1.0001	3.6105	1.0002
$0.255 \times 10^3$	2.2428	0.14045	1.0000	0.68023	0.99890	14.205	1.0001	3.6129	1.0008
$0.122 \times 10^4$	4.9053	0.14044	0.99993	0.67277	0.98794	14.206	1.0001	3.6683	1.0162
$0.2 \times 10^4$	6.2796	0.14042	0.99979	0.65948	0.96842	14.209	1.0004	3.7581	1.0411
$0.3 \times 10^4$	7.6883	0.14037	0.99943	0.63811	0.93705	14.214	1.0007	3.9112	1.0835
$0.4 \times 10^4$	8.8873	0.14030	0.99893	0.61567	0.90409	14.220	1.0011	4.0845	1.1315
$0.6 \times 10^4$	10.853	0.14012	0.99765	0.57558	0.84522	14.239	1.0025	4.4292	1.2270
$0.8 \times 10^4$	12.510	0.13987	0.99587	0.54459	0.79972	14.264	1.0042	4.7294	1.3101
$0.1 \times 10^5$	13.956	0.13956	0.99366	0.52110	0.76522	14.296	1.0065	4.9770	1.3787
$0.13 \times 10^5$	15.850	0.13901	0.98975	0.49523	0.72723	14.352	1.0104	5.2669	1.4590
$0.16 \times 10^5$	17.504	0.13839	0.98533	0.47630	0.69943	14.417	1.0150	5.4866	1.5199
$0.20 \times 10^5$	19.442	0.13748	0.97885	0.45728	0.67150	14.512	1.0217	5.7097	1.5816
$0.3 \times 10^5$	23.401	0.13511	0.96198	0.42502	0.62413	14.766	1.0396	6.0875	1.6863
$0.4 \times 10^5$	26.564	0.13282	0.94567	0.38624	0.56718	15.020	1.0574	6.3457	1.7579



Table 11 Numerical Results for a Curved Square Channel  $\gamma = 1$  with  $Pr = 10^2$

$c^2/r_c$	K	$\bar{w}$	$\bar{w}/(\bar{w})_0$	$ \bar{\theta} $	$\bar{\theta}/(\bar{\theta})_0$	fRe	$\frac{(fRe)}{(fRe)_0}$	Nu	$\frac{Nu}{(Nu)_0}$
0	0	0.14045	1	0.68098	1	14.204	1	3.6099	1
$0.25 \times 10^2$	0.70227	0.14045	1.0000	0.68063	0.99949	14.204	1.0000	3.6126	1.0007
$0.49 \times 10^2$	0.98316	0.14045	1.0000	0.67955	0.99790	14.204	1.0000	3.6197	1.0027
$0.64 \times 10^2$	1.1236	0.14045	1.0000	0.67855	0.99643	14.204	1.0000	3.6264	1.0046
$0.81 \times 10^2$	1.2642	0.14045	1.0000	0.67707	0.99426	14.204	1.0000	3.6363	1.0073
$0.1 \times 10^3$	1.4105	0.14045	1.0000	0.67519	0.99150	14.204	1.0000	3.6450	1.0097
$0.17 \times 10^3$	1.8323	0.14045	1.0000	0.66497	0.97649	14.204	1.0000	3.7105	1.0279
$0.255 \times 10^3$	2.2456	0.14045	1.0000	0.64882	0.95277	14.204	1.0000	3.8400	1.0637
$0.40 \times 10^3$	2.8107	0.14045	1.0000	0.61794	0.90743	14.204	1.0000	4.0812	1.1306
$0.625 \times 10^3$	3.5114	0.14046	1.0001	0.57519	0.84465	14.205	1.0001	4.4758	1.2400
$0.9 \times 10^3$	4.2133	0.14044	0.99993	0.53841	0.79064	14.206	1.0001	4.8679	1.3485
$0.122 \times 10^4$	4.9053	0.14044	0.99993	0.51020	0.74921	14.206	1.0001	5.2107	1.4434
$0.16 \times 10^4$	5.6171	0.14043	0.99985	0.48838	0.71717	14.207	1.0002	5.5022	1.5242
$0.2 \times 10^4$	6.2795	0.14041	0.99972	0.47265	0.69407	14.206	1.0001	5.7256	1.5860
$0.4 \times 10^4$	8.8569	0.14004	0.99708	0.42891	0.62984	14.271	1.0047	6.8296	1.8919







Table 12 Numerical Results for a Curved Square Channel  $\gamma = 1$  with  $Pr = 10^3$

$c^2/r_c$	K	$\overline{w}$	$\overline{w}/(\overline{w})_0$	$ \overline{\theta} $	$\overline{\theta}/(\overline{\theta})_0$	fRe	$\frac{(fRe)}{(fRe)_0}$	Nu	$\frac{Nu}{(Nu)_0}$
0	0	0.14045	1	0.68098	1	14.204	1	3.6099	1
$0.9 \times 10^1$	0.42136	0.14045	1.0000	0.67623	0.99302	14.205	1.0001	3.6421	1.0089
$0.16 \times 10^2$	0.56182	0.14045	1.0000	0.66678	0.97914	14.205	1.0001	3.7076	1.0271
$0.25 \times 10^2$	0.7022	0.14045	1.0000	0.64984	0.95427	14.205	1.0001	3.8302	1.0610
$0.49 \times 10^2$	0.98317	0.14045	1.0000	0.59945	0.88028	14.205	1.0001	4.2440	1.1757
$0.64 \times 10^2$	1.1236	0.14045	1.0000	0.57292	0.84132	14.205	1.0001	4.4966	1.2456
$0.1 \times 10^3$	1.4045	0.14045	1.0000	0.52877	0.77648	14.205	1.0001	4.9871	1.3815
$0.2 \times 10^3$	1.9864	0.14045	1.0001	0.47273	0.69419	14.204	1.0000	5.7324	1.5880



Table 13 Numerical Results for a Curved Square Channel  $\gamma = 1$  with  $Pr = 10^4$

$c^2/r_c$	K	$\overline{w}$	$\overline{w}/(\overline{w})_0$	$ \overline{\theta}  \times 10^{-2}$	$\overline{\theta}/(\overline{\theta})_0$	fRe	$\frac{(fRe)}{(fRe)_0}$	Nu	$\frac{Nu}{(Nu)_0}$
0	0	0.14046	1	0.68111	1	14.205	1	3.6104	1
$0.6 \times 10^1$	0.34405	0.14046	1.0000	0.57952	0.85085	14.205	1.0000	4.4317	1.2275
$0.1 \times 10^2$	0.44416	0.14046	1.0000	0.52883	0.77642	14.205	1.0000	4.9871	1.3813
$0.2 \times 10^2$	0.62813	0.14045	0.99993	0.47344	0.69510	14.205	1.0000	5.7260	1.5860
$0.3 \times 10^2$	0.72930	0.14045	0.99993	0.44894	0.65913	14.205	1.0000	6.0964	1.6886



Table 14 Comparison of Numerical Results with Exact Values  
for  $K = 0$  (straight channel)

	$\gamma$	0.2	0.5	1	2	5
Exact	(fRe)	19.091	15.540	14.225	15.540	19.091
Present Work	(fRe) <sub>I</sub>	19.046	15.517	14.204	15.517	19.046
	(fRe) <sub>II</sub>	19.080	15.563	14.240	15.563	19.080
Exact	Nu	5.7376	4.1245	3.6080	4.1245	5.7376
Present Work	(Nu) <sub>I</sub>	5.7414	4.1264	3.6099	4.1264	5.7414
	(Nu) <sub>II</sub>	5.7182	4.1151	3.6083	4.1151	5.7183
Divisions	M,N	16,40	20,20	32,16	40,10	80,8
Relaxation Factor	$\omega_{op}$	1.75	1.78	1.82	1.78	1.75





Table 15 Numerical Results of  $(\frac{\partial \bar{w}}{\partial n})_W$ ,  $\bar{w}$ , and  $4X|\frac{\partial \theta}{\partial n}|_W$   
for  $Pr = 0.73$

$\gamma$	0.2	0.5	1	2	5
K	79.298	103.37	100.12	121.43	106.58
$(\frac{\partial \bar{w}}{\partial n})_W$	0.99803	0.99468	0.99625	0.98963	0.99468
$\bar{w}$	0.10237	0.10337	0.10012	0.085862	0.087026
$4X \frac{\partial \theta}{\partial n} _W$	0.10260	0.10343	0.10029	0.086064	0.086916





B29908